NUREG/CR-1450
ORNL/NUREG/TM-392

ornl

OAK
RIDGE
NATIONAL
LABORATORY

UNION
CARBIDE

Multirod Burst Test Program Progress Report for July-December 1979

R. H. Chapman

Prepared for the U.S. Nuclear Regulatory Commission
Office of Nuclear Regulatory Research
Under Interagency Agreements DOE 40-551-75 and 40-552-75

OPERATED BY
UNION CARBIDE CORPORATION
FOR THE UNITED STATES
DEPARTMENT OF ENERGY

Printed in the United States of America. Available from
National Technical Information Service
U.S. Department of Commerce
5285 Port Royal Road, Springfield, Virginia 22161

Available from
GPO Sales Program
Division of Technical Information and Document Control
U.S. Nuclear Regulatory Commission
Washington, D.C. 20555

NUREG/CR-1450
ORNL/NUREG/TM-392
Dist. Category R3

Contract No. W-7405-eng-26

Engineering Technology Division

MULTIROD BURST TEST PROGRAM PROGRESS REPORT FOR JULY—DECEMBER 1979

R. H. Chapman

Manuscript Completed — July 17, 1980
Date Published — August 1980

Prepared for the
U.S. Nuclear Regulatory Commission
Office of Nuclear Regulatory Research
Under Interagency Agreements DOE 40-551-75 and 40-552-75

NRC FIN No. B0120

Prepared by the
OAK RIDGE NATIONAL LABORATORY
Oak Ridge, Tennessee 37830
operated by
UNION CARBIDE CORPORATION
for the
DEPARTMENT OF ENERGY

CONTENTS

FOREWORD

This report summarizes progress and preliminary results of the Multi-rod Burst Test (MRBT) Program (sponsored by the Division of Reactor Safety Research of the Nuclear Regulatory Commission) for the period July–December 1979.

Previous MRBT progress reports are

NUREG Report No.	ORNL Report No.	Period covered
	ORNL/TM-4729	July–September 1974
	ORNL/TM-4805	October–December 1974
	ORNL/TM-4914	January–March 1975
	ORNL/TM-5021	April–June 1975
	ORNL/TM-5154	July–September 1975
	ORNL/NUREG/TM-10	October–December 1975
	ORNL/NUREG/TM-36	January–March 1976
	ORNL/NUREG/TM-74	April–June 1976
	ORNL/NUREG/TM-77	July–September 1976
	ORNL/NUREG/TM-95	October–December 1976
	ORNL/NUREG/TM-108	January–March 1977
	ORNL/NUREG/TM-135	April–June 1977
NUREG/CR-0103	ORNL/NUREG/TM-200	July–December 1977
NUREG/CR-0225	ORNL/NUREG/TM-217	January–March 1978
NUREG/CR-0398	ORNL/NUREG/TM-243	April–June 1978
NUREG/CR-0655	ORNL/NUREG/TM-297	July–December 1978
NUREG/CR-0817	ORNL/NUREG/TM-323	January–March 1979
NUREG/CR-1023	ORNL/NUREG/TM-351	April–June 1979

Topical reports pertaining to research and development carried out by this program are

1. R. H. Chapman (comp.), *Characterization of Zircaloy-4 Tubing Procured for Fuel Cladding Research Programs*, ORNL/NUREG/TM-29 (July 1976).

2. W. E. Baucum and R. E. Dial, *An Apparatus for Spot Welding Sheathed Thermocouples to the Inside of Small-Diameter Tubes at Precise Location*, ORNL/NUREG/TM-33 (August 1976).

3. W. A. Simpson, Jr., et al., *Infrared Inspection and Characterization of Fuel-Pin Simulators*, ORNL/NUREG/TM-55 (November 1976).

4. R. H. Chapman et al., *Effect of Creep Time and Heating Rate on Deformation of Zircaloy-4 Tubes Tested in Steam with Internal Heaters*, NUREG/CR-0343 (ORNL/NUREG/TM-245) (October 1978).

5. J. F. Mincey, *Steady-State Axial Pressure Losses Along the Exterior of Deformed Fuel Cladding: Multirod Burst Test (MRBT) Bundles B-1 and B-2*, NUREG/CR-1011 (ORNL/NUREG/TM-350) (January 1980).

The following limited-distribution quick-look and data reports have been issued by this program:

1. R. H. Chapman (comp.), *Quick-look Report on MRBT No. 1 4 × 4 Bundle Burst Test*, Internal Report ORNL/MRBT-2 (September 1977).

2. R. H. Chapman (comp.), *Quick-look Report on MRBT No. 2 4 × 4 Bundle Burst Test*, Internal Report ORNL/MRBT-3 (November 1977).

3 R. H. Chapman, *Quick-look Report on MRBT No. 3 4 × 4 Bundle Burst Test*, Internal Report ORNL/MRBT-4 (August 1978).

4. R. H. Chapman et al., *Bundle B-1 Test Data*, ORNL/NUREG/TM-322 (June 1979).

5. R. H. Chapman et al., *Bundle B-2 Test Data*, ORNL/NUREG/TM-337 (August 1979).

6. R. H. Chapman et al., *Bundle B-3 Test Data*, ORNL/NUREG/TM-360 (January 1980).

SUMMARY

During this reporting period, 18 single-rod tests were conducted in the test facility that was recently modified to permit independent heating of the shroud and the fuel pin simulator as required for preprogrammed temperature paths as a function of time. Most of the tests were performed with shroud heating to investigate the importance of this parameter. Heating rate, steam flow (at very low Reynolds number), and burst temperature were also varied to examine the effect of these parameters. Four different fuel simulators were employed, including one of the two used in a previous series of scoping tests at low heating rates with unheated shrouds. Comparison of the previous series with this new series facilitates evaluation of test parameters.

Several of the tests are considered invalid because of (1) premature failure at defects introduced by the thermocouple spot welds or (2) essentially zero power levels in the fuel simulator during deformation. The latter situation was encountered in the isothermal creep-rupture tests. Although these tests are invalid for establishing strain limits, they provide potentially useful information for development of deformation models. In fact, some of the tests provided information of very high quality with respect to temperature behavior.

One important effect of shroud heating is to reduce the fuel simulator power requirements for maintaining a specified heating rate. This tends to increase temperature uniformity. The effect, which becomes less important as the heating rate increases, was not particularly significant at the highest heating rate used in these tests (28 K/s).

Because of the increased temperature uniformity, considerably greater deformation can be expected in heated shroud tests than in unheated shroud tests under otherwise similar conditions. This expectation was confirmed by the test results. Strains in the order of 100% were observed at the lowest heating rates; for comparable unheated shroud tests, strains in the range of 25 to 40% are observed.

The steam flow rates were varied in some of the low-heating-rate tests to assess the effect of convective cooling. Even though the flow was laminar in all these tests, the influence was significant in that

axial temperature gradients were induced, and as a consequence, deformation was highly localized near the exit steam end. The burst strain was not particularly affected because it is primarily a function of the local temperature and azimuthal temperature gradients.

One important objective of the tests was to determine if deformation in single-rod heated shroud tests is comparable to that observed in bundle tests. Based on these limited test results, we conclude that it is, provided the flow conditions produce comparable axial temperature conditions. Burst strain and tube heated length volume increase (related to average strain) in the 10 and 28 K/s heated shroud tests were in the range of data observed in the 4 × 4 bundle tests conducted earlier with these heating rates. However, the potentially important effect of rod-to-rod interactions on deformation is not present in the single-rod tests.

The ORNL correlation (published in the previous progress report) relating burst temperature to burst pressure and heating rate is based on unheated shroud test data. Since our practice (and that of most other investigators) is to define burst temperature as the maximum measured value, improved temperature uniformity in heated shroud tests increases the probability that the maximum measured temperature will be nearer the true burst value. For this reason, burst temperatures predicted by the correlation might be expected to be less than those observed in these heated shroud tests. This was generally true for the higher-temperature tests at 10 and 28 K/s heating rates. The lower-heating-rate data were in better agreement.

On the basis of the results discussed in this report, we conclude that single-rod heated shroud tests performed under appropriate conditions provide temperature distributions representative of those present in bundle tests. Because of this and the simplicity of the single-rod tests relative to bundle tests, these tests are highly desirable for studying the effects of various parameters on deformation behavior. Even so, certain data, such as rod-to-rod interactions, must be derived from bundle tests.

Five fuel pin simulators were delivered by a Japanese manufacturer for test and evaluation. These simulators are identical to those currently in use in Japanese Atomic Energy Research Institute (JAERI) cladding deformation investigations. Evaluation of the transient response of

these simulators, based on infrared characterization scans at a number of heating rates, is discussed and compared with similar data for ORNL simulators. In general, the axial temperature profiles of the Japanese simulators is less uniform at the higher heating rates. However, at heating rates in the range used in the JAERI tests, the distributions are comparable to Oak Ridge National Laboratory simulators. Plans are under way for performing burst tests on the simulators in the single-rod test facility.

Preparations are in progress for testing an 8 × 8 bundle. Facility modifications to expand the instrumentation and data acquisition equipment will be complete in early 1980. Approximately 90% of the required fuel pin simulators are completed. Present plans are for the test to be performed in mid-1980.

MULTIROD BURST TEST PROGRAM PROGRESS REPORT FOR JULY–DECEMBER 1979

R. H. Chapman

ABSTRACT

A series of scoping tests designed to explore the effect of shroud heating on Zircaloy cladding deformation was conducted in the single-rod test facility, which was recently modified to permit independent heating of the shroud under specified conditions. To facilitate comparison of the test results, the series included tests under conditions used previously. Significantly greater deformation was observed in heated shroud tests than would be expected from unheated shroud tests.

Fabrication of fuel pin simulators for the B-5 (8 × 8) bundle test continued with ~90% of the required number being completed.

Five fuel pin simulators, identical to the simulators used in the Japanese Atomic Energy Research Institute multirod bundle burst tests, were delivered by the Japanese manufacturer. The surface temperature distribution of the simulators was characterized for several heating rates by infrared scanning and was compared to similar characterizations of Oak Ridge National Laboratory simulators. Plans are under way for conducting burst tests on the Japanese simulators in the single-rod test facility.

---

1. INTRODUCTION

R. H. Chapman

The objectives of the Multirod Burst Test (MRBT) Program are to (1) delineate the deformation behavior of unirradiated Zircaloy cladding under conditions postulated for a large-break loss-of-coolant accident (LOCA) and (2) provide a data base that can be used to assess the magnitude and distribution of geometric changes in the fuel rod cladding in a multirod array and the extent of flow channel restriction that might result. Data are being obtained from single-rod and multirod experiments, both with and without electrical heating of the shroud surrounding the test arrays. The tests are designed to study possible effects of rod-to-rod interactions on ballooning and rupture behavior; a tentative test matrix was given in a previous report.[1] Although the test matrix includes

11 × 11 test arrays, these will be held in abeyance until a definite need, based on the results of 4 × 4 and 8 × 8 test arrays, is established.

Approximately 53 single-rod burst tests have been conducted with a heating rate of ~28 K/s; experimental details of these unheated shroud tests and preliminary results have been reported routinely. (All published reports pertaining to this research program are listed in the foreword of this report.) The data base covers a range of burst pressures from 770 to 19,150 kPa; the corresponding burst temperatures range from 1170 to 690°C. All the tests conducted before April 1977 were reevaluated for validity, and the results were summarized in a previous report.[2] Readers using results obtained in this program should be aware that some of the earlier data points have been removed as a result of this reevaluation.

Four steady-state single-rod creep-rupture tests were conducted at about 760°C to determine if large ballooning occurs over extended lengths of test specimens heated with internal fuel simulators. Test conditions were varied to cause failure in creep times of 49, 103, 162, and 250 s. Two transient (~28 K/s) burst tests were conducted with the same internal fuel simulators for comparison. The initial conditions for the transient burst tests were adjusted to cause failure at approximately the same temperature as in the creep-rupture tests; the results of these unheated shroud tests were reported.[3]

Subsequently, two transient burst tests, using each of the same two fuel simulators, were conducted at nominal heating rates of 5 and 10 K/s to bridge the span between the creep tests (~0 K/s) and the 28 K/s transient burst tests. Initial pressure conditions for these tests were adjusted to cause failure at ~760°C for comparison. The results of these low-heating-rate tests with unheated shrouds were reported.[4]

The creep-rupture and low-heating-rate tests were evaluated, and the results were reported in considerable detail in a topical report.[5]

Two transient (28 K/s) burst tests were conducted to investigate the effect of steam flow rate on burst location. The steam flow rate in one test [Reynolds (Re) number ~800] was typical of that normally employed in the single-rod tests; in the other, the flow (Re ~180) was comparable to

that employed in the B-1 and B-2 bundle tests. The results of these tests have also been reported.[4]

Each of the single-rod tests discussed previously was conducted with an unheated shroud (ambient temperature of about 340°C) surrounding the fuel pin simulator. Since this arrangement causes significant heat losses from the simulator and enhances the circumferential temperature gradients therein, deformation observed in these tests is probably less than that expected in a fuel rod surrounded by others at about the same temperature.

Two 4 × 4 multirod tests, one (B-1) with and the other (B-2) without electrical heating of the shroud, have been conducted with a bundle heating rate of ~30 K/s. Initial pressure conditions for these tests were selected to cause failure at ~860°C. Another 4 × 4 array (B-3) was tested with an electrically heated shroud using a bundle heating rate of ~10 K/s; initial pressure conditions were selected to cause failure at ~760°C to provide a basis for comparison with the low-heating-rate single-rod tests.

Detailed results and interpretations of the bundle tests have been reported.[3,4,6-8] A topical report[9] interpreting the B-1 and B-2 water flow tests has been published. Data reports[10-12] giving detailed results of the B-1, B-2, and B-3 tests without interpretation have been published. Some results of further analysis of the B-3 test data are included in this report.

The substantial quantities of data accumulated in the MRBT Program to date have all been obtained from single-rod unheated shroud tests and from heated and unheated shroud 4 × 4 bundle tests in which (1) the shroud temperature at the time of burst was no closer than within about 80°C of the bundle temperature and (2) the rods were not confined sufficiently in their outward (radial) movement to simulate the radial restraint in a reactor core. The importance of closely simulating the thermal surroundings (thermal boundary) and confinement (deformation boundary) is not clear at this time, but the value of the data base will be increased by investigating these concerns in future tests. One conclusion that has remained valid throughout the testing is that at a given deformation temperature level, temperature gradients determine deformation behavior; the more uniform the temperature distribution, the greater (and more uniform) the

deformation. Therefore, deformation results will be dependent not only on the inherent metallurgical properties of Zircaloy, but also on all factors that determine the temperature gradients, including the method and uniformity of heating, heating rate, heat losses to coolant and surroundings, and axial distribution of heat losses; recent reports[13,14] by Hindle and Mann discussed the influence of these variables. Essentially all of our tests to date have been conducted at relatively low steam flow rates, and heat losses to the steam coolant have been small but are still an important factor to consider.

Major emphasis of this report period was devoted to (1) a scoping series of single-rod tests to explore the effect of a heated shroud on deformation and (2) preparations for an 8 × 8 bundle (B-5) test in which radial movement of the outer ring of rods will be restrained with a suitably positioned and supported reflective shroud. (The outer ring of rods may be regarded as sacrificial and as providing both a good thermal boundary and a good deformation boundary for the inner 6 × 6 bundle.) These and related activities are summarized in this report.

2. PROGRAM PLANS AND ANALYSIS

2.1 Programmatic Activities

R. H. Chapman

Data reports on the B-2 and B-3 tests were published[11,12] during this reporting period. These reports follow the format of the previous one[10] in that they give detailed data acquired during the tests and results of pretest and posttest examinations without interpretations.

A topical report[9] which analyzes and interprets the results of the B-1 and B-2 flow tests was also published. Two additional topical reports, one describing the development and fabrication of MRBT fuel simulators (heaters) and the other discussing MRBT thermometry techniques and errors, have been drafted.

A review of MRBT, JAERI, and REBEKA bundle flow restriction data as well as comments and suggestions for resolving recent FLECHT SEASET thermocouple and fuel pin simulator failures was presented to the FLECHT SEASET Program Management Group Meeting in Pittsburgh, Pennsylvania, on July 25. There appears to be rather good agreement between MRBT and REBEKA test results, considering the differences in test objectives and conditions. On the other hand, MRBT and JAERI results are somewhat less in agreement, although test conditions appear to be comparable. To investigate the lack of good agreement, we procured five fuel pin simulators, conforming to the JAERI design specifications for characterization and evaluation.

The simulators have been infrared (IR) scanned and radiographed over the full length; one simulator was partially disassembled for additional study. Burst tests will be conducted with the other four simulators. Since the electrical and thermal characteristics of the fuel simulators (internal heaters) are quite different from the characteristics of our simulators, evaluation of the transient heating performance is not a trivial matter. For the same reasons, modifications to the single-rod test facility will be necessary to perform burst tests under conditions comparable to those used in the JAERI bundle tests. For comparison purposes, we plan to test and evaluate our fuel pin simulators (we normally scan only the fuel simulator for characterization) under comparable conditions.

2.2 Single-Rod Test Results

R. H. Chapman

2.2.1 Introduction

In the past, our single-rod tests have been conducted in a test configuration (Fig. 2.1) in which the temperature of the flow shroud surrounding the fuel pin simulator remained essentially at ambient conditions (~340°C). This arrangement most likely causes significant heat loss from the test simulator and enhances the circumferential temperature gradients therein. As a result, deformation observed in tests conducted in this assembly is probably less than that expected in a fuel rod surrounded by others at about the same temperature. The results of our 4 × 4 bundle tests, in which the deformation was significantly greater than that observed in our single-rod tests (in this test configuration) at comparable test conditions, imply this to be the case.

To investigate this implication, we recently modified (after test SR-46) our single-rod test facility to incorporate a separate power supply and an integrated control system for heating the shroud surrounding the simulator. The modifications, which were described in detail in the previous report,[6] also included a new test configuration (Fig. 2.2). (This configuration was first used in test SR-47, and it will be used in all subsequent tests.)

During this report period we conducted a series of scoping tests to investigate the effect of shroud temperature on cladding deformation. Eighteen tests were conducted, 15 with and 3 without shroud heating, under temperature and pressure conditions typified by the transients shown in Fig. 2.3. These conditions were selected to facilitate comparison with an earlier unheated shroud test series[5] in which the effect of simulator heating rate was investigated.

Four different fuel simulators (internal heaters) were used in the tests. Three of these (MNL-009, MNL-046, and MNL-085) were selected from the lot fabricated recently[6] at Oak Ridge National Laboratory (ORNL), using BN preform technology. The other simulator (SEMCO 2828031) was used in the earlier test series and was selected for the current series to

permit direct comparison of heated and unheated shroud test results without consideration of fuel simulator characteristics. Based on the pretest IR characterization scans (Fig. 2.4), the ORNL-fabricated simulators selected for this test series were of slightly better quality (i.e., more uniform heat generation) than the one used in the previous scoping series.

The fuel pin simulator design and test instrumentation were not changed. In other words, we continue to spot weld twelve 0.25-mm-diam bare-wire, type S (Pt vs Pt + Rh) thermocouples to the outside of the Zircaloy tube to obtain axial and circumferential temperature gradients. The lower eight thermocouples are averaged and used by the rod power controller to maintain the specified temperature as a function of time. Six thermocouples (of the same type) are attached (two diametrically apart at elevations of 20, 38, and 50 cm from start of heated zone) to the outside surface of the shroud. These are averaged and used by the shroud power controller to maintain the specified temperature as a function of time.

Table 2.1 gives pertinent characteristics of the tests conducted during this reporting period. As the table shows, a wide range of conditions were employed to assess the effect of a number of important parameters. Preliminary evaluation of the data revealed that several of the tests are invalid, and this is indicated under the "Remarks" column. Some were invalidated on the basis that the failure was caused by the presence of a thermocouple and hence was premature. Others were invalidated on the basis that the power in the fuel simulator decreased during the time deformation was occurring to levels well below decay heat power in nuclear fuel rods. This situation occurred with the isothermal creep tests and resulted from the fact that the heated shroud virtually eliminated heat losses from the fuel pin simulator. This aspect will be discussed in greater detail below.

Table 2.2 tabulates pertinent results from the tests. As is our custom, we have presented both the valid and invalid results, since much can be learned from the invalid tests. However, any use of those data determined to be invalid should be considered carefully; otherwise, misleading or incorrect conclusions may result.

The tests and results will be discussed in the following subsections according to the heating rate used.

Table 2.1. Test conditions for evaluating the effect of shroud heating

Test No.	Fuel simulator identification	Heating rate (K/s)		Simulator linear power rating (kW/m)	Inlet steam Reynolds No.	Remarks
		Simulator	Shroud			
SR-47	SEMCO-031	10	10	3.3	735	TE caused premature burst, invalid test
SR-48	MNL-085	10	0	5.5	735	Shroud unheated to compare ORNL and SEMCO fuel simulators
SR-49	MNL-046	5	5	1.8	715	Compare with unheated shroud results of SR-55
SR-50	MNL-009	10	10	3.[illegible]	760	α + β phase test
SR-51	SEMCO-031	0	0	0.002[a]	755	Creep test, 10 K/s to hold temperature, TE caused premature burst, invalid test
SR-52	MNL-085	10	10	3.4	745	Compare with SR-48 with unheated shroud and same fuel simulator
SR-53	MNL-046	0	0	0.3	715	Creep test, 10 K/s to hold temperature, shroud 60°C less than simulator
SR-54	SEMCO-031	10	0	4.3	775	Shroud unheated to compare with SR-41 with same fuel simulator
SR-55	MNL-046	5	0	3.5	750	Compare with heated shroud results of SR-49
SR-56	SEMCO-031	0	0	0.005[a]	715	Creep test, 10 K/s to hold temperature, TE caused premature failure, invalid test
SR-57	MNL-046	0	0	0.005	810	Creep test, 10 K/s to hold temperature, invalid test
SR-58	SEMCO-031	0	0	0.001[a]	725	Creep test, 10 K/s to hold temperature, failure at TE, invalid test
SR-60	MNL-009	28	28	10.0	750	α + β phase test
SR-61	SEMCO-031	28	28	9.5	720	Compares heated shroud with unheated shroud results with same simulator
SR-62	MNL-009	28	28	10.5	745	α + β phase test
SR-63	SEMCO-031	0	0	0.3	5025	Creep test, 10 K/s to hold temperature, increased convective cooling
SR-64	MNL-046	5	5	2.1	4040	Increased convective cooling compared with SR-49
SR-65	MNL-046	5	5	1.7	330	Decreased convective cooling compared with SR-49

[a]During isothermal hold time.

Table 2.2. Summary of preliminary results of single-rod tests in steam

Test No.	Fuel simulator No.	FPS gas volume[a] (cm^3)	Initial conditions		Maximum pressure (kPa)	Burst conditions				Time from power-on to burst (s)	Burst strain (%)	Tube heated length change (%)	
			Temperature (°C)	Pressure (kPa)		Pressure (kPa)	Temperature[b] (°C)	TE No.	TE position relative to tube burst			Volume	Length
SR-47	SEMCO-031	51.0	335	11,460	11,875	9,730	786	203	4.5 cm below, 180° around	43.10	65.1	46.9	−3.7
SR-48	MNL-085	50.5	343	10,520	11,000	9,800	770	206	14.0 cm above, 135° around	42.00	27.1	23.0	−1.3
SR-49	MNL-046	51.2	341	9,565	9,895	7,635	783	206	9.0 cm above, 25° around	86.10	95.4	65.7	−4.9
SR-50	MNL-009	51.0	350	5,315	5,580	4,590	897	208	6.0 cm above, 150° around	56.70	55.9	40.3	+0.4
SR-51	SEMCO-031	51.0	338	8,085	8,365	6,950	810	206	At burst, 0° around	54.08	90.9	44.8	−3.1
SR-52	MNL-085	51.3	352	11,505	11,970	9,910	761	203	10.3 cm below, 135° around	40.90	48.7	37.3	−2.4
SR-53	MNL-046	50.8	327	6,610	6,900	5,835	762	207	24.5 cm above, 90° around	116.55	83.2	37.6	−2.6
SR-54	SEMCO-031	51.7	347	10,700	11,105	9,800	754	211	11.5 cm above, 135° around	41.70	27.4	25.1	−1.4
SR-55	MNL-046	51.3	356	8,855	9,195	8,010	790	210	7.0 cm below, 30° around	82.85	22.4	27.6	−1.2
SR-56	SEMCO-031	51.1	334	6,630	6,930	5,405	787	210	At burst, 8° around	80.95	67.0	50.6	−3.3
SR-57	MNL-046	51.5	328	6,105	6,420	4,985	779	211	5.5 cm above, 60° around	114.25	109.8	46.4	−1.6
SR-58	SEMCO-031	51.3	347	5,965	6,250	5,030	787	203	At burst, 0° around	174.68	137.0	42.5	−2.5
SR-60	MNL-009	50.3	349	7,815	8,215	7,145	879	204	1.7 cm below, 30° around	18.55	24.2	29.8	−1.5
SR-61	SEMCO-031	51.5	333	15,855	16,570	14,295	762	203	0.5 cm above, 17° around	14.60	31.4	26.9	−1.1
SR-62	MNL-009	51.9	349	4,390	4,665	4,195	937	207	6.5 cm above, 45° around	22.40	30.8	25.0	+0.3
SR-63	SEMCO-031	51.7	346	5,980	6,285	5,670	760	206	At burst, 10° around	140.6	98.9	19.7	−1.3
SR-64	MNL-046	50.4	343	9,595	10,020	8,490	766	205	5.5 cm above, 5° around	83.95	109.9	34.3	−2.3
SR-65	MNL-046	49.9	333	11,275	11,750	9,010	748	211	9.7 cm below, 80° around	83.20	74.4	55.3	−4.0

[a] Fuel pin simulator volume measured at room temperature; includes pressure transducer and connecting tube.

[b] Maximum measured by any thermocouple at time of burst; thermocouple number and location indicating burst are listed.

2.2.2 28 K/s tests

Three tests (SR-60, SR-61, and SR-62) were conducted with both the shroud and the fuel pin simulator heated at a rate of 28 K/s. Initial pressures were adjusted to cause failures at 762°C (SR-61), 879°C (SR-60), and 937°C (SR-62). The fuel simulator used in SR-61 was the same as employed in SR-37, which was part of the unheated shroud scoping series.[5] The burst temperatures in the two tests were nearly identical. Pertinent test conditions and results are given in Tables 2.1 and 2.2.

Figure 2.5 shows the pressure and temperature data of SR-60 for the instrumented cross section very near the burst location. The burst temperature (879°C) was obtained from TE-204, whose trace is included in the plot. As the figure shows, significant circumferential temperature gradients developed during the deformation phase of the test because of relatively fast heating in the high alpha temperature range. The temperature perturbation in the first few seconds of the test reflects action of the controller.

Figure 2.6 shows the eight-thermocouple rod average temperature, which is used through a feedback loop to control the rod power supply; the six-thermocouple shroud average temperature; the fuel simulator linear power rating; and the simulator internal pressure (channels 62, 63, 64, and 55, respectively). The rod and shroud average temperatures were rather close during deformation. The power required at the start of the transient was relatively large, but the average during the deformation phase was about 10 kW/m.

Figure 2.7 shows the axial distribution of the posttest circumferential elongation in SR-60; the burst strain was 24%. The pretest IR characterization scan of the fuel simulator is shown for reference purposes, and the planes of the thermocouples are indicated on the scan. Figure 2.8 shows two views of the burst. The locations of thermocouples TE-203 and TE-204, whose traces are plotted in Fig. 2.5, are indicated. Thermocouples TE-205 and TE-206, not evident in the photographs, were located diametrically opposite TE-203 and TE-204, respectively.

Test SR-61 was conducted to compare the results of a heated shroud test with those of an unheated shroud test (SR-37) using the same internal fuel simulator. An earlier attempt to perform the SR-61 test was

aborted because of an equipment malfunction. During the aborted attempt, the temperature reached a value of ~525°C before the power was terminated. The pressure was maintained on the simulator for ~15 min during cooldown from this temperature level. The Zircaloy tube suffered no apparent damage, and the test was conducted at a later time without modifications to the test specimen.

Based on past experience with this particular simulator, thermocouples (four equally spaced around the tube at each of three axial locations) were attached in regions of most interest. Figure 2.9 shows the pressure and temperature traces for the four thermocouples located on the plane near the burst. The burst temperature was obtained from TE-203, whose trace is included in the figure. The axial distribution of circumferential elongation is plotted in Fig. 2.10; the burst strain was 31%. The pretest IR characterization scan of the fuel simulator and the axial locations of thermocouples are also included in the figure. Photographs of the burst are shown in Fig. 2.11, with the remains of the thermocouples at the lower two instrumented elevations. The four temperature traces plotted in Fig. 2.9 are for the thermocouples nearest the burst location.

The initial pressure in the third test in this series (SR-62) was adjusted to cause failure in the alpha-plus-beta two-phase temperature region. Figure 2.12 shows internal pressure and temperatures from the four thermocouples, equally spaced around the tube, located nearest the burst. The burst temperature (937°C) was obtained from TE-207, whose trace is included in the figure. The deformation profile, the pretest IR characterization scan of the fuel simulator, and the axial locations of the thermocouples are shown in Fig. 2.13. The burst strain was 31%.

These three tests, all with heated shrouds, burst with approximately the same strain, even though there was a span of about 175°C in their burst temperatures. The burst strains were in close agreement, although a few percent (<10%) higher, with unheated shroud test results.[5]

2.2.3 10 K/s tests

Five tests were conducted in this series; in three of these (SR-47, SR-50, and SR-52), the shroud was heated at the same rate as the fuel pin

simulator, and in the other two (SR-48 and SR-54), the shroud was not heated. Test conditions and results are summarized in Tables 2.1 and 2.2.

Test SR-47 was the first test conducted after the facility was modified to permit heating of the shroud at the same rate as the fuel pin simulator. Test conditions were selected to approximate those used in the B-3 bundle test[12] and in SR-41 from the previous series of scoping tests.[5] The fuel simulator used in SR-41 was also employed in SR-47. The thermocouples were located in regions of interest based on our previous experience and the pretest IR characterization scan of this particular simulator.

Although this test has been judged to be invalid (see Table 2.1) because of premature failure at one of the thermocouples, many useful results were obtained. Since we believe our understanding is increased by every test, the results of this one are included.

Figure 2.14 depicts pressure, rod and shroud average temperatures, and fuel simulator power (channels 55, 62, 63, and 64, respectively) during the test. The average linear power rating during the test was about 3.3 kW/m.

Figures 2.15 and 2.16 show temperatures measured at the two instrumented planes in the region of greatest deformation. One thermocouple at each plane was inoperative (TE-206 and TE-209 at the 19- and 24-cm elevations, respectively); these traces are omitted from the plots. Both figures show very small circumferential gradients throughout the test, with a small gradient developing in the last 3 s. Figure 2.17 shows temperatures measured at each of the three instrumented planes. The burst temperature (786°C) was indicated by one of the thermocouples (TE-203) at the 19-cm elevation. This temperature was about 10°C higher than those measured at the 24-cm elevation, as Fig. 2.17 shows.

The axial profile of the circumferential elongation is plotted in Fig. 2.18, together with the pretest IR characterization scan and the axial locations of the thermocouples. The burst occurred between the wires of TE-209 (Fig. 2.19), which was inoperative throughout the test, and as Fig. 2.18 shows, at a position slightly higher in elevation than the two strain peaks (78%) in the profile. The strain at the burst was only 65%; because (1) this value was less than the maximum, (2) the failure occurred between the two thermocouple wires, and (3) this was the highest

temperature zone, we may conclude that the burst was initiated by a defect introduced by the thermocouple spot welds. Even though the failure was premature, the pressure trace (Fig. 2.17) indicates failure was imminent; thus, it was premature by an extremely short time interval. The maximum and burst strains were consistent with the upper range of strains observed in the B-3 bundle,[12] which the conditions of this test were supposed to approximate.

The SR-48 fuel simulator came from the lot produced at ORNL,[6] and initial conditions for the test were selected to approximate those in tests SR-41 and SR-42 with SEMCO fuel simulators to facilitate comparison of simulator quality. Consistent with this goal, the shroud was unheated in SR-48. Figure 2.20 depicts the rod and shroud average temperatures, the simulator pressure, and linear power (channels 62, 63, 55, and 64, respectively) during the test. As the figure shows, the power required to maintain the specified heating rate increased to compensate for heat losses as the temperature increased until it averaged about 5 kW/m during the deformation phase. As a result of the high heat losses, large circumferential temperature gradients developed during this portion of the transient (Fig. 2.21). The burst temperature (770°C) was indicated by TE-206, whose trace is included in the plot.

The axial profile of the circumferential elongation is plotted in Fig. 2.22, together with the pretest IR characterization scan of the fuel simulator and the axial locations of the thermocouples. The burst strain (27%) was essentially the same as observed in the unheated shroud tests (SR-41 and SR-42) conducted earlier[5] with the same heating rate. However, the strain was considerably less than in SR-47, which was conducted at the same heating rate but with the shroud heated. As would be expected, the effects of an unheated shroud are to increase the simulator power (and thus the temperature gradients) and to decrease the burst strain.

The third test (SR-50) in the 10 K/s heating rate category was conducted with the shroud heated at the same rate as the fuel pin simulator. Initial conditions were selected to cause failure in the alpha-plus-beta temperature range. Figures 2.23 and 2.24, respectively, indicate axial and circumferential temperature gradients during the test. The former shows temperatures measured at the 21- and 55-cm elevations, and the

latter shows temperatures measured around the tube at the 37-cm elevation; the fourth thermocouple (TE-210) at this elevation was inoperative during the test. The burst temperature (897°C) was obtained from TE-208 in this group of thermocouples.

The axial profile of the circumferential elongation is plotted in Fig. 2.25, together with the pretest IR characterization scan and the axial locations of the thermocouples. The deformation profile shows the effect of a local instability developing and producing rather large strains in a region of fairly uniform temperature as inferred from the IR scan and the measured temperatures. The burst strain (56%) was consistent with SR-47 (with a heated shroud) and thus was considerably greater than that of the unheated shroud tests.

Test SR-52 was conducted with a heated shroud using the fuel simulator from SR-48. Comparison of these two tests shows the effect of shroud heating with a very uniform fuel simulator.[6] Initial conditions selected were essentially the same as used in the B-3 test[12] so that the comparison could be extended to include the strain results of that test.

Figure 2.26 depicts the simulator pressure, rod and shroud average temperatures, and fuel simulator and shroud power requirements (channels 55, 62, 63, 64, and 65, respectively) during the test. The plot shows that fuel simulator power remained fairly constant (at 3.4 kW/m) throughout the test, while shroud power increased more or less linearly to compensate for its electrical characteristics and heat losses to the steam and surroundings.

Figure 2.27 depicts temperatures measured at the 21-cm elevation. As the previous heated shroud tests demonstrated, circumferential gradients were very small throughout the transient. The burst temperature (761°C), obtained from one of the thermocouples (TE-203) at this elevation, was in good agreement with B-3 results.[12]

The axial profile of the circumferential elongation is plotted in Fig. 2.28, together with the pretest IR characterization scan and axial locations of the thermocouples. The burst strain (49%) was considerably greater than that observed in an unheated shroud test (SR-48) with the same fuel simulator. The burst strain was consistent with the lower range of strains observed in the B-3 test.

Test SR-54 was conducted to compare results from the modified test facility (Fig. 2.2) with those obtained in the previous test configuration using the same fuel simulator (Fig. 2.1). By comparison with SR-47, which used the same fuel simulator, the effects of shroud heating could be elucidated further. Initial conditions for SR-54 were essentially the same as those in SR-41 (Ref. 5).

Based on experience and the pretest IR characterization scan, the thermocouples were located at axial positions at which the failure might be expected. Temperature data obtained at two of these locations are shown in Figs. 2.29 and 2.30. We define the burst temperature as the maximum measured value (of those considered to be reliable) at the time of failure without regard to the location of the thermocouple relative to the burst. Normally, this definition presents no difficulty since the thermocouple traces usually exhibit clear evidence of malfunctions that occur during the transient. This test was one of the rare cases in which problems occur. The trace of TE-207 (Fig. 2.29) shows very unusual behavior near the end of the transient and is considerably higher than the other temperatures plotted in the two figures. The appearance of the oxide on the tube surface at the instrumented elevations indicated that the temperature variation was not nearly as large as the TE-207 data would suggest. Furthermore, the temperature indicated by TE-207 at the time of failure is 40 to 50°C higher than would be expected from the burst pressure. For these reasons we concluded that TE-207 provided unreliable data during the last 7 s of the transient, and it should not be used to define the burst temperature. Instead, TE-211 data were used to define the burst temperature (754°C). This value is in very good agreement with all the other data from this test and agrees well with the temperature predicted by our correlation for the observed burst pressure.

The axial profile of the circumferential elongation is plotted in Fig. 2.31, together with the pretest IR characterization scan of the fuel simulator and axial locations of the thermocouples. The burst strain (27%) was the same as that observed in SR-41 under similar test conditions with the same fuel simulator, although the burst location was different.[5] The strain was considerably less than that in SR-47 with the same simulator and a heated shroud.

2.2.4 5 K/s tests

Four tests were performed in this group; in three of these (SR-49, SR-64, and SR-65) the shroud was heated and the shroud was unheated in SR-55. Also, as noted in Table 2.1, the steam flow in SR-64 was a factor of ~5.7 greater than that normally used, while in SR-65 the flow was about half the normal value. Other test conditions and pertinent results are compared in Tables 2.1 and 2.2.

The fuel simulator selected for SR-49 came from the lot produced at ORNL and had a very flat axial heat generation profile as judged from the pretest IR characterization scan (Fig. 2.32); the figure also shows the pretest location of the thermocouples and the axial profile of the circumferential elongation.

Figures 2.33 through 2.35 show the temperatures measured at the three instrumented elevations. As would be expected from the axial heat generation profile, the presence of a heated shroud, and the use of a low heating rate, very small circumferential temperature gradients developed. Figure 2.36 shows the axial temperature distribution as measured by the thermocouples located at the 45° azimuthal position at each elevation. The small gradient along the tube accounts for the steep strain gradient (Fig. 2.32) in this region. The burst temperature (783°C) was indicated by TE-206, whose trace is plotted in Figs. 2.33 and 2.36.

The abnormal behavior of TE-203, shown in Fig. 2.33, had an unusual effect on the rod average temperature and simulator power. Figure 2.37 shows a slight increase in rod average temperature (channel 62) occurring at the time of the step increase in TE-203 as a result of the automatic averaging circuit in the power controller. Before the step increase, TE-203 was outside the limits for inclusion in the average, but the step increase was sufficient to permit it to be included, increasing the average by 2 to 3°C. This slight increase in average temperature was sensed by the controller and resulted in a sudden decrease in simulator power (channel 64). Simultaneously, the shroud controller sensed that the shroud average temperature (channel 63) was slightly less than that of the rod and suddenly increased shroud power (channel 65) to compensate for the difference. This is a good example of the ability of the integrated

control system to sense and correct small differences in programmed temperature transients.

Photographs of the burst are shown in Fig. 2.38; the remains of the thermocouples, whose traces are plotted in Fig. 2.33, are evident. These appear approximately at the 21.7-cm elevation. The difference in this position and that plotted in Fig. 2.32 is due to axial shrinkage of the tube (4.9%) during deformation. The slight depression in the deformation profile at about 22.5 cm (Fig. 2.32) might seem to be attributed to a cooling effect of the thermocouples, but careful study of the photographs in Figs. 2.38 and 2.39 shows the strain depression to be upstream (colder steam) side of the thermocouples. If the fin effect of the thermocouples had caused local cooling of the tube, the strain depression would have been located at the actual location of the thermocouples; the photographs show clearly that this is not the case. Instead, the slight depression is attributed to the small depression in the axial heat generation as evidenced by the pretest IR characterization scan in Fig. 2.32. Again, axial shrinkage of the tube during deformation caused the shift of the scan relative to the posttest deformation profile evident in this region of the figure.

Photographs of the tube over a greater portion of the heated length (Fig. 2.39) illustrate the "carrot-type" deformation discussed by Hindle and Mann.[13,14]

Test SR-55 was performed with an unheated shroud with steam conditions essentially the same as in SR-49. Also, the same fuel simulator was used in the two tests to facilitate comparison of the effect of shroud heating on deformation with a simulator having a very uniform axial heat generation profile.

The thermocouple arrangement was altered in this test to obtain additional information on the axial temperature profile. Figure 2.40 shows the axial locations of the thermocouples, together with the pretest IR characterization scan of the fuel simulator and the axial distribution of the circumferential elongation. Temperatures measured at the instrumented cross section at the 24-cm elevation are plotted in Fig. 2.41. They show the behavior typical of tests performed in the high alpha temperature range. The burst temperature (790°C) was obtained from TE-210, whose trace is included in the plot. Figure 2.42 depicts temperatures measured

at the same circumferential position at three axial locations (see Fig. 2.40). The relatively uniform axial temperature distribution is consistent with the more or less uniform deformation profile.

Test SR-64 was assembled with the same fuel simulator as used in SR-49 and tested with a heated shroud. The Reynolds number of the steam at the start of the SR-64 heated zone was a factor of about 5.7 greater than that in SR-49, giving rise to increased convective heat losses along the length of the fuel pin simulator. As might be expected, this had a significant effect on the axial distribution of both the temperature and deformation.

The thermocouple arrangement in SR-64, the same as in SR-55, is shown in Fig. 2.43, together with the pretest IR characterization scan of the fuel simulator and the axial distribution of the circumferential elongation. The deformation was highly localized near the exit end of the steam, reflecting the influence of convective cooling along the tube length. In addition, deformation in the vicinity of the burst was fairly symmetrical about the axis of the tube (Fig. 2.44), indicating a very uniform temperature distribution around the tube. Average strain as deduced from the volume increase of the heated length (Table 2.2) was modest.

This is borne out by the temperatures measured at the 12-cm elevation as depicted in Fig. 2.45. The burst temperature (766°C) was measured by TE-205 at this location. The angular position of this thermocouple was almost in line with the burst (Fig. 2.44). Temperatures measured at the next highest elevation, plotted in Fig. 2.46, show essentially the same behavior as observed at the lowest elevation. The maximum temperature measured (by TE-209 at the same relative angular position as TE-205) at this cross section at the time of burst was only 0.6°C less than that measured by TE-205. Temperatures measured by the upper four thermocouples, plotted in Fig. 2.47, show significant cooling of the tube by the increased steam flow. The temperature measured at the time of burst by TE-211 was only 3.9°C less than that measured by TE-205, indicating nearly uniform temperature distribution over the lower portion of the rod.

As Fig. 2.48 shows, the increased steam flow also affected the axial temperature distribution of the shroud significantly for thermocouples

located at the 20- (TE-305), 38- (TE-303), and 56-cm (TE-301) elevations (all at the same relative azimuthal position).

Further evidence of the increased steam flow is shown by the significantly greater simulator and shroud power requirements (channels 64 and 65, respectively) as given in Fig. 2.49 compared with those plotted for SR-49 in Fig. 2.37.

Test SR-65 was assembled with the same fuel simulator as used in SR-64 and performed with a heated shroud. The effect of convective cooling was further investigated by reducing the steam flow to approximately half that normally used. The thermocouples were arranged in the same pattern as used in SR-64. Since the steam flow in these two tests differed by a factor of about 12, reporting the same type of data for the two tests will facilitate comparison.

The axial distribution of the circumferential elongation is plotted in Fig. 2.50, together with the pretest IR characterization scan of the fuel simulator and the axial locations of the thermocouples. The average strain in SR-65 was greater (as inferred from the volume increase over the heated length tabulated in Table 2.2) than in SR-64, although the burst strain was significantly less. Moreover, comparison of the two strain profiles shows that the deformation was distributed more uniformly in SR-64, indicating more uniform temperatures.

This is borne out by the measured temperatures. Figure 2.51 shows that very small temperature differences (maximum difference of 6.7°C at time of burst) existed at the 12-cm elevation; the maximum temperature at this instrumented location was 740°C (from TE-205). Temperatures measured at the 24-cm elevation are plotted in Fig. 2.52. The maximum difference measured at this location at the time of burst was 11.2°C, with the maximum temperature being 744°C (from TE-209). Temperatures measured along the upper portion of the tube are plotted in Fig. 2.53. The burst temperature (748°C) was indicated by TE-211, while the temperature at the uppermost thermocouple was 725°C. A comparison of these temperature plots with the corresponding ones for SR-64 shows smaller temperature variations in the low steam flow test (SR-65).

As expected, the shroud axial temperature distribution was also more uniform in this test (Fig. 2.54). Another consequence of reduced

convective cooling is a reduction in the power required to maintain the programmed heating rate, as shown in Fig. 2.55, which also shows the rod and shroud average temperatures and the simulator pressure.

As mentioned previously, SR-49, SR-64, and SR-65 were tested at different steam flow rates, using the same fuel simulator, to determine the effect of this parameter on axial distribution of temperature and deformation. The temperature distributions are plotted in Fig. 2.56 with time as a parameter; the uppermost group of curves are plotted for the respective burst times. The maximum measured temperature was selected for each of those elevations having multiple thermocouples, that is, at elevations of 24, 38, and 48 cm in SR-49 and at elevations of 12 and 24 cm in SR-64 and SR-65.

As expected, the temperature distribution remained relatively flat throughout the transient for the lowest convective cooling case, and very small azimuthal temperature gradients were measured (Figs. 2.51 and 2.52). Also, the deformation profile (Fig. 2.50) is consistent with a uniform axial temperature profile.

Although the Reynolds number (upstream of the heated zone) in SR-49 was about a factor of 2 greater than that of SR-65 and a factor of about 5.7 less than that of SR-64, the measured axial temperature distributions (over the instrumented portions) in SR-49 and SR-64 were very similar and were strongly skewed, as would be expected for increased convective cooling conditions. The power requirements (Table 2.1) were also higher, and larger azimuthal temperature gradients (particularly in SR-64 as shown in Fig. 2.46) were observed. Also, the shroud axial temperature distribution was more strongly skewed for the two higher-flow-rate tests (compare Figs. 2.48 and 2.54). Deformation in the two higher-flow-rate tests was highly localized in the high-temperature regions (Figs. 2.32 and 2.43), and greater burst strains resulted.

The results of these tests show a strong influence of convective cooling on temperature distribution and thus on deformation. They also reconfirm earlier observations that deformation is strongly dependent on small temperature differences.

2.2.5 Isothermal creep-rupture tests (~0 K/s heating rate)

In a previous series of tests[5] conducted with an unheated shroud, deformation observed under essentially isothermal heating conditions was not significantly different from that observed at heating rates of 5, 10, and 28 K/s. Subsequent tests have now shown that the presence of a heated shroud reduces the simulator power required to maintain a specified heating rate and improves temperature uniformity in the tube surrounding the fuel simulator; as a result, greater deformation is observed. During this reporting period, six isothermal creep-rupture tests (SR-51, SR-53, SR-56, SR-57, SR-58, and SR-63) were conducted with a heated shroud. One of the fuel simulators used in the previous series was used in four of these tests to permit direct comparison with the earlier results. The other two tests were conducted with one of the more uniform simulators produced in ORNL facilities; this permits comparison of results on the basis of uniformity of axial heat generation.

This series of tests was conducted by ramping the fuel simulator and shroud from the initial temperature to the hold temperature at a rate of 10 K/s. (Tests[5] in the previous series were ramped 13 K/s.) When the specified test temperature was attained, the power levels were reduced, via actions of the integrated temperature control system, to maintain the desired temperature at a constant value. The initial pressure was adjusted to a value expected to cause failure after 50 to 150 s of isothermal creep, that is, in the range of the previous tests.[5] Tables 2.1 and 2.2 summarize test conditions and pertinent results.

The first test (SR-51) in this group was assembled with a fuel simulator from the previous series. Four thermocouples (equally spaced around the tube) were located at axial elevations of 19, 24, and 68.6 cm. The two lower elevations were at pronounced peaks in the pretest IR characterization scan of the fuel simulator where earlier tests had failed. As anticipated, deformation was large and highly localized in this region (Fig. 2.57). Photographs of the burst (Fig. 2.58) show that failure occurred between the two thermocouple wires of TE-206.

Although the initial pressure suggested that failure would occur after 50 to 150 s of isothermal heating, the plots of rod (channel 62)

and shroud (channel 63) average temperatures (Fig. 2.59) show that the tube failed after about 9 s of near isothermal conditions. This observation, together with the fact that the failure occurred between the wires of TE-206, leads us to conclude that the failure initiated at a defect introduced by spot welding one of the thermocouple wires.

Electrical power to the fuel simulator decreased from ~3.3 kW/m during the ramp to about 2 W/m during the "near-isothermal" hold time as shown by channel 64 in the figure. The heated shroud essentially eliminated heat losses from the simulator, and in effect the test was much the same as if it had been conducted in a furnace. This absence of heat generation within the fuel pin simulator permitted the cladding temperature to equilibrate and become very uniform. Since linear power ratings in the range required in this test (~2 W/m) to maintain the cladding temperature constant are much below the decay heat level of interest, we conclude this test to be invalid for use in describing deformation limits under simulated accident conditions.

Although we consider this test to be invalid for certain applications, the temperature data may be of considerable interest for development of deformation models. Figures 2.60 through 2.62 show the temperatures measured at the 19-, 24-, and 68.6-cm elevations, respectively. As the plots show, small circumferential gradients existed at each level, consistent with the test conditions. The burst temperature (810°C) was indicated by TE-206, which was directly on the burst (Fig. 2.58). Two thermocouples at each of the two lower instrumented elevations showed rapidly increasing temperatures near the time of burst. The presence of "noise spikes" in the data from the lowest elevation (Fig. 2.60) made it difficult to separate real temperature increases from extraneous electrical noise. This was circumvented by exposition of the data on greatly expanded time and temperature scales. For example, TE-206 and TE-210, which were located at the same relative azimuthal position, are plotted in Fig. 2.63 on expanded scales covering about the last 10 s of the heating transient. The thermocouples showed similar behavior and nearly identical temperatures during most of this time period, except for obvious erratic behavior of TE-206 in the time interval of ~49.3 to ~51.8 s. The plot does not show clearly whether the rapid increase over the 0.5-s period

preceding the burst is real. Figure 2.64 shows the data from the lowest instrumented section as actually recorded (at 5-ms intervals) by the computer-controlled data acquisition system for a 0.5-s interval around the time of burst. The plot shows that TE-203, TE-204, and TE-206 were stable up to the time of burst, with TE-206 indicating a value of 810°C at the time of burst as indicated by the change in slope of the pressure curve, and that the noise spikes occurred 20 ms later. A negative noise spike is evident on TE-205 53.9 s after power-on. The noise spikes show exponential decay (or buildup) to stable readings immediately after the spikes.

Test SR-53 was assembled with one of the simulators fabricated at ORNL and tested to determine deformation under creep conditions with a simulator having a reasonably uniform axial heat generation profile. The test was marked by unusual disturbances in the thermocouple circuitry and by inadvertent shroud temperature controller settings. As a result of this error, the shroud power supply was programmed for constant power until its average temperature became 60°C less than the average rod temperature, after which the power supply was automatically controlled to maintain this difference.

Figure 2.65 shows the rod average temperature (channel 62) throughout the transient and the shroud average temperature (channel 63) during that portion of the test in which the shroud average was within the automatic power control range, that is, 60°C less than the rod average. The shroud average departed from the automatic control range after about 10 s of heating and came back in at about 70 s and remained in range for the remainder of the test. The figure also depicts the simulator pressure and the fuel simulator power. Operation with the shroud 60°C less than the rod caused significant heat losses from the rod. As a result, the fuel simulator power during the constant temperature portion of the test was about 0.3 kW/m, considerably greater than necessary to maintain constant temperature conditions in SR-51 (Fig. 2.59).

The simulator power required to compensate for heat losses was apparently sufficient to cause circumferential temperature gradients to increase throughout the test (Figs. 2.66 through 2.68). The burst temperature (762°C) was indicated by TE-207, whose trace is included in

Fig. 2.67. The effect of improper shroud power controller action is reflected by comparison of the temperatures plotted in Fig. 2.69.

Deformation in SR-53 was highly localized as shown by the plot in Fig. 2.70. The figure also shows the pretest IR characterization scan of the fuel simulator and the axial locations of the thermocouples. Although moderate temperature gradients existed at the instrumented elevations, the magnitude of the strain at the burst elevation suggests that very small gradients existed in this region.

Test SR-56 was assembled with one of the fuel simulators used in the previous series[5] of low-heating-rate tests to investigate the effect of shroud heating on deformation while minimizing the influence of the simulator. As with many of our previous tests, 12 external bare-wire thermocouples (four equally spaced around the tube at each of three axial locations) were attached at positions of interest as shown on the pretest IR characterization scan of the fuel simulator (Fig. 2.71). The axial distribution of the circumferential elongation is also plotted in the figure, with the burst location being noted slightly to the right of the lower strain peak.

Although the initial pressure was adjusted to cause failure after 50 to 150 s of creep at constant temperature, the failure occurred about 36 s after these conditions were realized. The premature failure was caused by a defect introduced by attaching a thermocouple. A photograph of the burst is shown in Fig. 2.72, with thermocouple identifications. Also evident is a potential defect adjacent to TE-206. Such defects are more serious in large deformation tests since the ratio of defected wall thickness to total wall thickness is much greater; consequently, the relative tube strength is reduced during the latter stages of deformation.

The heated shroud was effective in reducing the fuel pin simulator losses during the period of constant temperature operation. As a result, the automatic controller reduced the fuel simulator power to only about 5 W/m, much below the range of interest for simulating decay heat levels in a LOCA. This condition was conducive to equilibration of the temperature distribution and enhancement of deformation. Figure 2.73 is a plot of the temperatures measured at the burst elevation during the test. The burst temperature (787°C) was indicated by TE-210, the thermocouple which

was located adjacent to the burst and whose trace is plotted in the figure. Thermocouple TE-209 was inoperative during the test, as shown by its trace in the figure. The maximum temperature difference measured at this elevation at the time of failure was 10.1°C. Similarly, maximum differences of 8.1 and 4.3°C were measured at the 19- and 69-cm elevations, respectively. Figure 2.74 shows temperatures measured at each of the three instrumented sections. The temperature at the highest elevation decreased slightly as the test progressed because of the cooling effect of the incoming steam (at the top of the heated zone) with essentially zero power in the fuel simulator during the constant temperature portion of the test.

Test SR-57 was assembled with one of the fuel simulators fabricated at ORNL, having a very uniform axial heat generation profile to investigate the effect of this parameter with a heated shroud. Thermocouples were attached to provide azimuthal and axial temperatures at locations indicated on the pretest IR characterization scan of the fuel simulator in Fig. 2.75. The figure also shows that deformation in the test was large and highly localized, suggesting very uniform temperatures over the lower portion of the tube.

Figure 2.76 shows very small azimuthal gradients at the 24-cm elevation during the 45-s ramp and the ~70 s of constant temperature operation. Similar information was obtained at the 12-cm elevation. Temperatures measured at the four upper instrumented locations are shown in Fig. 2.77. As the figure shows, axial gradients developed during the test and became pronounced during the time creep was occurring. As with most of the other heated shroud creep tests, the fuel simulator power required to maintain constant temperature at the control thermocouples was extremely low (~5 W/m) during this phase. As a result, the incoming steam cooled the upper portion of the tube but had negligible effect on the lower portion, as shown in the axial temperature distributions plotted in Fig. 2.78. In particular, the three curves at the top of the figure show how the distribution became extremely skewed during the time creep was taking place. The burst temperature (779°C), which was obtained from TE-211, and burst location are noted on the distribution existing at the time of burst.

Since SR-56 failed prematurely, SR-58 was assembled with the same fuel simulator and tested under conditions approximating those used in

SR-56. The test was marked by several unusual occurrences of particular interest.

Thermocouples were located at the same relative positions as in SR-56, namely four thermocouples equally spaced around the tube at three axial locations as indicated on the pretest IR characterization scan of the fuel simulator in Fig. 2.79. The figure also shows extreme localization of the strain centered about the lower instrumented section. The burst strain (137%) was the greatest we have observed in any of our tests. As with SR-56, the failure occurred at one of the thermocouples, as shown in Fig. 2.80. In fact, two failures occurred simultaneously, as shown more clearly in Fig. 2.81. Comments noted earlier about the depth of the thermocouple weld-affected zone relative to total wall thickness are even more appropriate in this large deformation test. Assuming constant cross-sectional area, the calculated wall thickness for 137% strain is only 0.250 mm, which can be compared with the original nominal thickness of 0.635 mm. Even though the deformation was large, presumably it would have been larger if the thermocouple spot welds had not initiated the failure. Figures 2.80 and 2.81 show the thermocouples located at the position of maximum deformation, and there is no evidence that their presence caused localized cooling of the tube. If this were true, local flat spots should be visible in the profiles of the very symmetrically ballooned regions. Temperatures measured at this axial position were very uniform and increased near the end of the test.

Malfunctioning of a component at the interface between the automatic controller and the shroud power supply caused the unusual behavior illustrated in Fig. 2.82, which depicts the rod and shroud average temperatures and simulator pressure (channels 62, 63, and 55, respectively), as well as steam inlet and outlet temperatures (TE-102 and TE-103, respectively). As the plot shows, the shroud average temperature cycled above and below the rod average during the ~135 s of near-constant temperature operation. The steam outlet temperature also cycled with the shroud average but about 7 to 8 s out of phase. Fuel simulator (channels 58 and 59) and shroud (channels 60 and 61) power parameters, plotted in Fig. 2.83, show the cyclic behavior with the shroud power lagging slightly behind the simulator

power. Near-constant power operation was achieved during the last 20 to 22 s of the test, with the simulator power being less than about 2 W/m.

Figure 2.84 shows the temperatures measured on the shroud during the test. These thermocouples (0.25 mm diam, type S, bare wire) were welded on the outside surface of the 0.79-mm-thick Inconel shroud at the 20-, 38-, and 56-cm elevations (TE-306, TE-304, and TE-302, respectively); all were at an azimuthal position of 300°. The figure shows negligible axial temperature gradients throughout the test and almost constant temperature during the last 20 to 22 s.

Temperatures measured around the tube at burst elevation, plotted in Fig. 2.85, show very small (2 to 3°C) azimuthal gradients during most of the test. However, gradients developed during the last 2 to 3 s are shown more clearly by Fig. 2.86, an expanded-scale plot of the data for about 5 s preceding the failure. Locations of the thermocouples from which the data were obtained are noted in the figure. The burst occurred at one of the wires of TE-203 (Fig. 2.80). This particular thermocouple and the others to a lesser extent indicated a significant temperature increase even though the simulator power was only 1 to 2 W/m during this time.

Temperatures measured on the outside surface of the ohmic-heated shroud are shown in the figure for comparison. Heat losses from the outside of the shroud (see Fig. 2.2 for physical arrangement) and the method of heating probably caused a small radial gradient in the shroud, and the temperature on the inside surface was somewhat higher than plotted in the figure.

Temperatures measured along the tube (see Fig. 2.79 for elevations) at the 30° azimuthal position are plotted in Fig. 2.87. The behavior of TE-210 is of particular interest in that it does not show an increase during the last few seconds, even though it was located just 5 cm directly above TE-206. Also, azimuthal gradients at the elevation of TE-210 were very small (2 to 3°C) throughout the test. Since the temperature of the shroud at this elevation was essentially the same as measured at the burst elevation, these observations appear to eliminate heat transfer from the shroud as being responsible for the significant increase indicated by the simulator thermocouples. The very symmetrical (and large) ballooning and the increase observed on all four thermocouples at the burst elevation

also seem to cast doubt that the increase was caused by texture effects usually observed in high alpha temperature tests. The time range over which the increase occurred appears too long for rapid deformation effects on the tube and/or thermocouples to be the cause.

Test SR-63 was assembled with the fuel simulator from SR-58 and tested with the same conditions except for increased convective cooling, as indicated in Tables 2.1 and 2.2. The flow was about a factor of 7 greater, (inlet Reynolds number of 5025 vs 725). The thermocouples were located to obtain both axial and azimuthal temperature gradients, since it was anticipated that strong gradients would be introduced by the better convective cooling. Locations of the thermocouples are indicated on the pretest IR characterization scan of the fuel simulator in Fig. 2.88. The figure also shows that the deformation was highly localized at the lower end of the heated zone. A photograph of the burst is shown in Fig. 2.89 with the remains of some of the thermocouples in place.

Figure 2.90 depicts the rod (channel 62) and shroud (channel 63) average temperatures and the rod (channel 64) and shroud (channel 65) power levels. The rod average temperature was the average of the eight thermocouples at the lower two instrumented locations. This average and the shroud average remained constant for about 98 s during which creep occurred. The power levels also remained constant during this period. Evidently the increased convective cooling was sufficient to require a power level of about 0.3 kW/m in the fuel simulator. The steam inlet (TE-102) and outlet (TE-103) temperatures are compared with the rod and shroud averages in Fig. 2.91. The outlet steam increased slightly during the constant temperature portion of the test.

Figure 2.92 depicts the temperatures measured at the burst elevation. The burst temperature (760°C) was indicated by TE-206, which was located adjacent to the burst (Fig. 2.89). Temperatures measured by the four upper thermocouples are plotted in Fig. 2.93. The figure shows development of a strong axial temperature gradient as the test progressed. This is shown perhaps somewhat better in Fig. 2.94. As this plot shows, the cooling effect of the steam concentrated the high-temperature zone near the

exit end, resulting in highly localized deformation (Fig. 2.88). Deformation in this test was considerably less than in SR-58, presumably the result of the more pronounced temperature gradients.

2.3 Overview of Single-Rod Tests

R. H. Chapman

The previous section discussed 18 tests performed under a variety of conditions to investigate the effects of heating rate, convective cooling, shroud heating, and uniformity of fuel simulator axial heat generation. All the tests were conducted in the new test facility (Fig. 2.2), which includes separate power supplies for independent heating of the shroud and fuel pin simulator. An integrated control system provides automatic control of the power supplies to maintain programmed temperature histories during the test. Pertinent test conditions and results are summarized in Tables 2.1 and 2.2. Some of the tests were performed with one of the two fuel simulators used in an earlier series[5] of tests conducted in the previous test facility (Fig. 2.1) without shroud heating. Since the test facility did not have automatic control capability at that time, those tests were conducted under essentially constant power conditions. As a result, heating rate varied, depending on losses during the tests. Comparison of the results reported herein with those reported[5] for the previous series can provide considerable insight to the deformation behavior under a range of test conditions.

As noted in Table 2.1 and in the previous discussion of the tests, a number of the tests are considered invalid for establishing deformation limits that might be anticipated in reactor accidents. Some of the tests were invalidated because of premature failures resulting from defects introduced in spot welding thermocouples to the tubes. Others, primarily the isothermal creep-rupture tests, were invalidated because the fuel simulator power during deformation (essentially zero) was considerably below that due to decay heat in the time frame of interest in a LOCA.

As might be expected, one effect of shroud heating is to reduce the fuel simulator power required to maintain a specified cladding heating

rate. This is shown in Fig. 2.95, which compares power requirements at 700°C for heated and unheated shroud tests. For all practical purposes, the heated shroud curve represents the power input required to increase the cladding temperature at a given rate in the absence of external losses and is independent (except for simulator physical property changes) of temperature level. Since the losses are dependent on cladding temperature, the unheated shroud curve is one of a family of curves: this particular one is for 700°C, representing the power input required to increase simulator stored energy and to compensate for losses as a function of heating rate. The difference between the two curves represents the power required to compensate for external losses, and for the range of conditions covered in our single-rod tests, this is equivalent to about 1.3 kW/m when the cladding is at 700°C. A calculated zero-loss performance curve for a TMI-2 fuel rod is shown for comparison with experimental results for the fuel pin simulator used in our tests.

These data show that a major portion of the input power is required to increase the stored energy of the test assembly at the highest heating rate used in these tests. As the heating rate is decreased, the fraction of the input power required for increasing the stored energy is decreased, and the fraction that appears as losses is increased. In the limit, for isothermal transients, all the power goes to losses and none to increasing the stored energy. This explains why in all except two of the heated shroud isothermal creep-rupture tests, the input power required to compensate for fuel pin simulator losses was in the range of 1 to 5 W/m. The two exceptions involved unusual test conditions, one case (SR-63) with increased convective cooling and very large axial temperature gradients and one case (SR-53) in which the shroud was 60°C less than the fuel pin simulator.

At one time it was thought that short-term (50- to 200-s) isothermal creep-rupture tests might be a convenient limiting case for the simulation of reactor accident conditions. However, based on the previous discussion, this no longer appears to be a valid test condition, and we do not plan to conduct further tests of this nature. Instead, we will adopt a heating rate of 1 K/s as a convenient lower limit for test purposes.

Another important comparison is shown in Fig. 2.95, and that is how well power requirements in single-rod heated shroud tests agree with average bundle power levels determined under comparable conditions in the three 4 × 4 bundle tests. Based on the good agreement evident in the figure, we conclude that single-rod heated shroud tests do model losses and thus induce temperature gradients representative of individual rods in 4 × 4 bundles.

The tests performed during the reporting period also provided an opportunity to compare strain results from heated shroud tests with those from bundle tests and burst temperatures with predicted values obtained from the correlation[8] developed from unheated shroud tests. In heated shroud tests, the temperature is more uniform, and there is an increased probability that the highest measured temperature is nearer the true burst temperature. Therefore, the experimental results will be higher than those predicted from the correlation. Figure 2.96 compares the results for each heating rate with a family of curves (for 0, 5, 10, and 28 K/s heating rates) calculated from the correlation. All the data from the previous series[5] and this series (including the invalid tests) are plotted in the graphs. Figure 2.96(a), for the 0 K/s tests, shows consistent results, except for SR-51, between the heated and unheated shroud tests. Figure 2.96(b), for the 5 K/s tests, exhibits the best agreement between unheated and heated shroud tests, although all the heated shroud results are underpredicted by 10 to 15°C. Figure 2.96(c), for the 10 K/s tests, indicates fair agreement for the burst pressures in the range of 9600 to 10,000 kPa. The one heated shroud test result at 4590 kPa burst pressure was underpredicted by about 45°C. Figure 2.96(d), for the 28 K/s tests, indicates that the correlation underpredicts the heated shroud results by 30 to 35°C at temperatures above 850°C. This may indicate the need to base the correlation on heated shroud data to improve its predictive capability.

Figure 2.97 compares the burst strain for the same data sets with the data[2] band obtained for unheated shroud tests at 28 K/s. The figures show that another effect of shroud heating is to increase the burst strain over that obtained in unheated shroud tests, with the greatest increase being

observed for the lowest heating rates. Very little increase was observed in the 28 K/s tests.

One goal of this test series was to compare deformation in single-rod heated shroud tests with that observed in bundle tests. Figure 2.98, from the previous progress report, shows the B-1 and B-3 bundle results (B-2 was essentially the same as B-1) in relationship to single-rod unheated shroud test data. Comparison of Fig. 2.97(c) with this figure shows that the single-rod heated shroud test results are about midrange of the B-3 bundle. Similarly, Fig. 2.97(d) shows that the single-rod heated shroud results tend to be in the lower range of the B-1 values.

Burst strain data are widely reported and used in assessing the effect of deformation on thermal-hydraulic performance, although it is a highly localized parameter. Average strain along the tube may be more important than burst strain in determining the flow resistance in a deformed bundle. Consequently, we routinely report the percentage volume increase of the tube over the heated length. This parameter can be used to calculate an average strain value or, perhaps, to generate bundle blockage using statistical techniques. Figure 2.99 compares this parameter for the two data sets with the data band derived from 28 K/s unheated shroud tests. Figure 2.100, also from the previous progress report, shows the relationship of this parameter for the three bundle tests to single-rod unheated shroud results. Comparison of Fig. 2.99(c) with this figure shows that single-rod heated shroud results are in agreement with the lower range of the B-3 data. A similar conclusion is evident by comparing Fig. 2.99(d) with the B-1 and B-2 results.

Plotting data in this manner tends to deemphasize highly localized deformation and reorders the data in some instances. However, the conclusion remains the same; that is, a heated shroud improves temperature uniformity and results in greater deformation than observed in unheated shroud tests, with the effect being more pronounced at the lowest heating rates. The effect was not particularly important in the 28 K/s tests.

Based on the results of this test series with a heated shroud, which produced deformation data consistent with the ranges observed in the three 4 x 4 bundle tests, we conclude that single rods tested in this way are

subjected to temperature conditions representative of those in multirod arrays. While burst and average (i.e., volume increase) strains are representative of rods in bundles, the potentially important effect of rod-to-rod interaction on deformation is omitted. Thermal-hydraulic conditions, such as convective cooling, play a major role in the axial distribution of deformation, and appropriate test conditions should be employed to produce reasonably uniform axial temperature distributions. We believe that single-rod heated shroud tests are desirable and appropriate for studying the effects of various parameters on deformation behavior.

This test series also showed that isothermal creep-rupture tests with a heated shroud can produce misleading results. The heated shroud essentially eliminated losses from the fuel pin simulator under the conditions tested and resulted in essentially zero power in the fuel simulator during deformation. Such conditions are not representative of decay heat levels in the time frame of interest in LOCAs, and we do not plan further tests under these conditions. We will instead adopt a heating rate of 1 K/s as the lower limit of interest in our test program.

2.4 Additional Bundle B-3 Results

D. O. Hobson*

Enlarged (~5×) photographs of the B-3 cross sections were examined in the same manner as reported[6] earlier for the B-1 and B-2 bundles to determine the variations in the direction of maximum tube wall thinning in each of the sections. The directions were identified and correlated according to the view sectors and nomenclature described by Figs. 2.19 through 2.21 of Ref. 6. Figure 2.101 shows the percentages of the total observations occurring in each of the eight sectors.

Briefly, 58% of the thinned areas of the type I rods (corner positions) were in the two sectors (1 and 3) facing the nearest neighbors, that is, the type II (side) rods. The side rods, in turn, thinned predominantly toward the four type III (center) rods with ~30% of the thinned

*Metals and Ceramics Division.

areas facing sector 3, the next nearest neighbor in the inner array. The center rods (type III) thinned preferentially toward the outer ring of rods (types I and II). Very few (~5%) of the thinned areas faced neighboring inner rod positions (sectors 4 and 6). These observations compare well with the burst directions in the B-3 test.

2.5 Digital Simulation of Bundle Tests

M. D. White L. J. Ott

Since MRBT experimental data have shown that both steam flow rate and bundle heating rate have an effect on the axial location of simulator bursts, a transient digital simulator was developed to facilitate establishment of steam conditions for future bundle tests. The digital simulator consists of a thermal-hydraulic computer program that models a fuel pin simulator in the various types of coolant channels present in a bundle test. The model was shown to closely approximate observed behavior in the previous bundle tests. Following this verification, the model was used to generate a number of typical operating curves that can be used in the future to aid selection of appropriate test conditions.

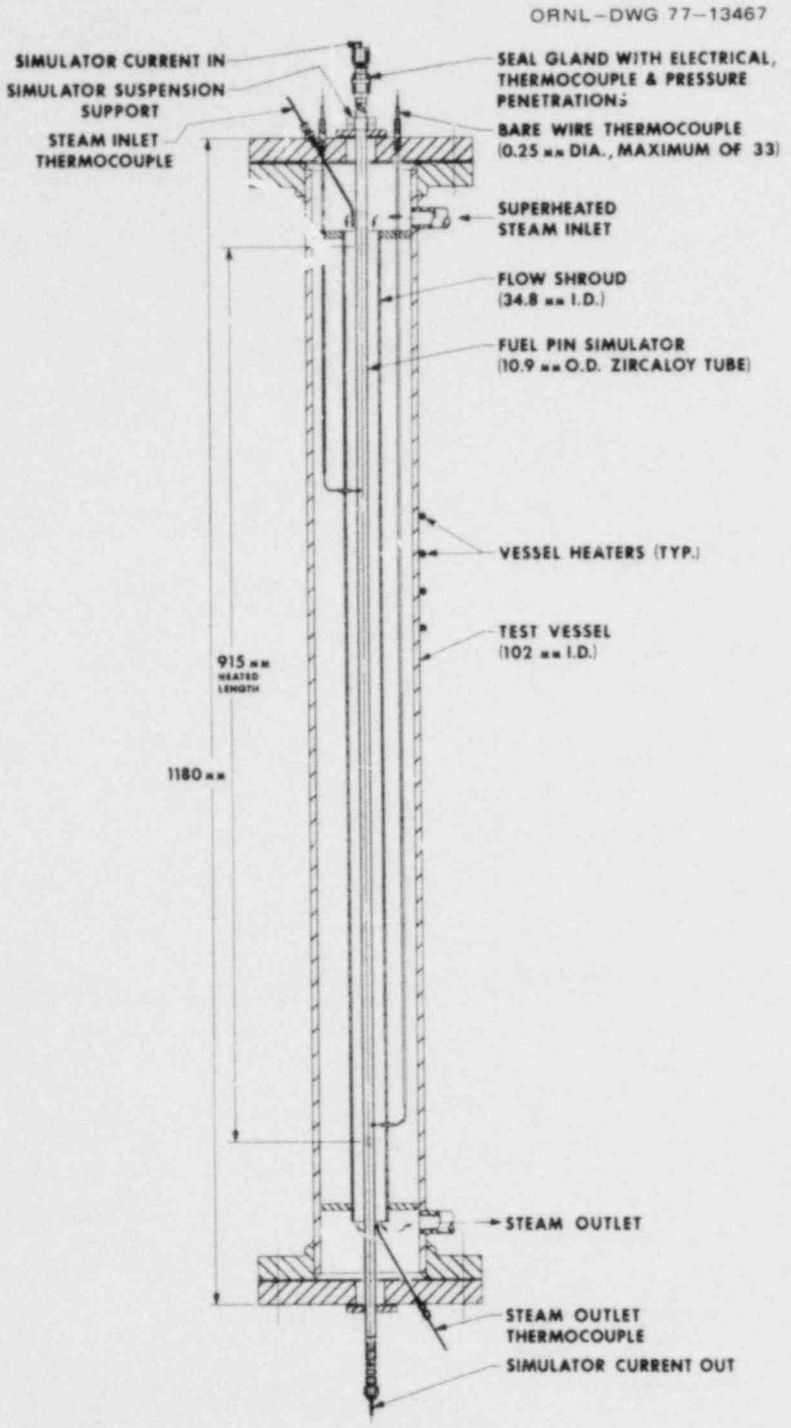

Fig. 2.1. Single-rod test assembly with unheated shroud.

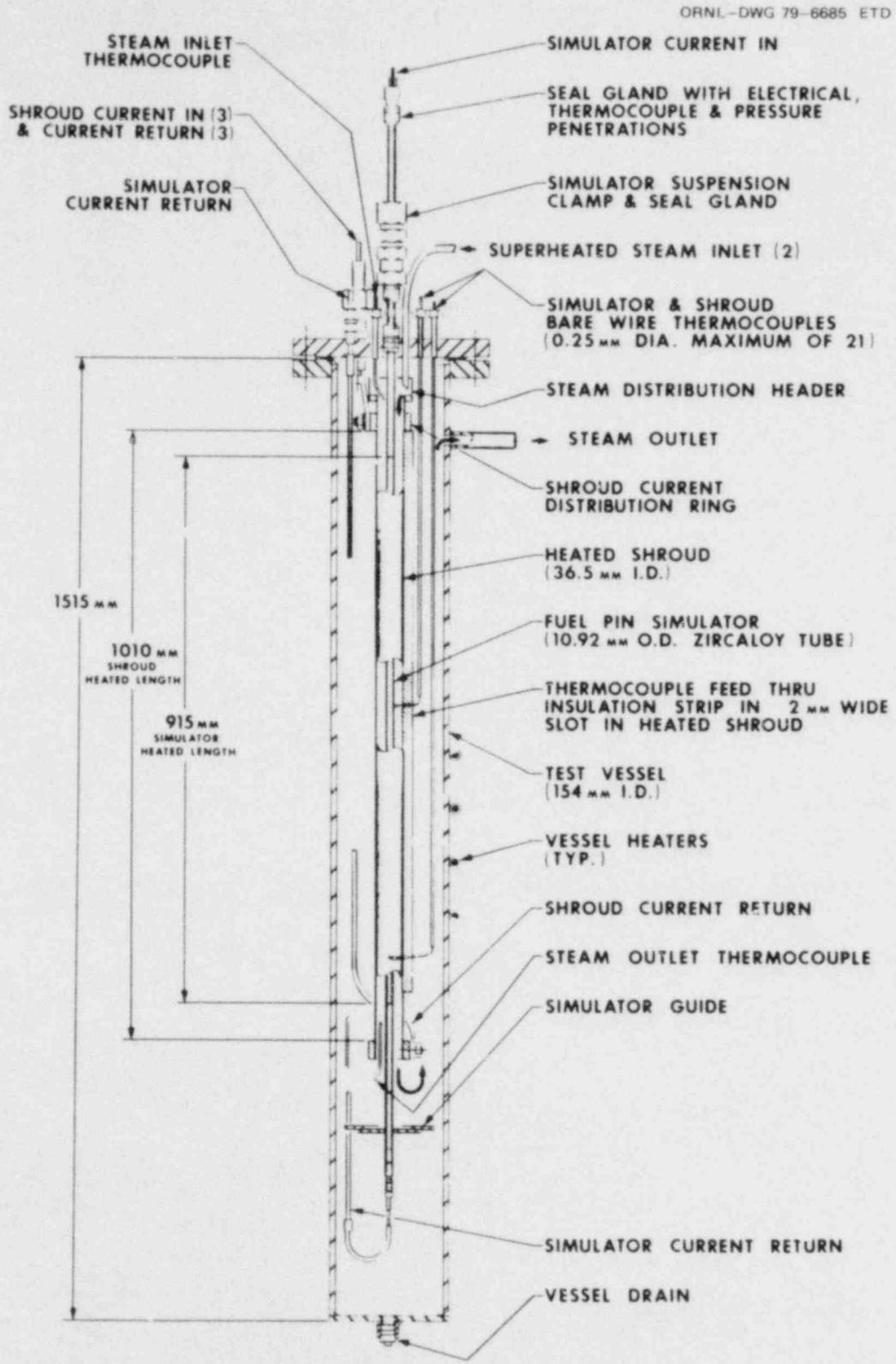

Fig. 2.2. Single-rod test assembly with heated shroud.

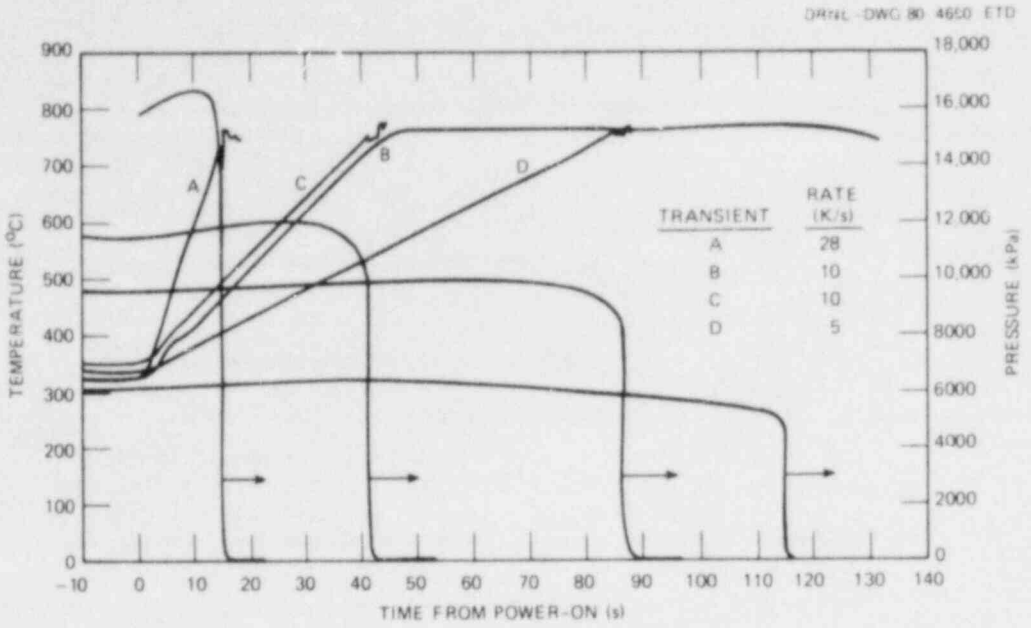

Fig. 2.3. Typical transients for low-heating-rate and creep-rupture single-rod burst tests with heated shroud.

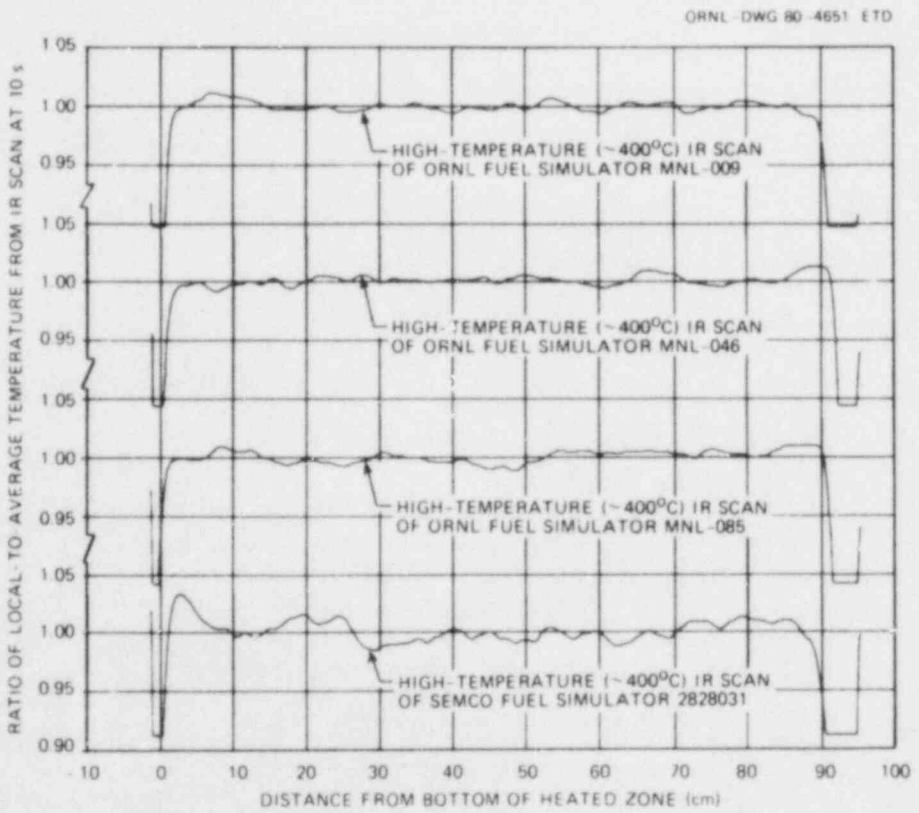

Fig. 2.4. Comparison of IR characterization scans of fuel simulators used in single-rod heated shroud tests.

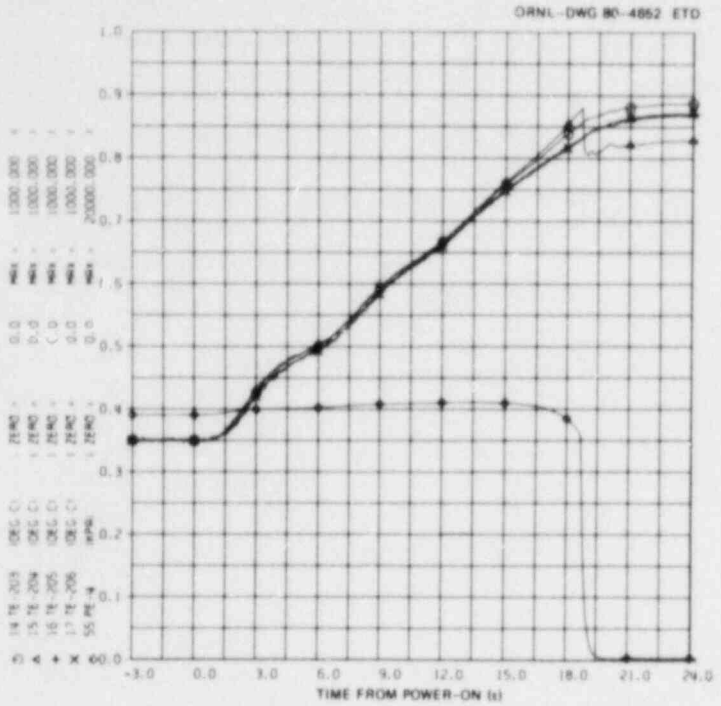

Fig. 2.5. Quick-look data plot for thermocouples near burst location in SR-60.

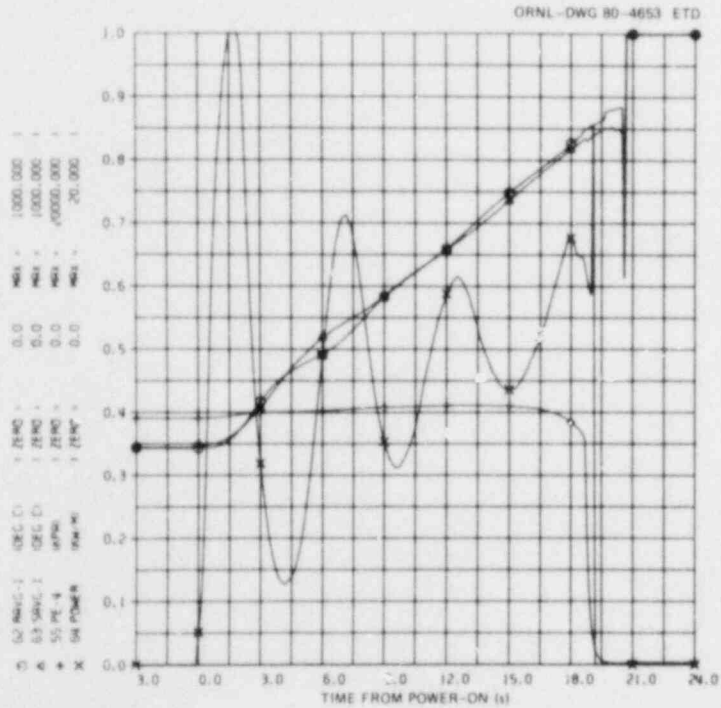

Fig. 2.6. Rod and shroud average temperatures, rod power, and pressure in SR-60.

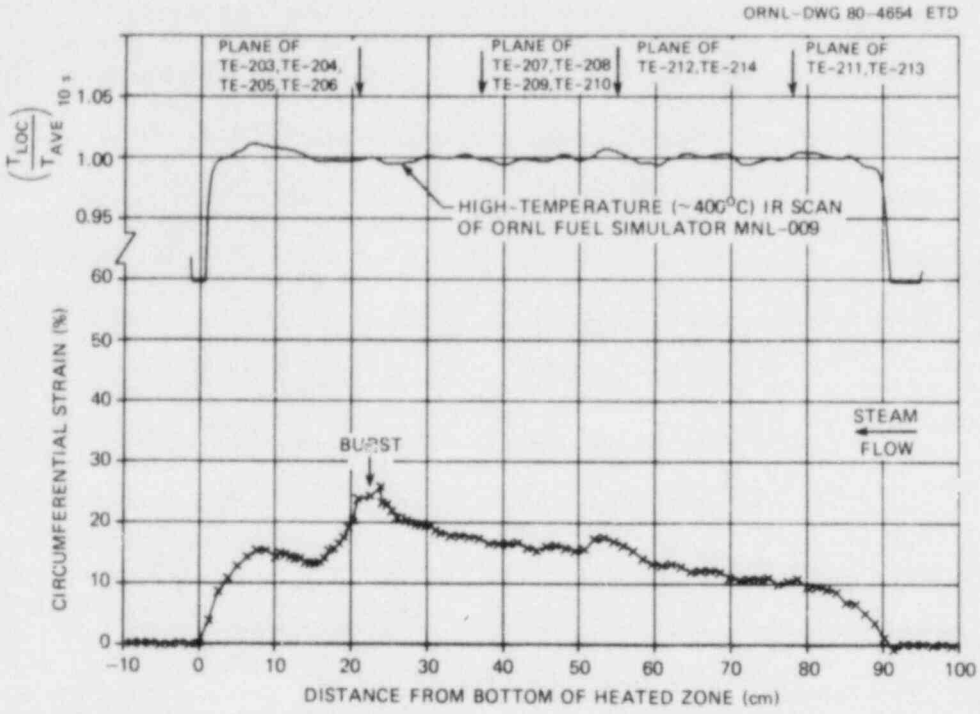

Fig. 2.7. Deformation profile of SR-60.

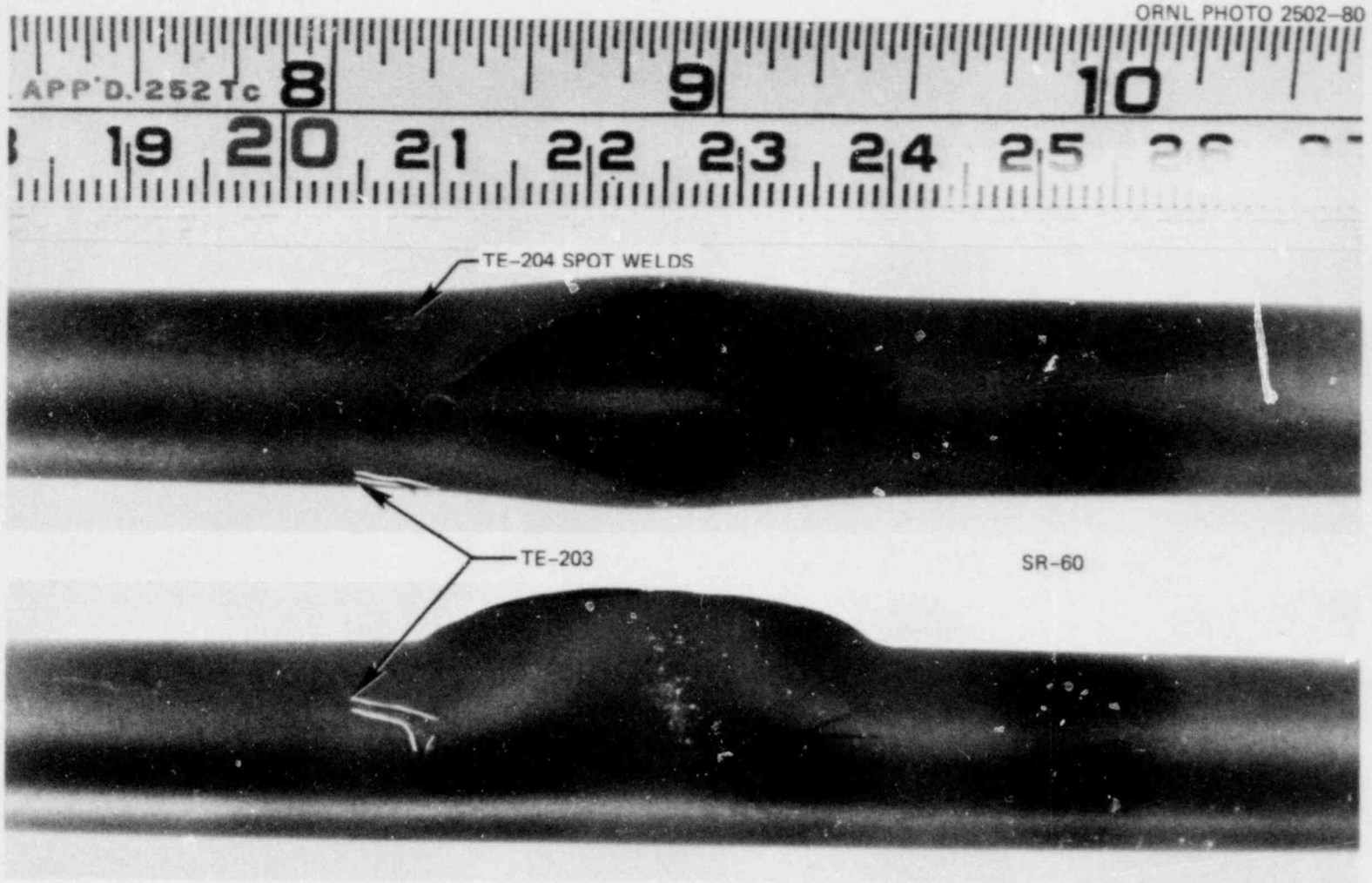

Fig. 2.8. Views of burst in SR-60 showing remains of thermocouples located very near the failure.

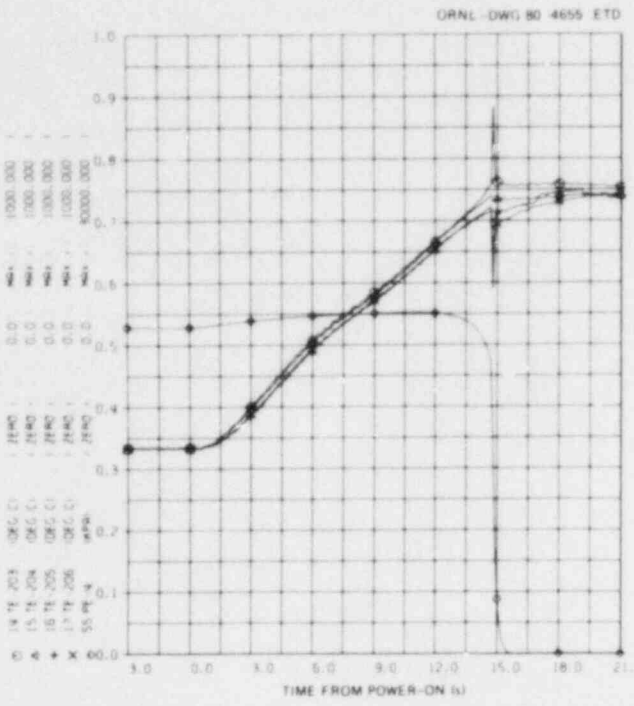

Fig. 2.9. Quick-look data plot for thermocouples near burst location in SR-61.

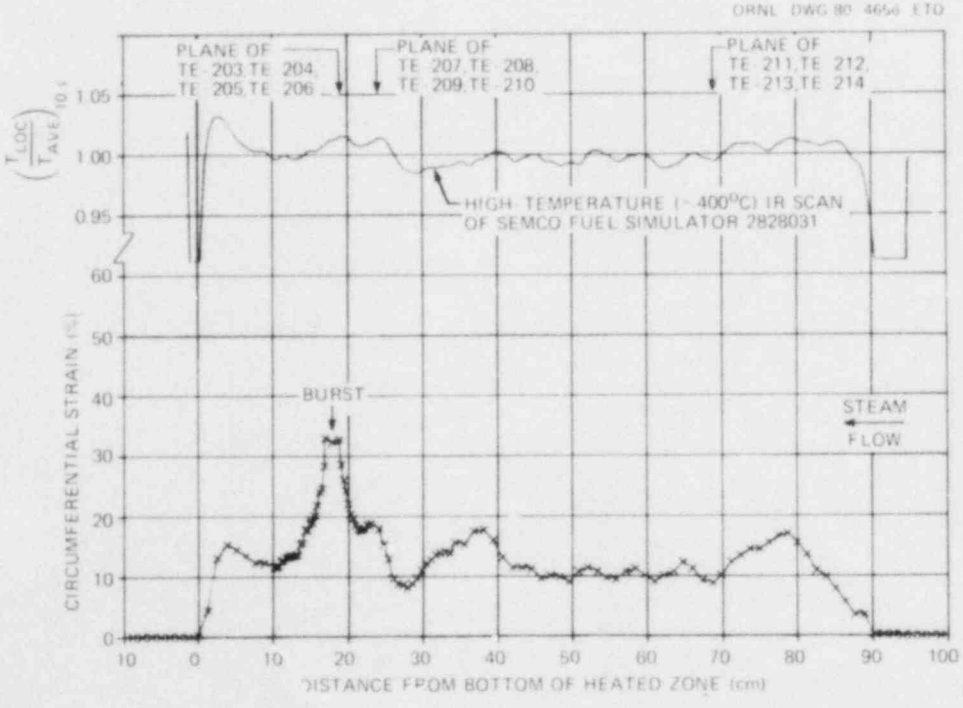

Fig. 2.10. Deformation profile of SR-61.

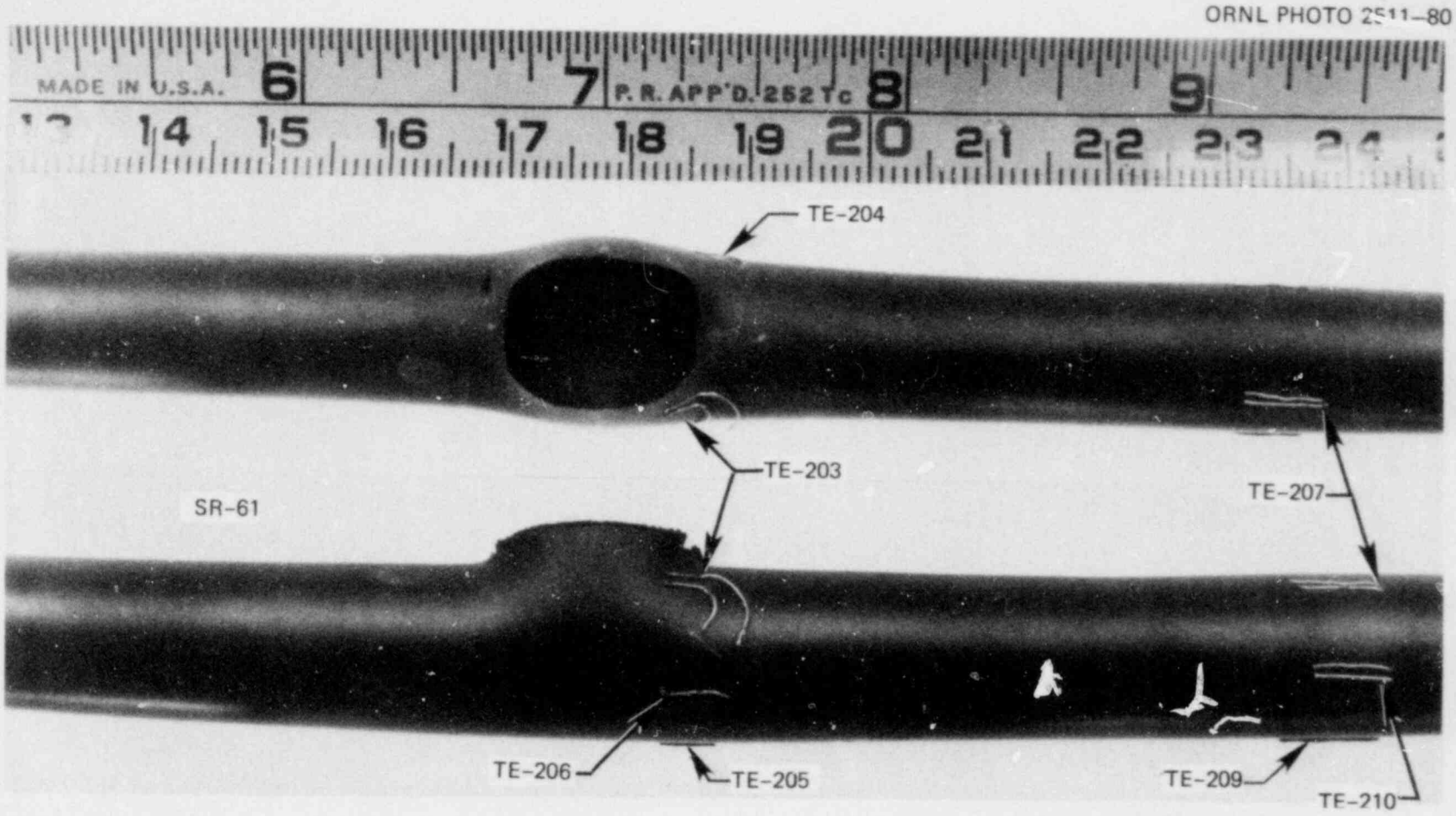

Fig. 2.11. Burst in SR-61 with thermocouple remains located near the failure.

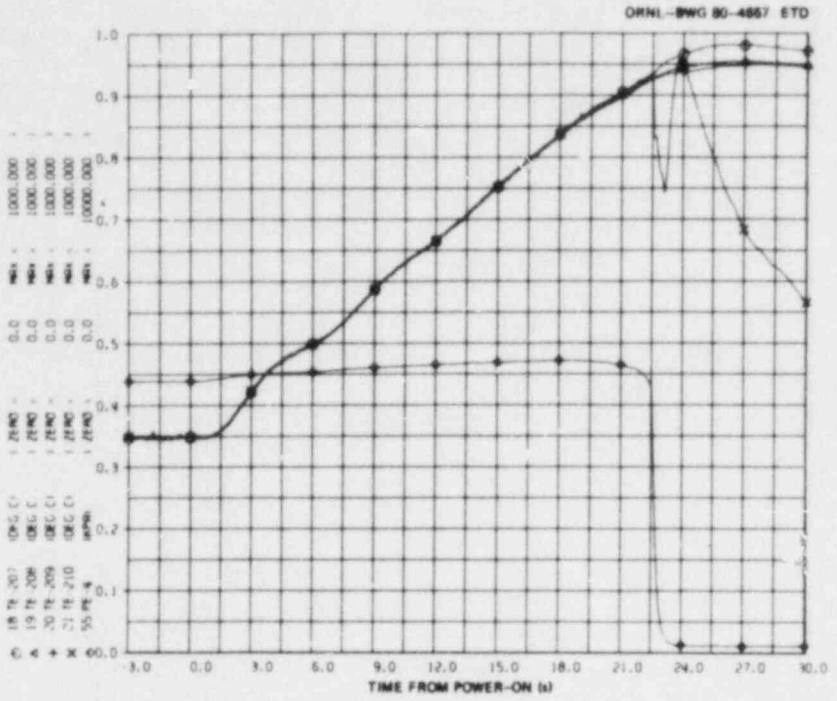

Fig. 2.12. Quick-look data for SR-62.

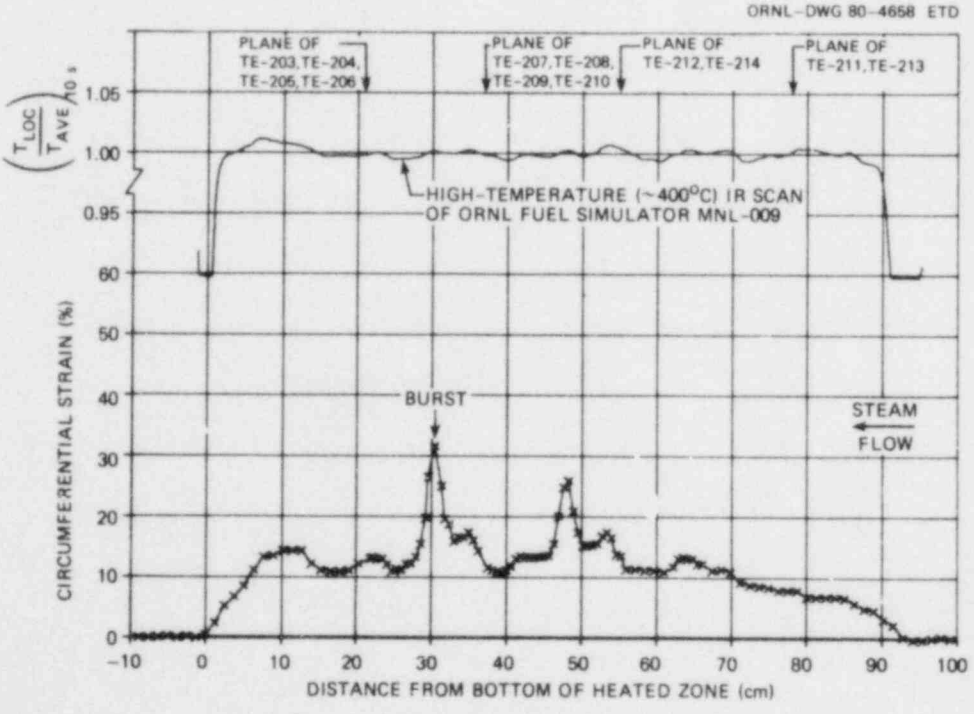

Fig. 2.13. Deformation profile of SR-62.

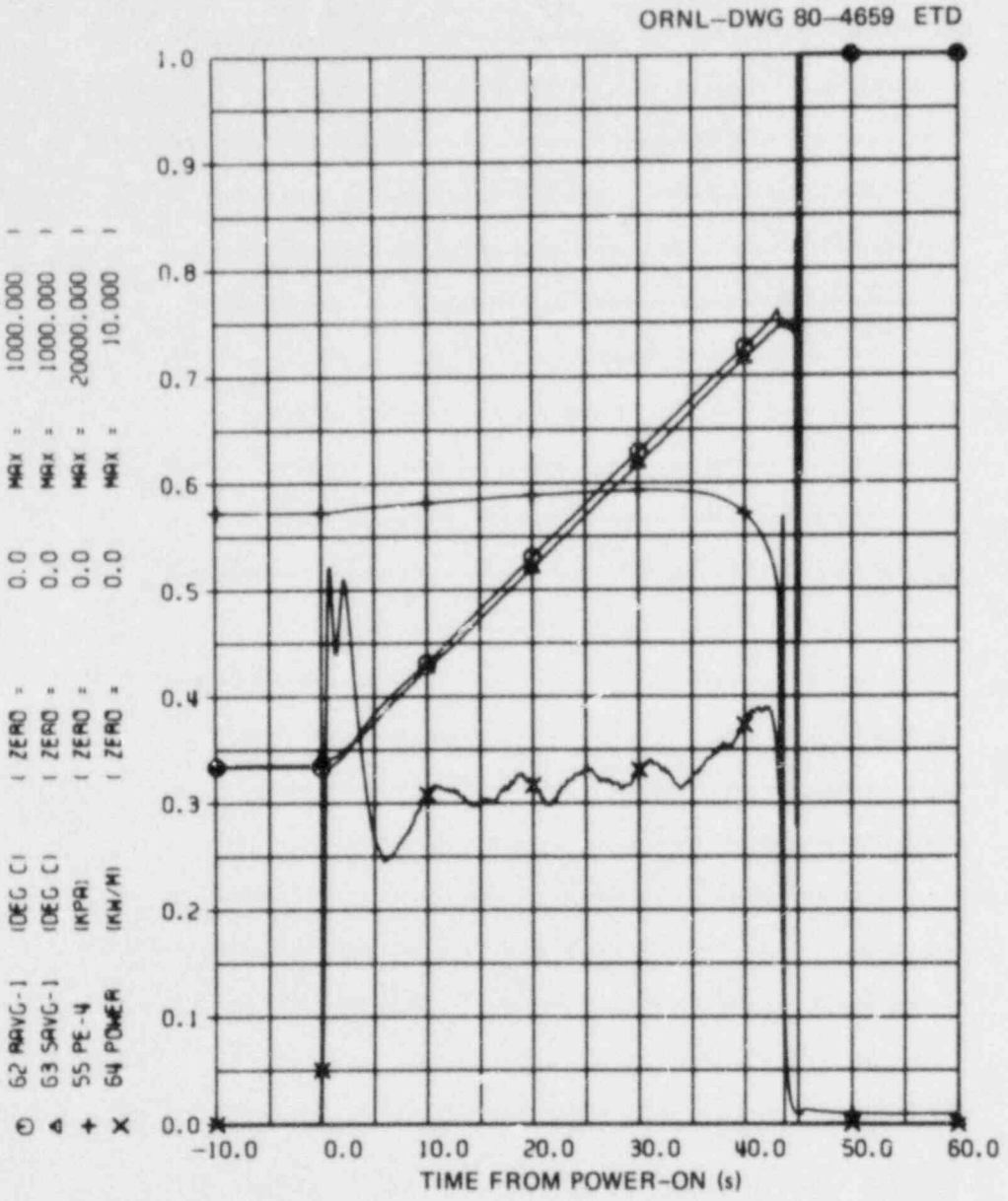

Fig. 2.14. Rod and shroud average temperatures and simulator pressure and power in SR-47.

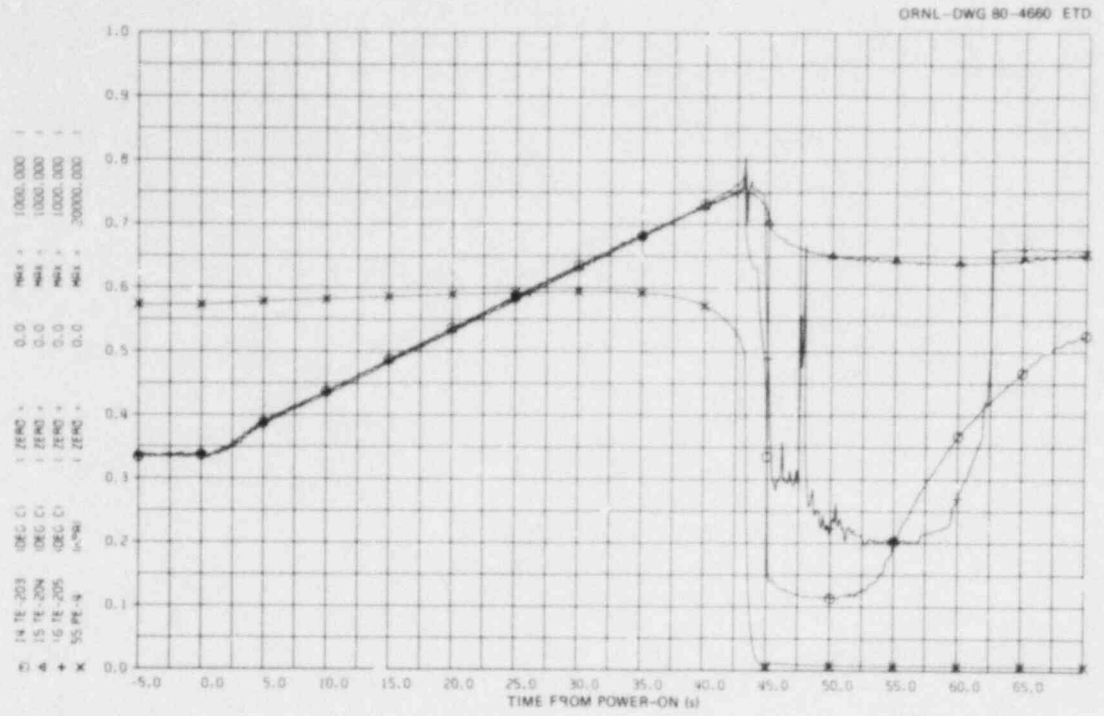

Fig. 2.15. Temperatures measured at 19-cm elevation in SR-47.

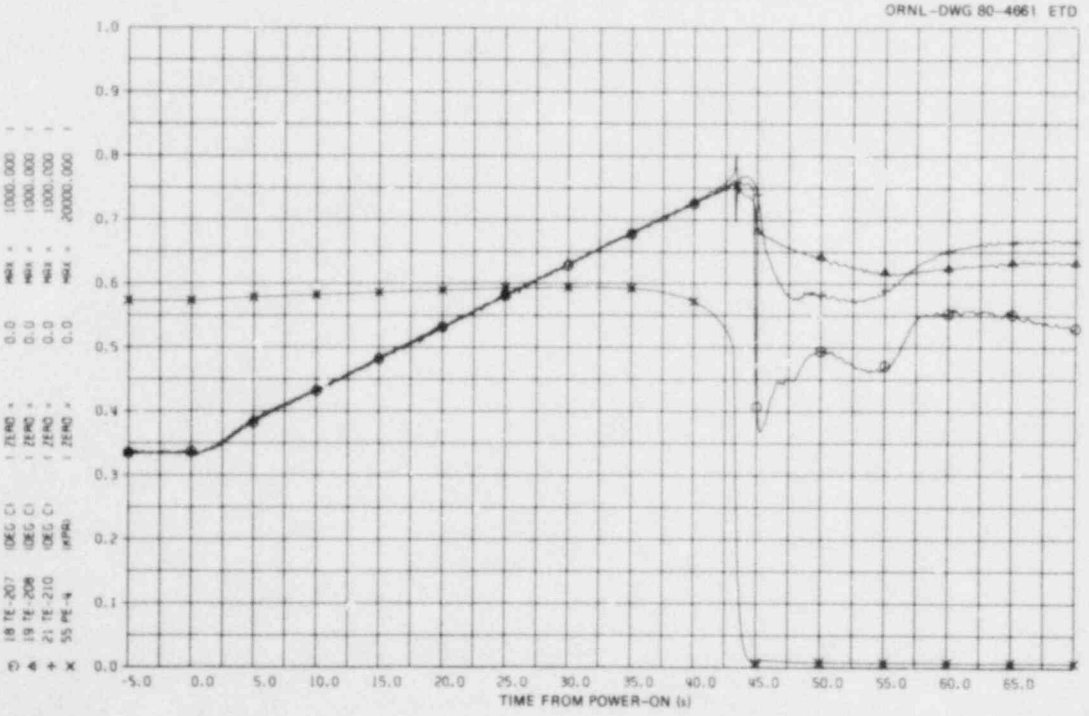

Fig. 2.16. Temperatures measured at 24-cm elevation in SR-47.

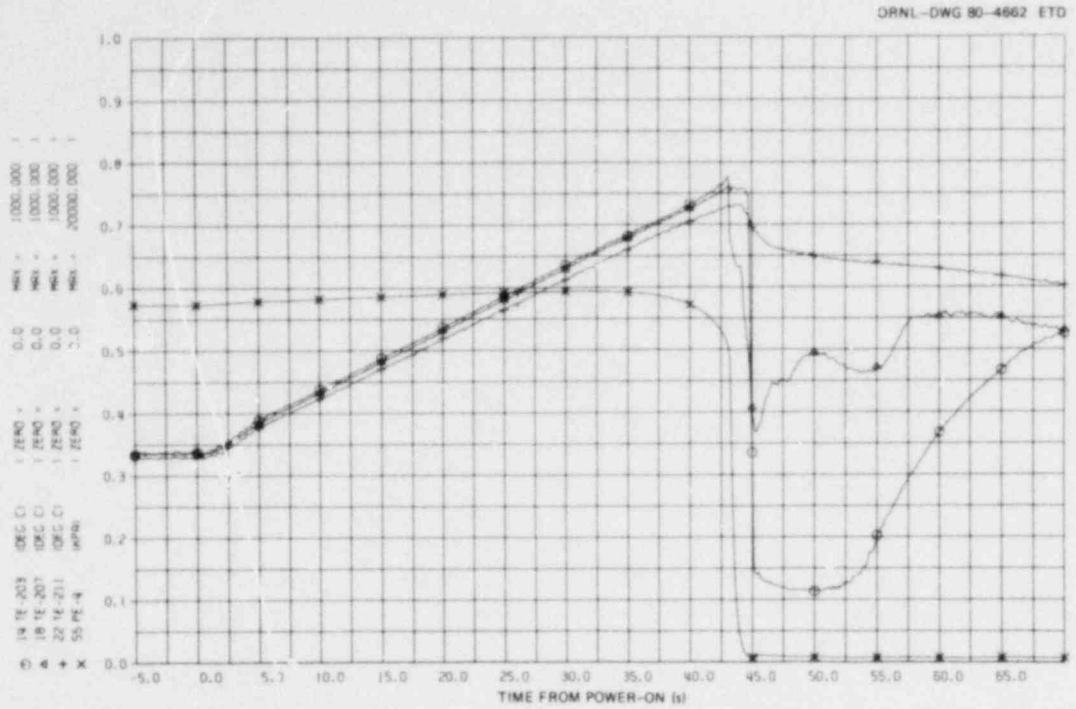

Fig. 2.17. Temperatures measured at the three instrumented elevations in SR-47.

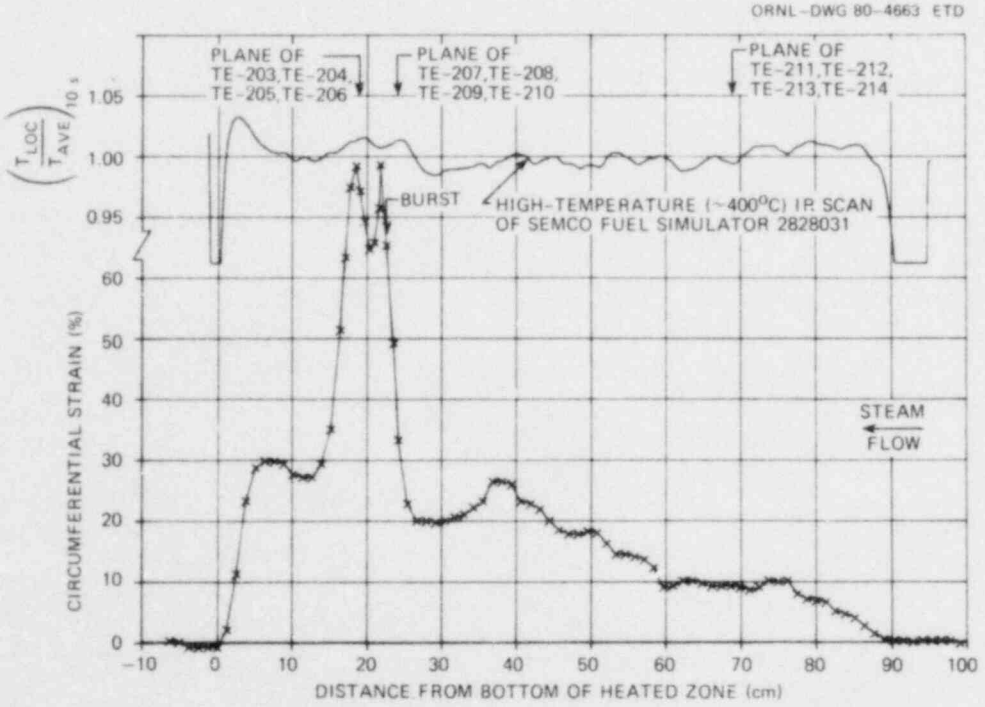

Fig. 2.18. Deformation profile of SR-47.

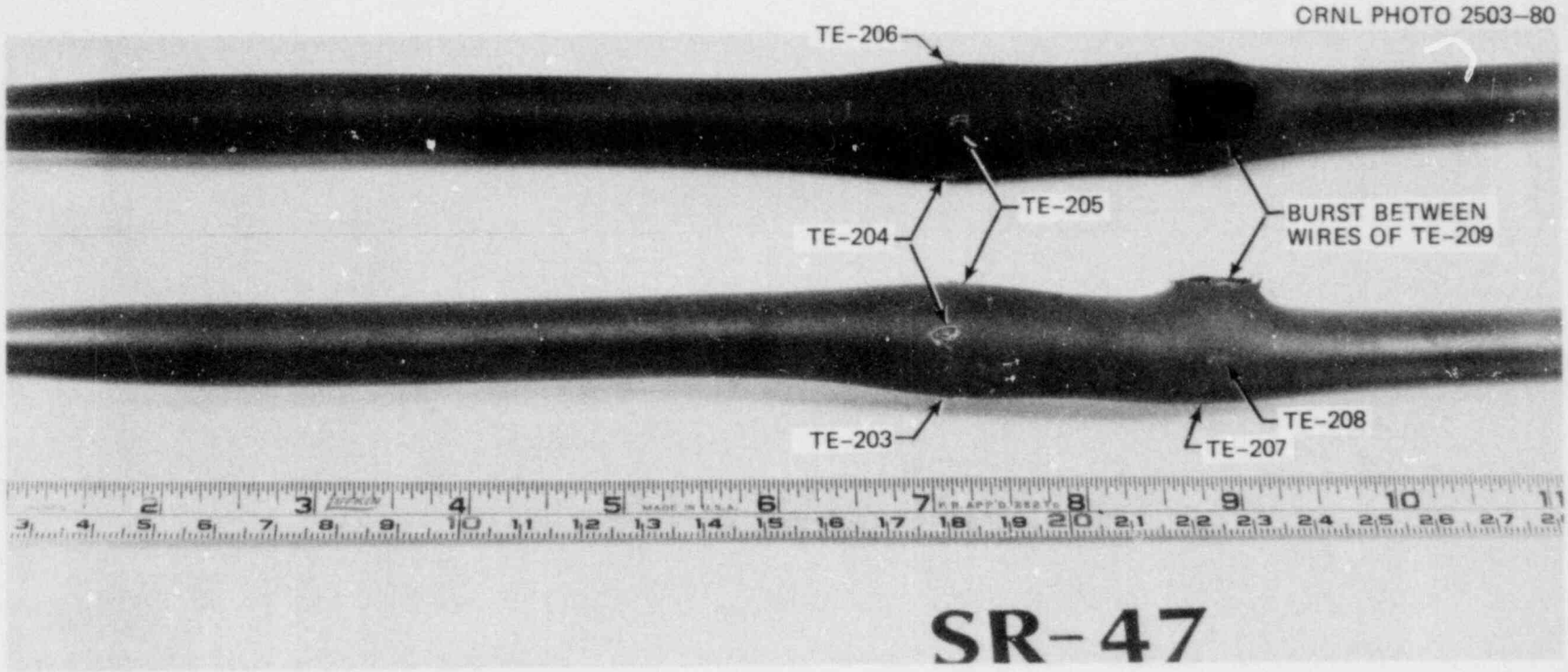

Fig. 2.19. Burst in SR-47 with remains of thermocouples in region of greatest deformation.

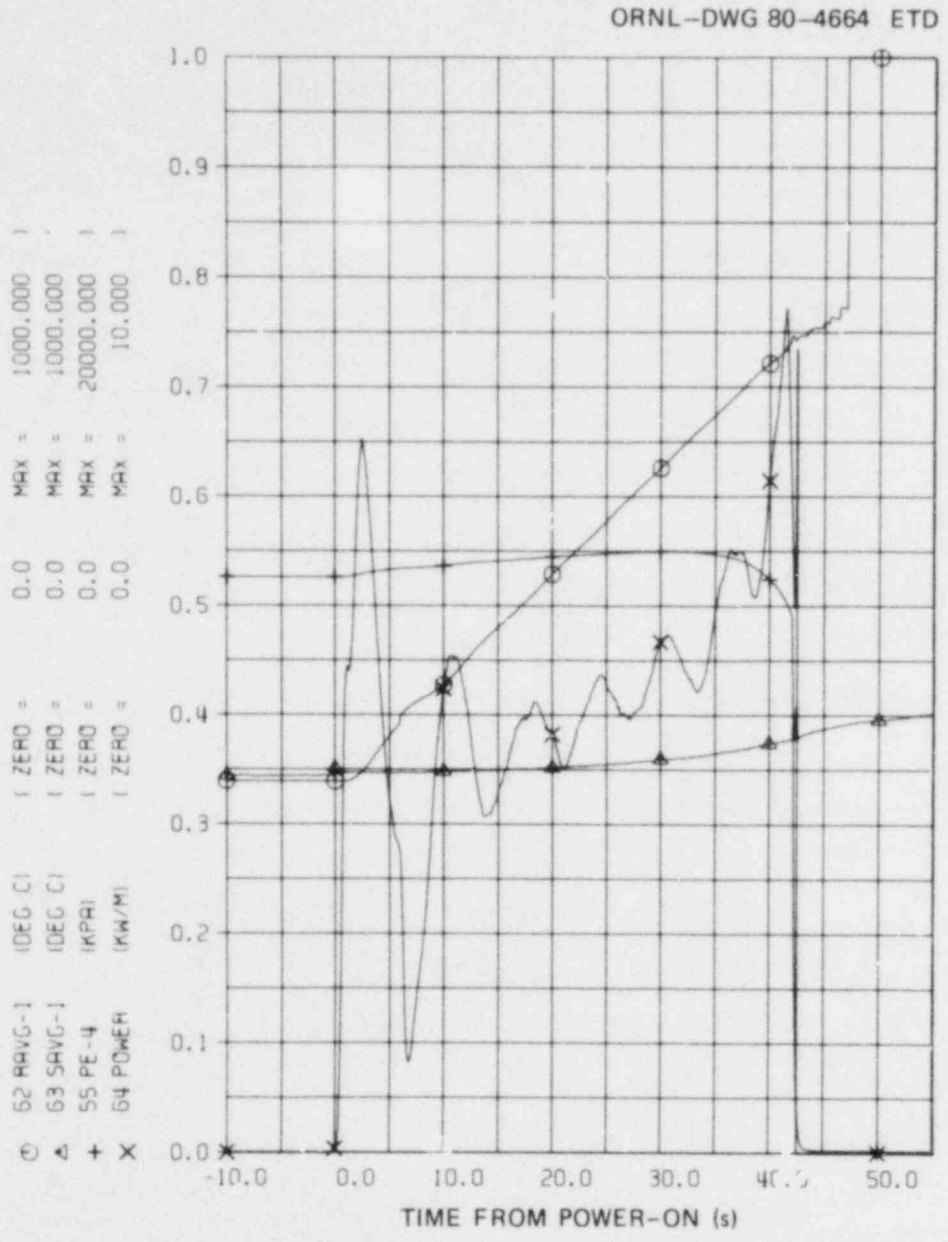

Fig. 2.20. Rod and shroud average temperatures and simulator pressure and power in SR-48.

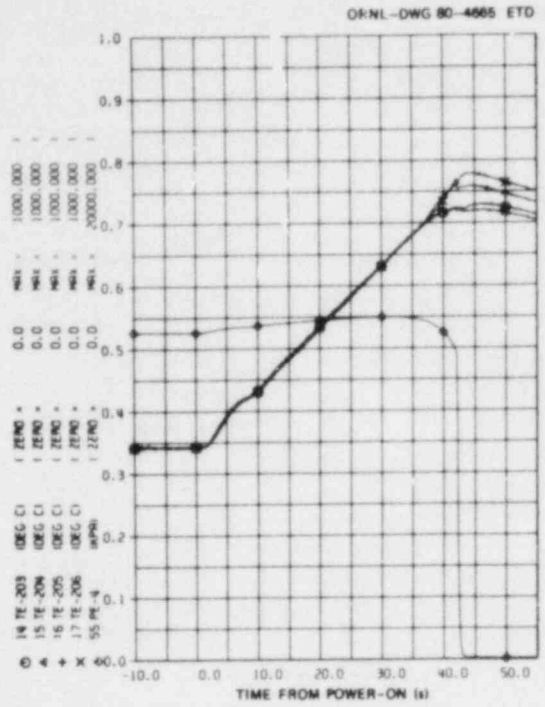

Fig. 2.21. Temperatures measured at lowest instrumented elevation in SR-48.

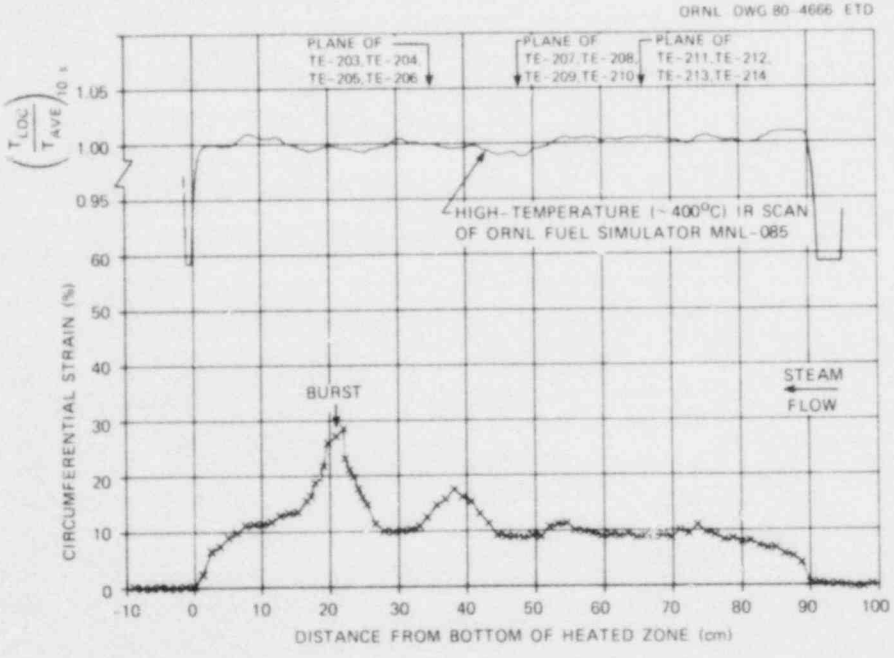

Fig. 2.22. Deformation profile of SR-48.

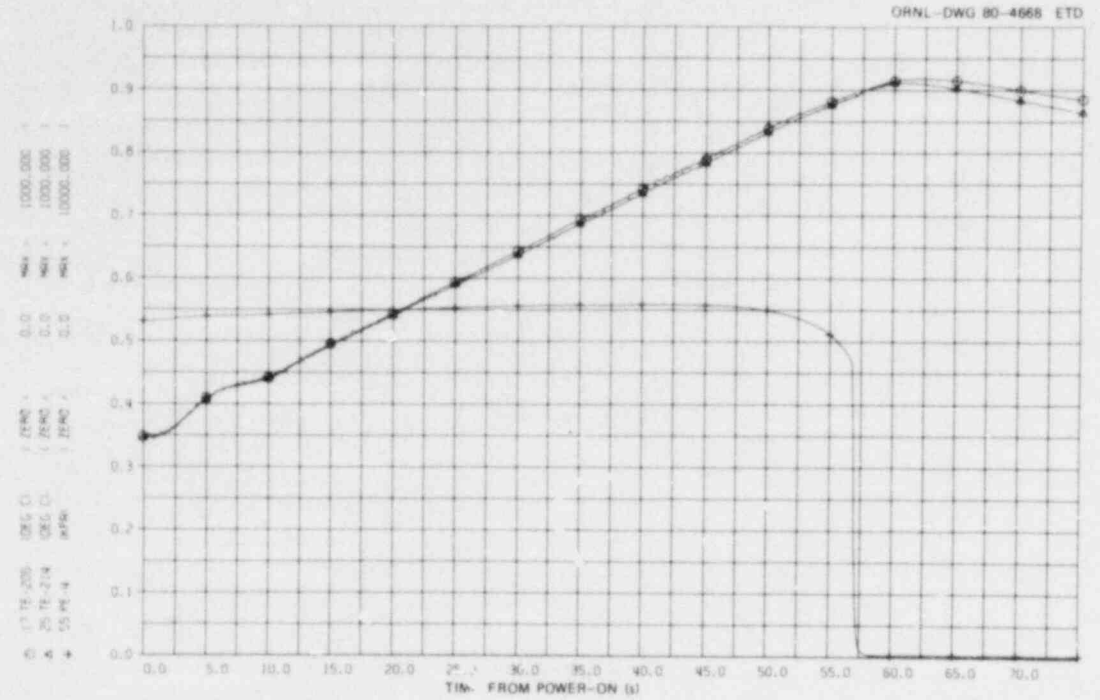

Fig. 2.23. Temperatures measured at 21- and 55-cm elevations in SR-50.

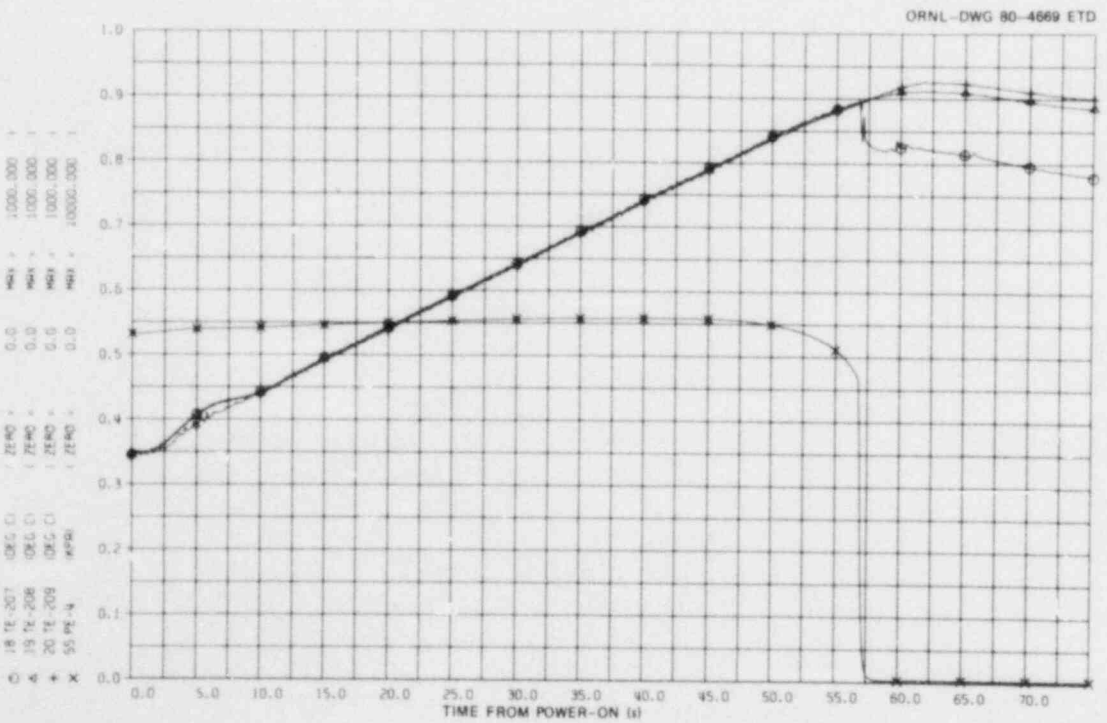

Fig. 2.24. Temperatures measured at 37-cm elevation in SR-50.

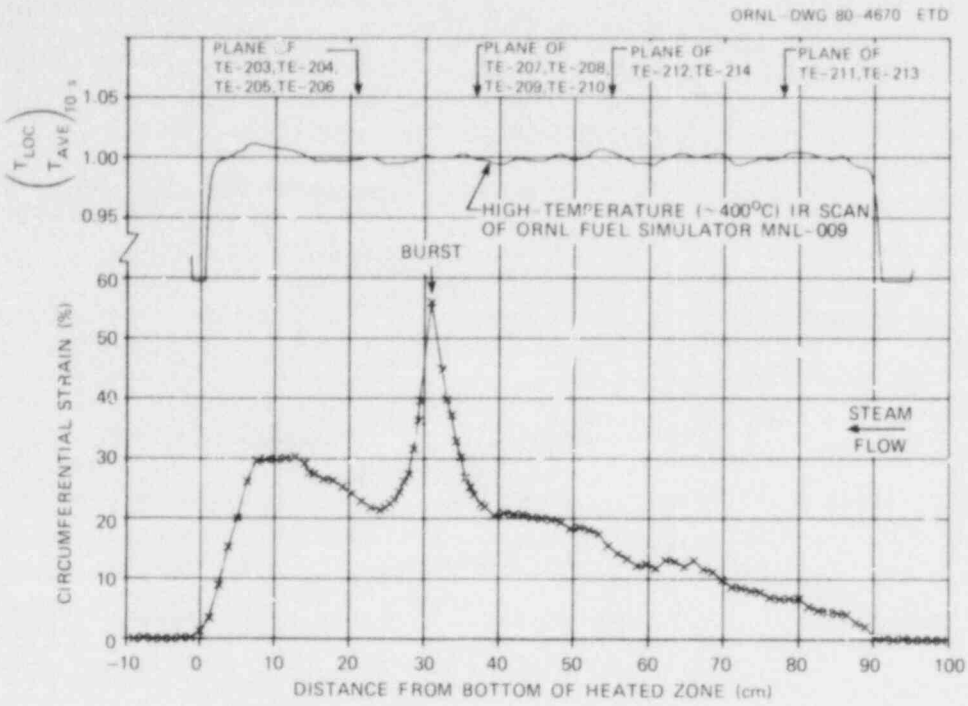

Fig. 2.25. Deformation profile of SR-50.

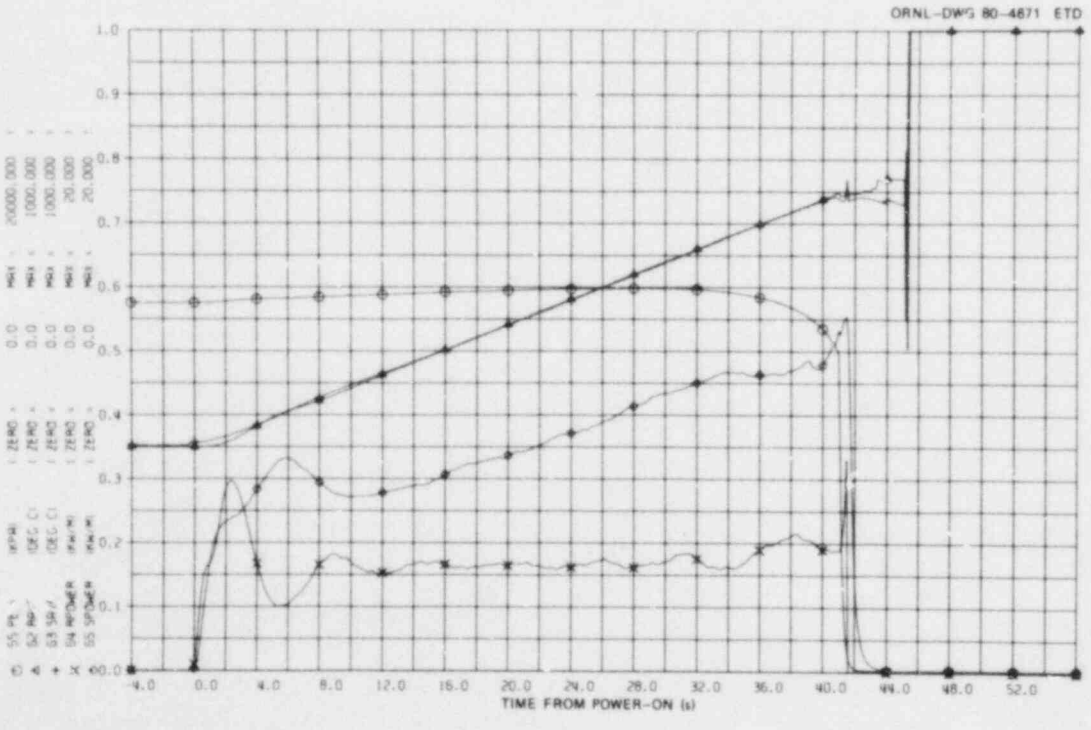

Fig. 2.26. Pressure, average temperatures, and power requirements in SR-52.

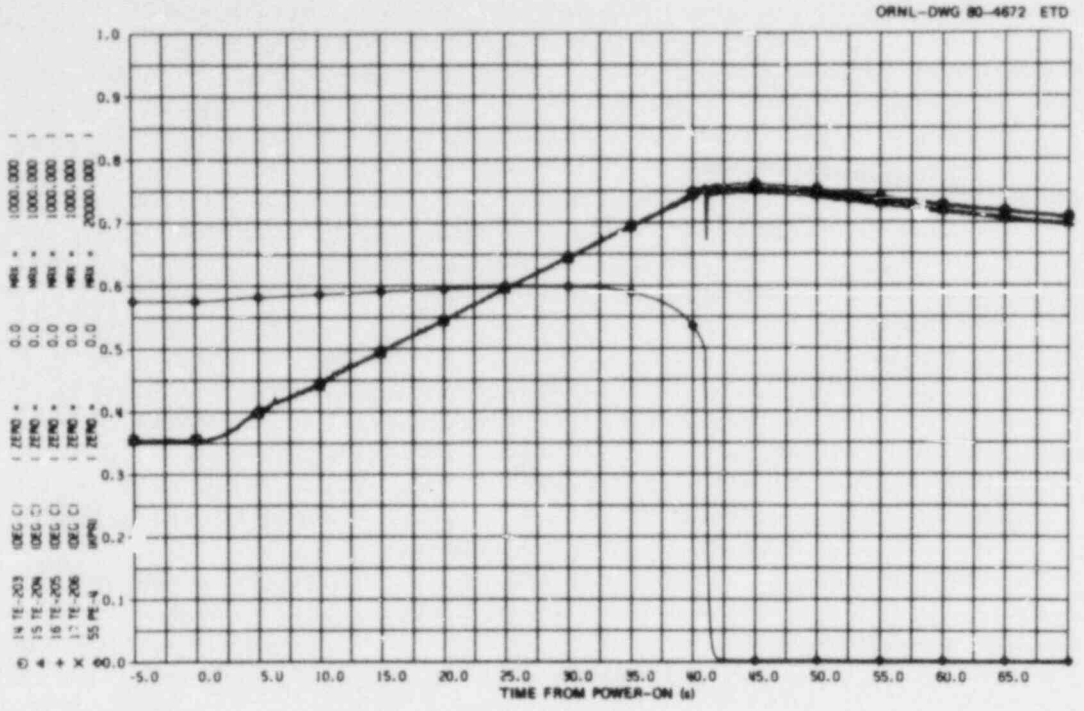

Fig. 2.27. Temperatures measured at 21-cm elevation in SR-52.

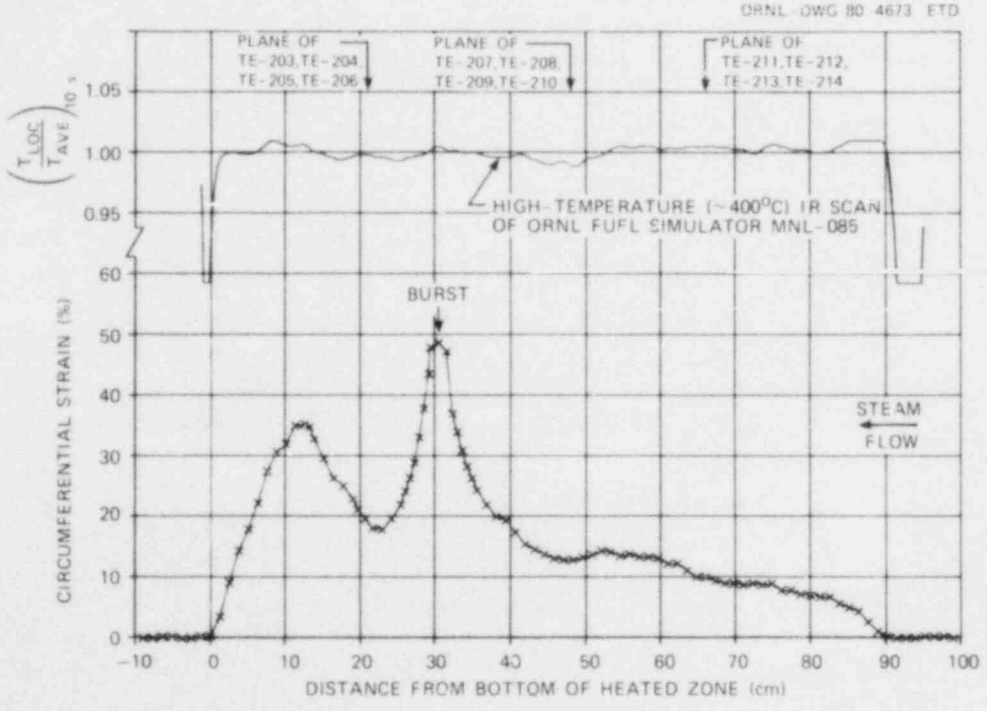

Fig. 2.28. Deformation profile of SR-52.

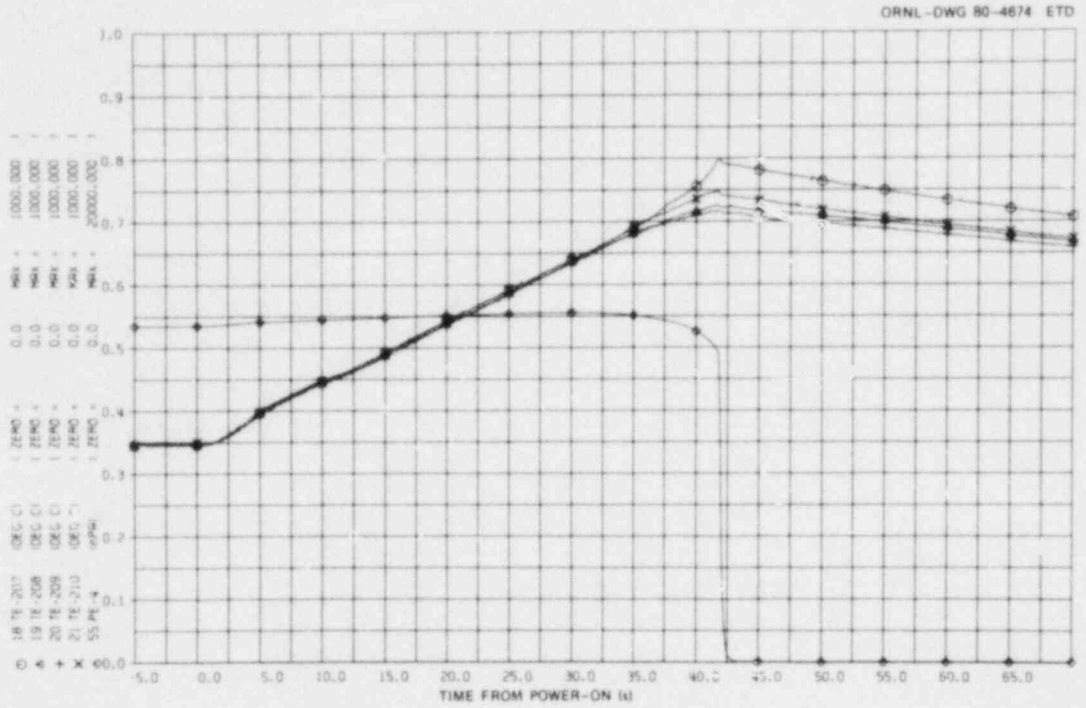

Fig. 2.29. Temperatures measured at 24-cm elevation in SR-54.

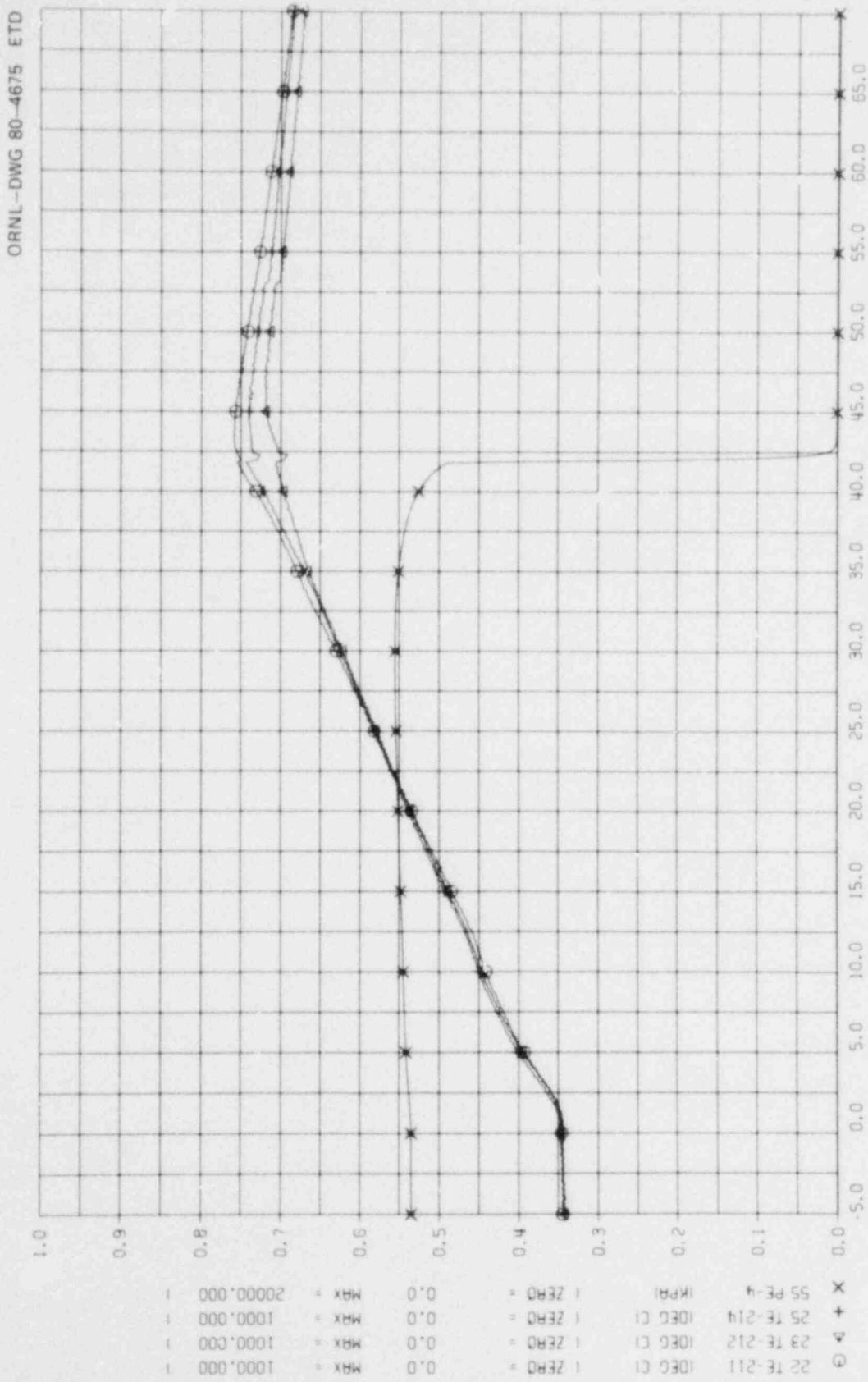

Fig. 2.30. Temperatures measured at 69-cm elevation in SR-54.

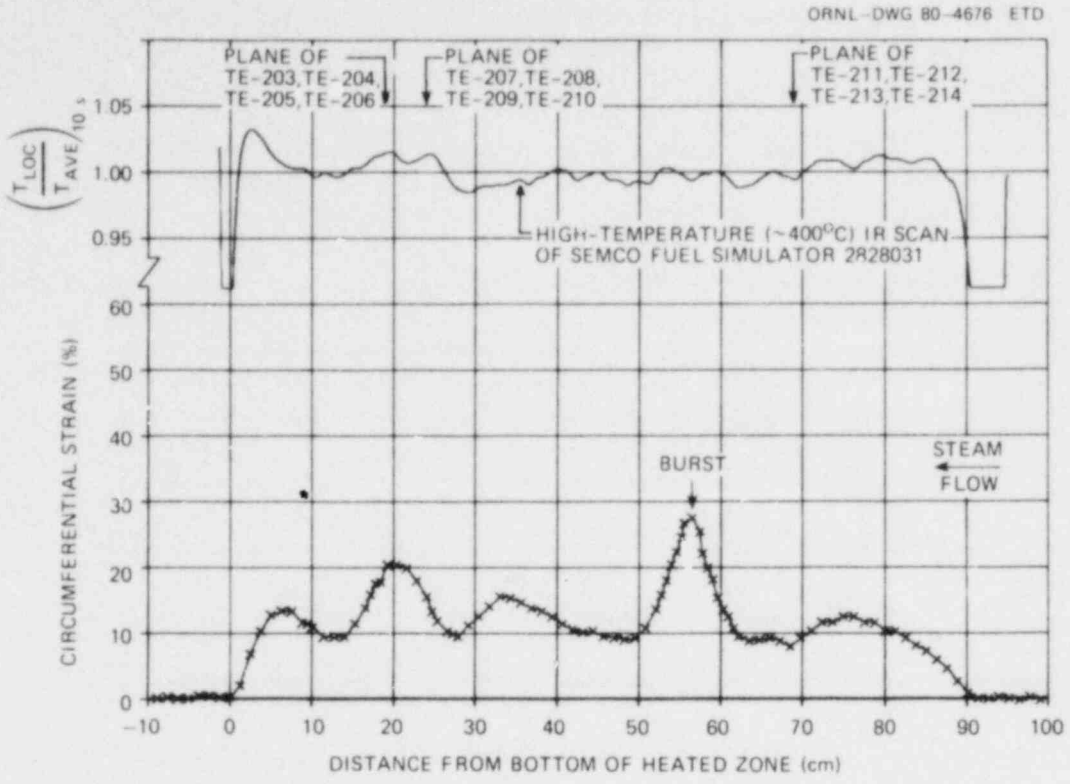

Fig. 2.31. Deformation profile of SR-54.

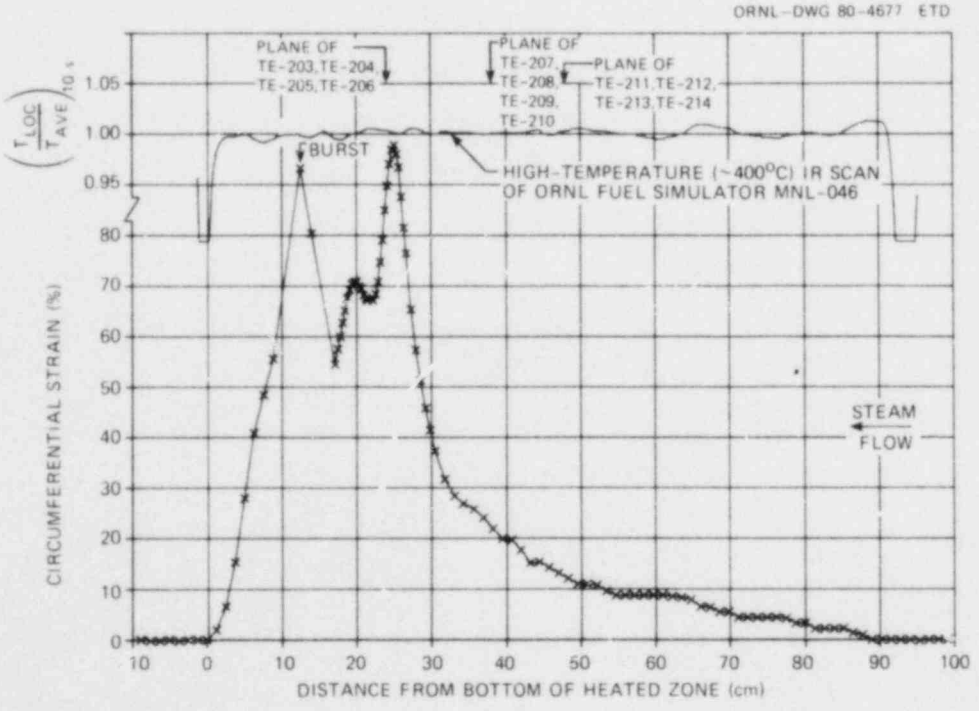

Fig. 2.32. Deformation profile of SR-49.

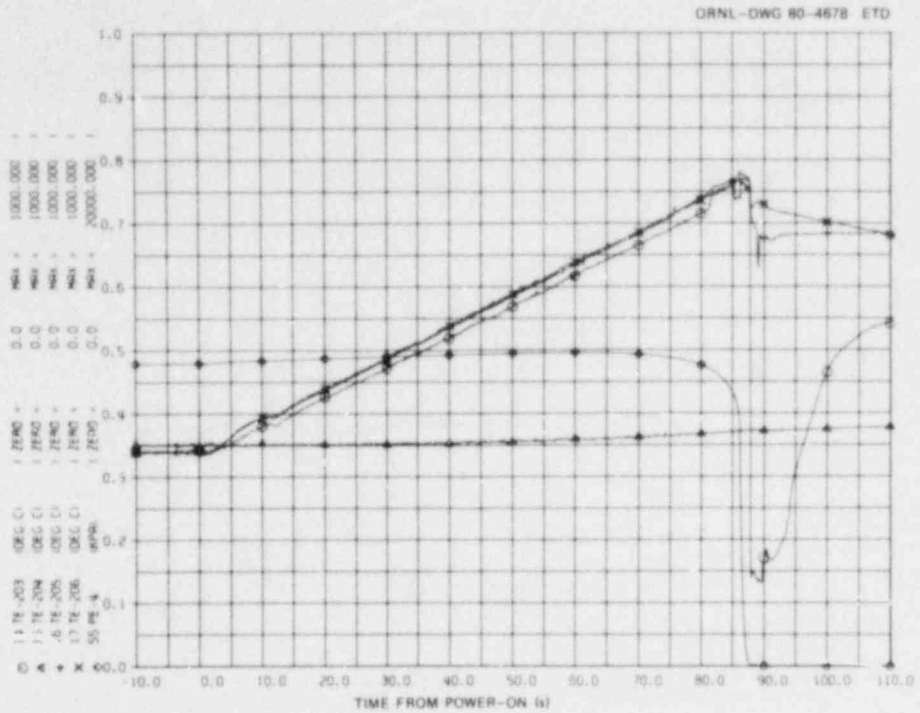

Fig. 2.33. Temperatures measured at 24-cm elevation in SR-49.

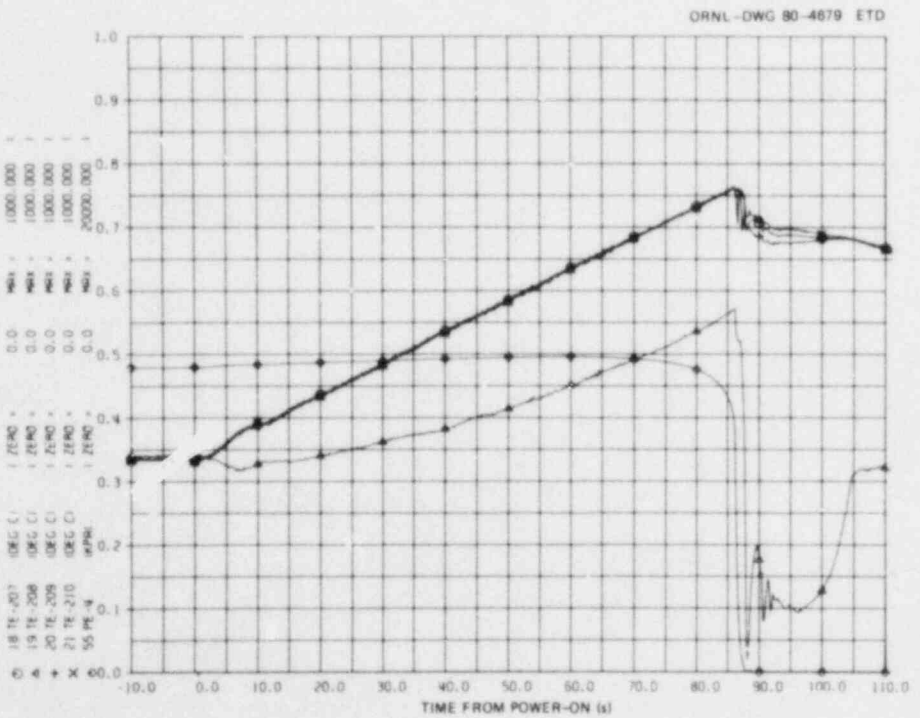

Fig. 2.34. Temperatures measured at 38-cm elevation in SR-49.

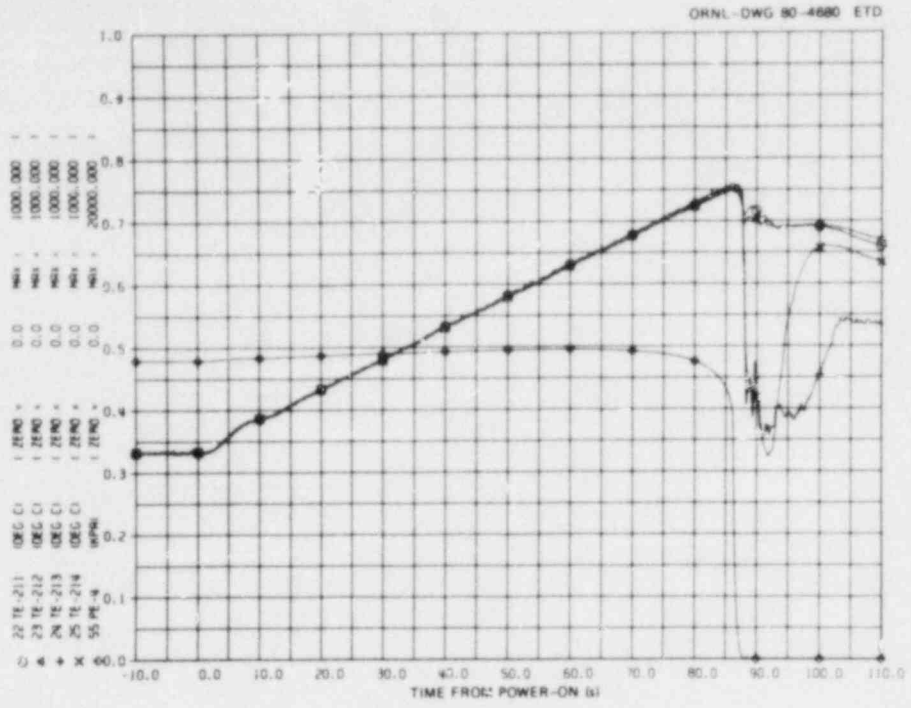

Fig. 2.35. Temperatures measured at 48-cm elevation in SR-49.

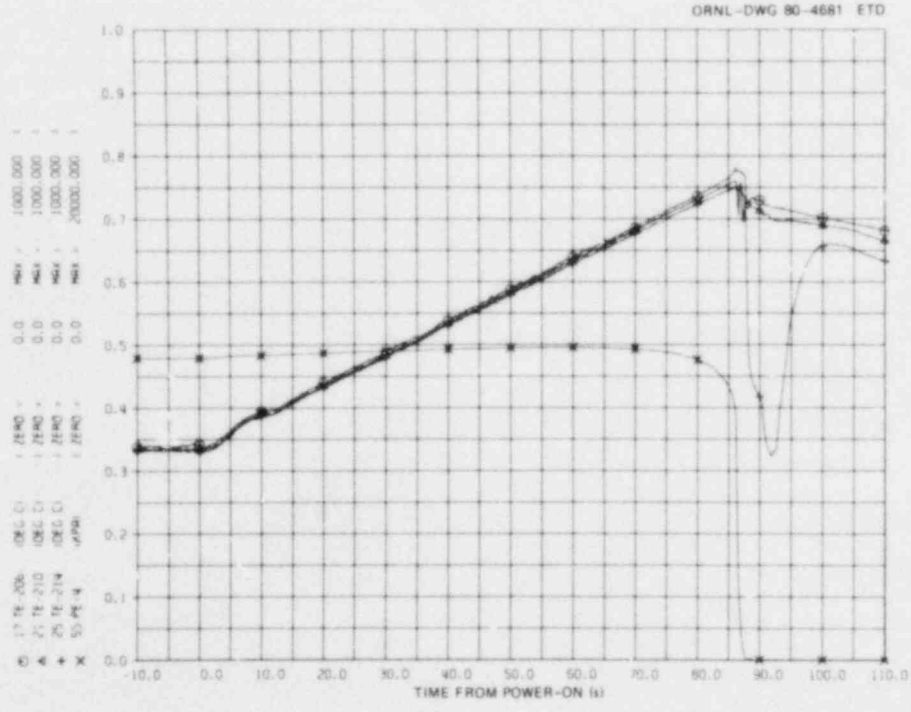

Fig. 2.36. Axial temperature distribution in SR-49.

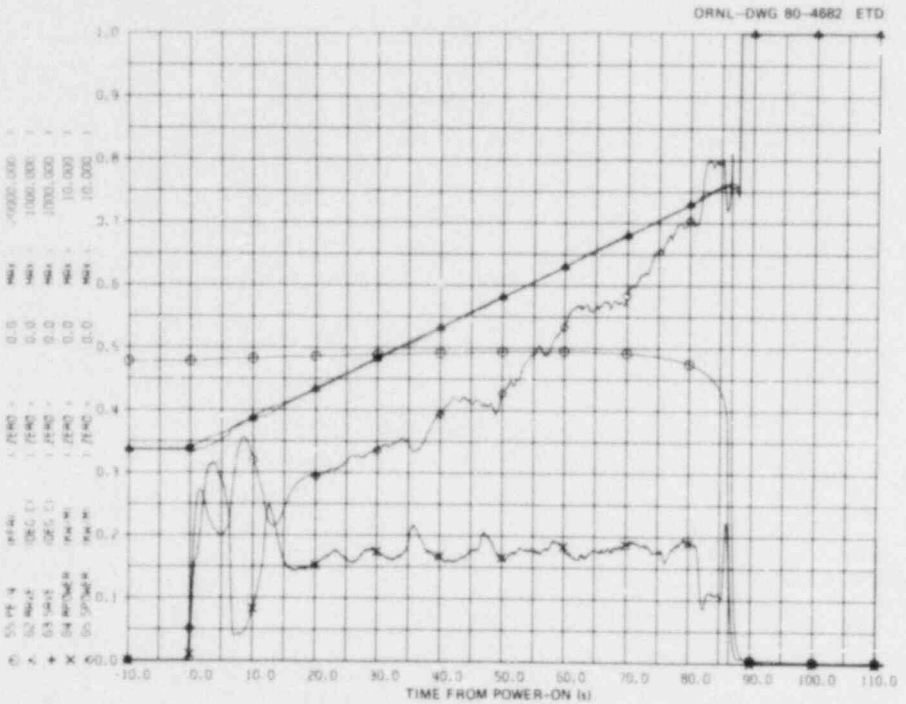

Fig. 2.37. Rod and shroud average temperatures, simulator and shroud powers, and simulator pressure in SR-49.

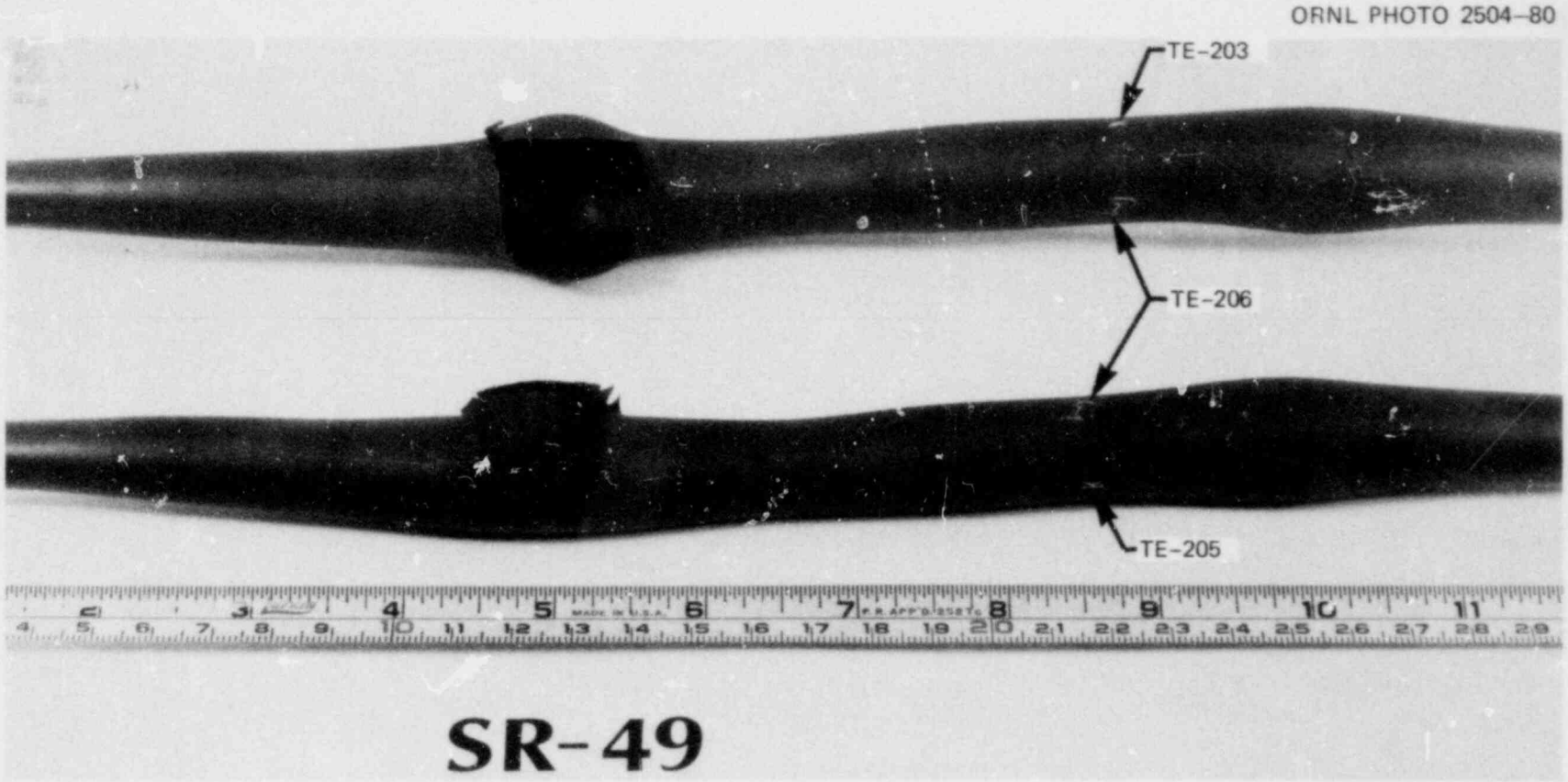

Fig. 2.38. Burst in SR-49.

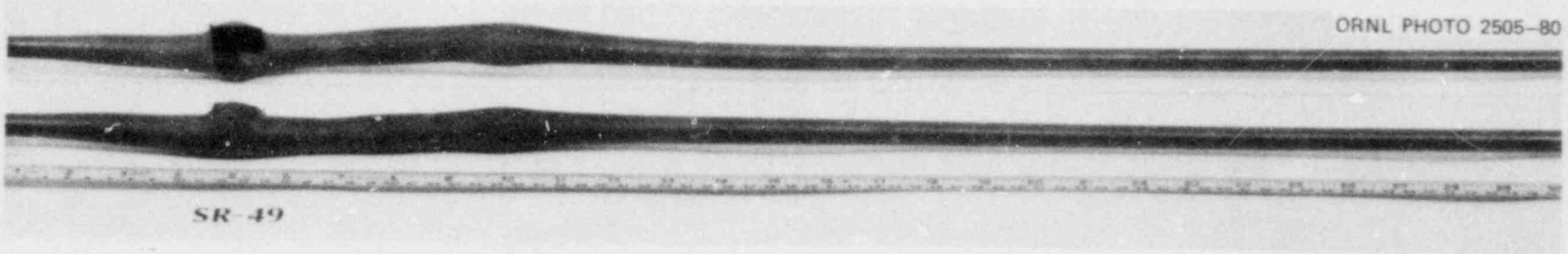

Fig. 2.39. "Carrot"-type deformation in SR-49.

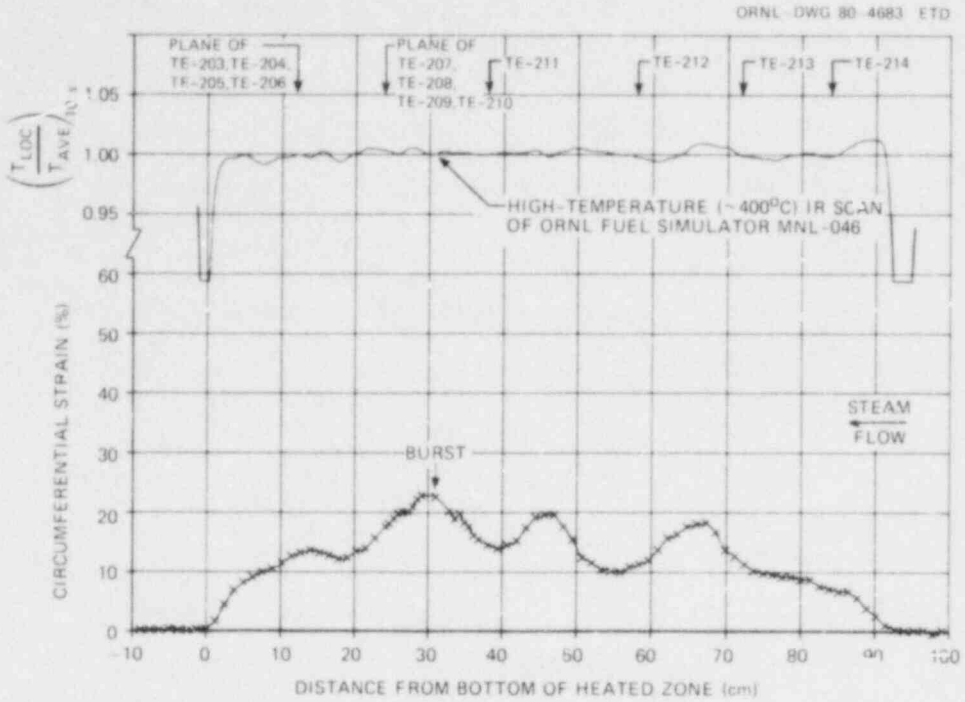

Fig. 2.40. Deformation profile of SR-55.

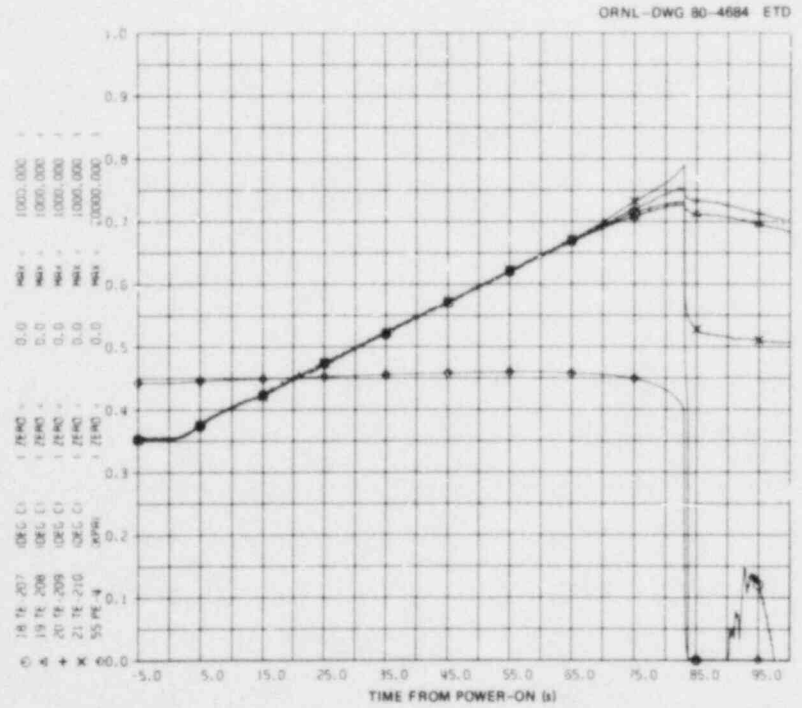

Fig. 2.41. Temperature measured at 24-cm elevation in SR-55.

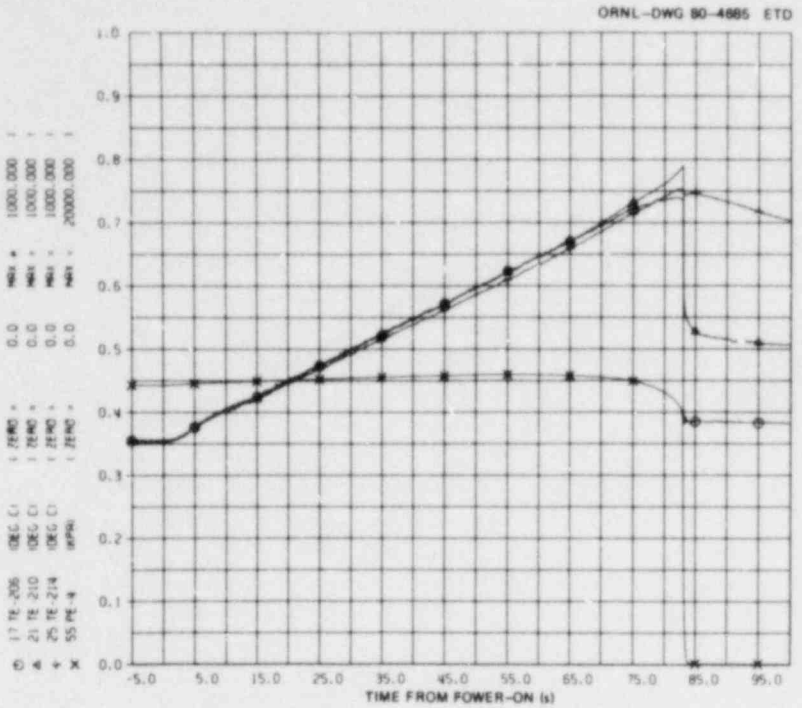

Fig. 2.42. Axial temperature profile in SR-55.

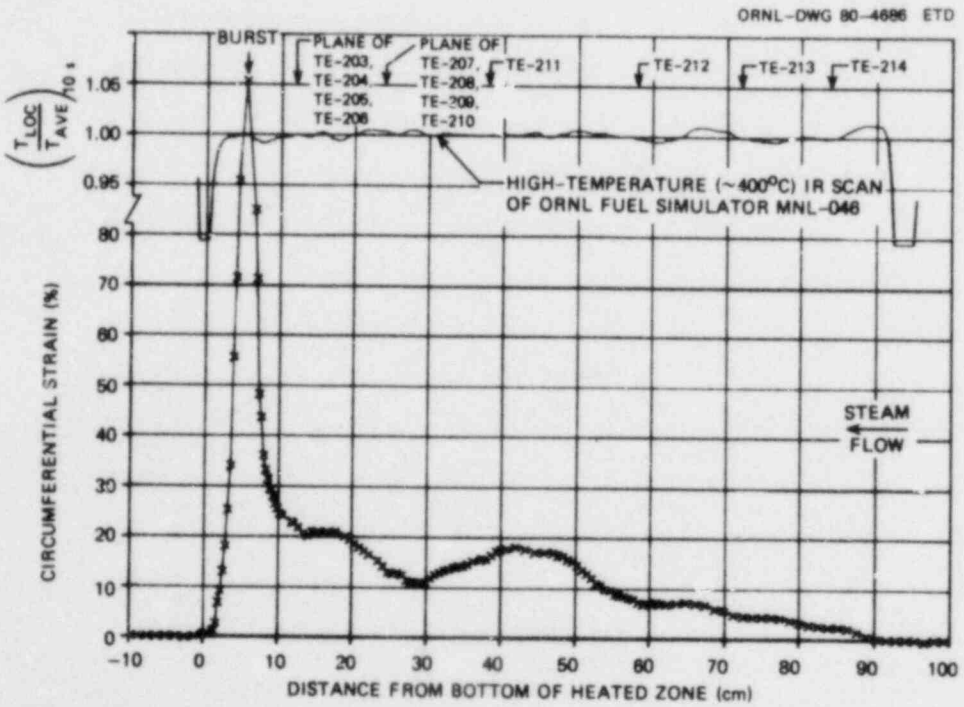

Fig. 2.43. Deformation profile of SR-64.

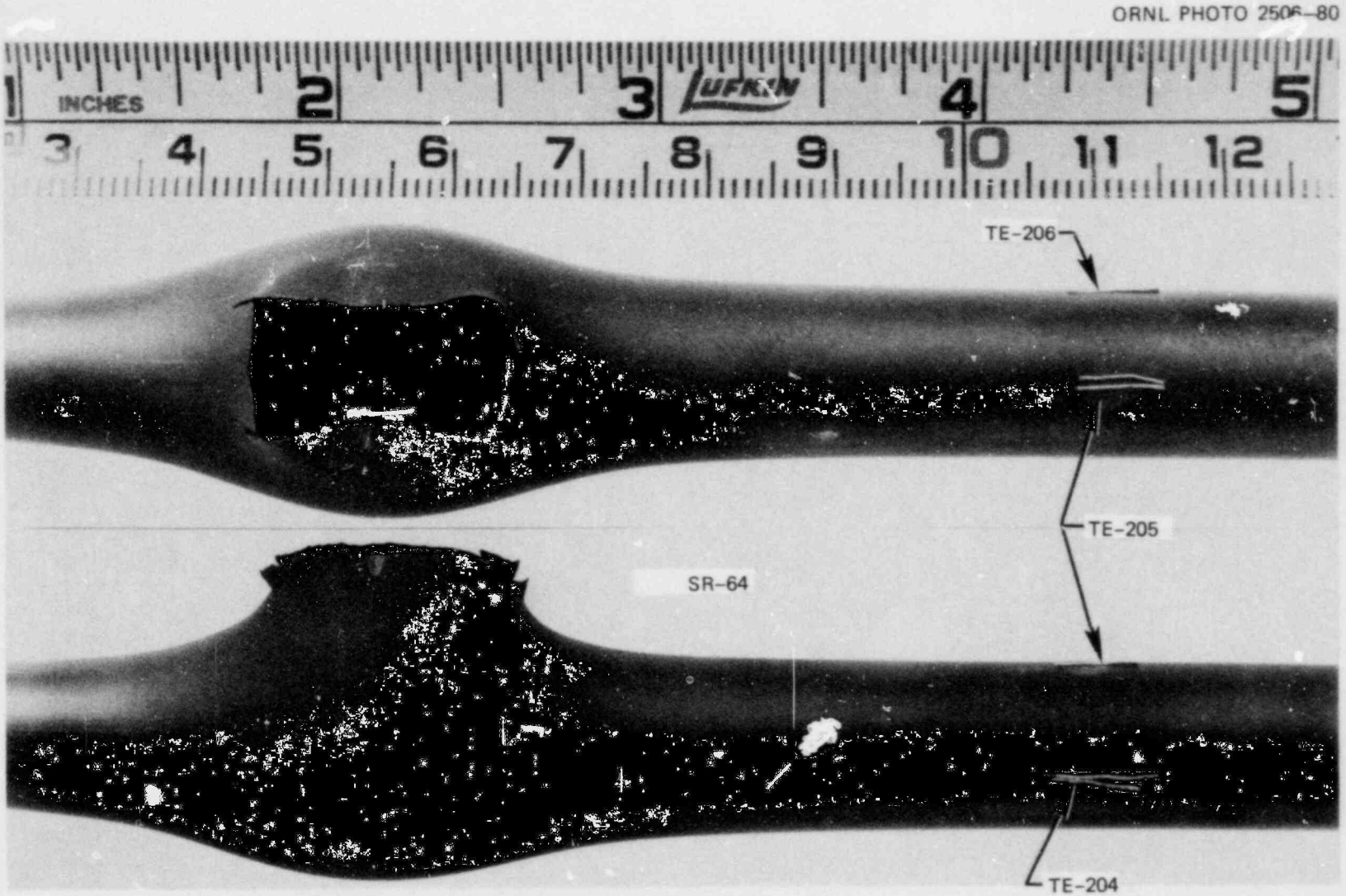

Fig. 2.44. Burst in SR-64.

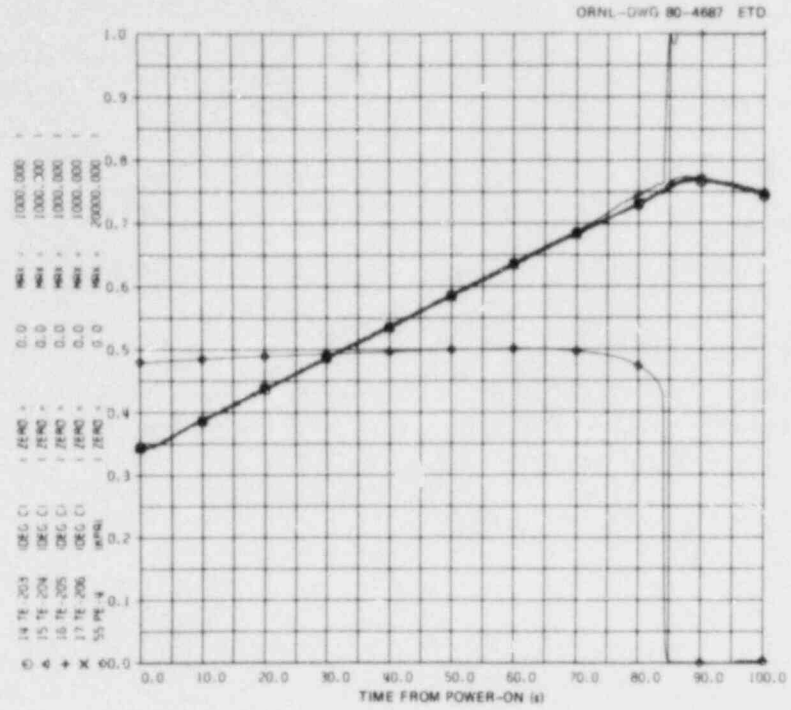

Fig. 2.45. Temperatures measured at 12-cm elevation in SR-64.

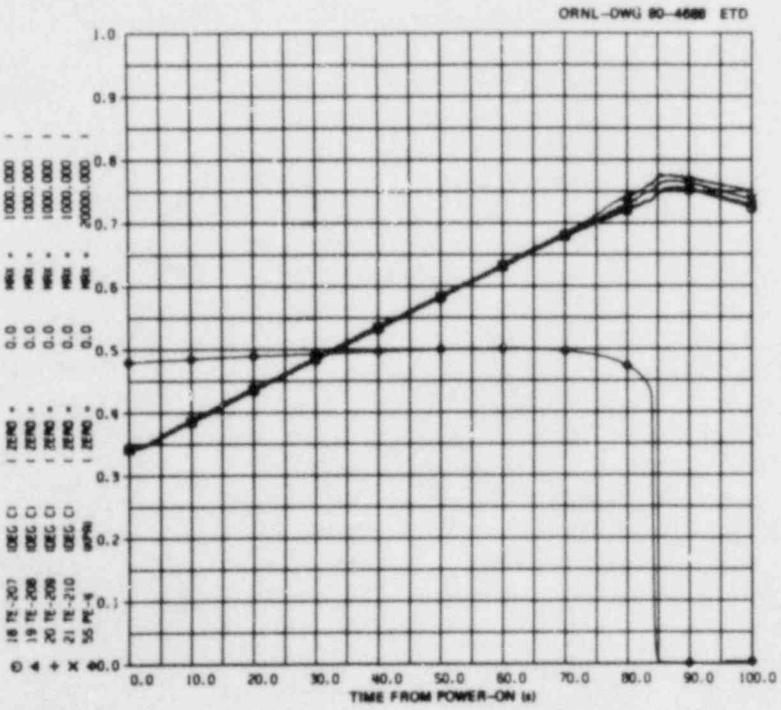

Fig. 2.46. Temperatures measured at 24-cm elevation in SR-64.

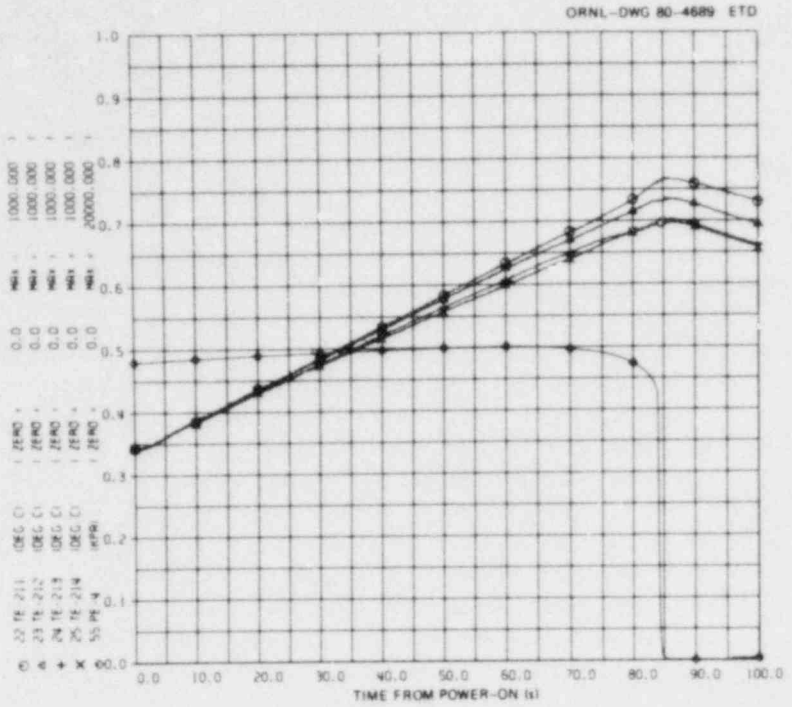

Fig. 2.47. Temperature distribution along upper portion of SR-64.

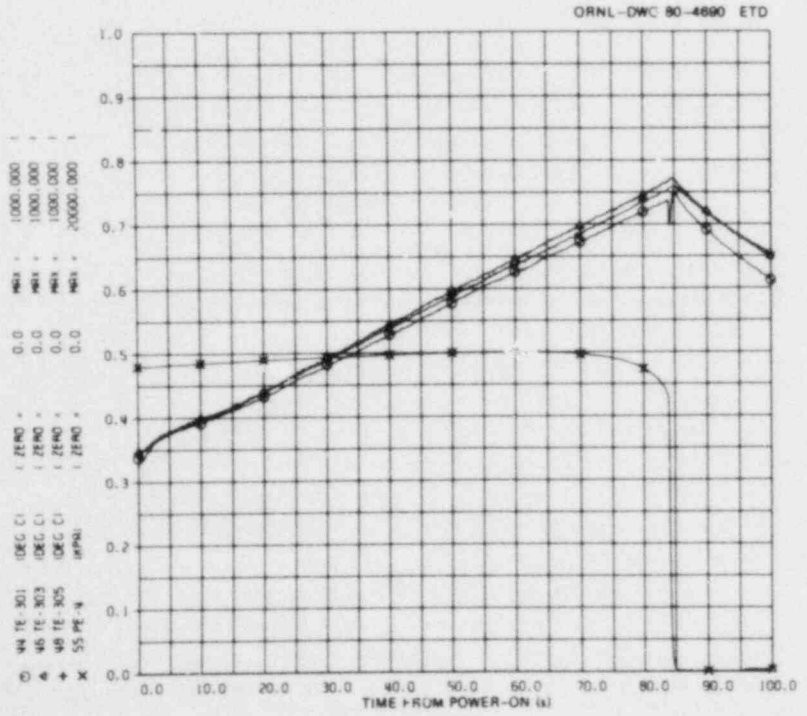

Fig. 2.48. Axial temperature distribution of heated shroud in SR-64.

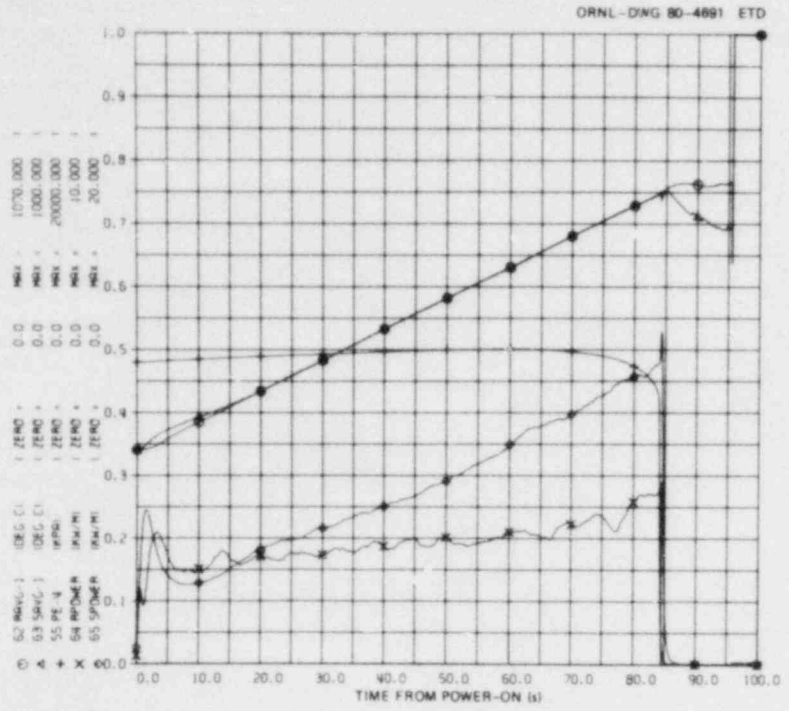

Fig. 2.49. Rod and shroud average temperatures, simulator and shroud powers, and simulator pressure in SR-64.

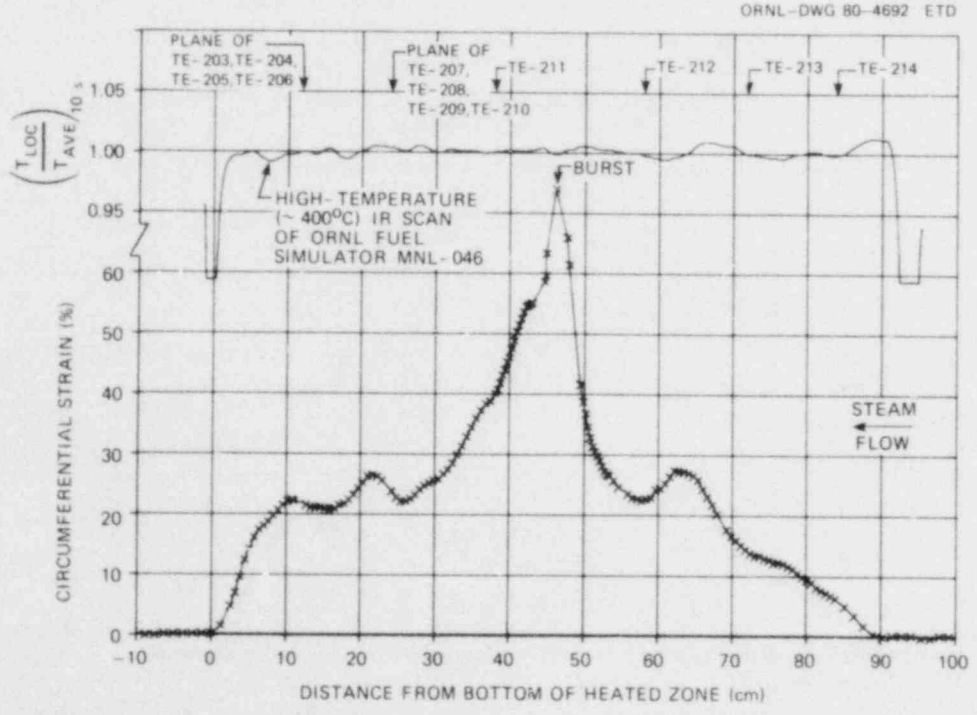

Fig. 2.50. Deformation profile of SR-65.

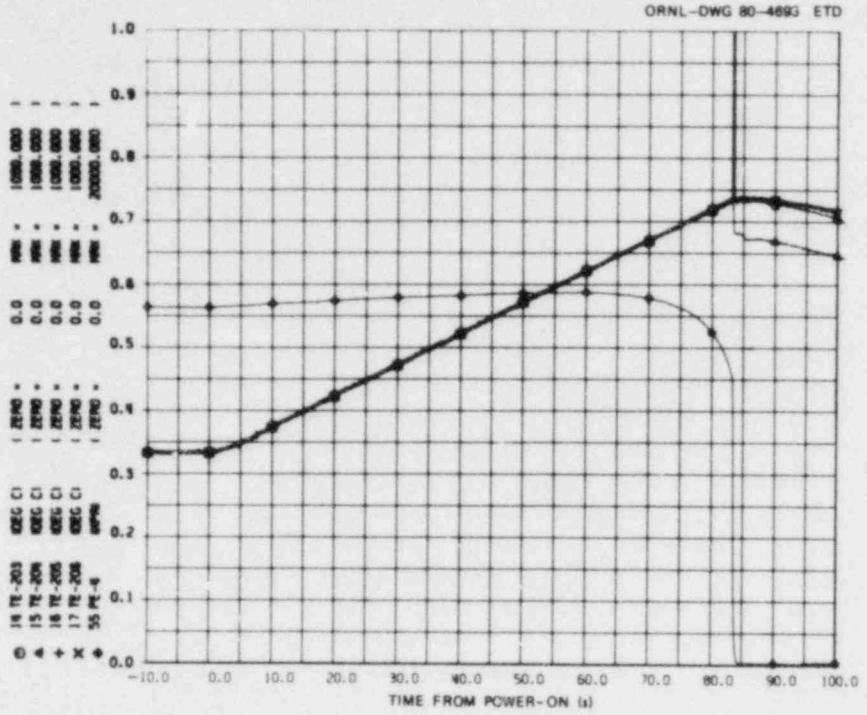

Fig. 2.51. Temperatures measured at 12-cm elevation in SR-65.

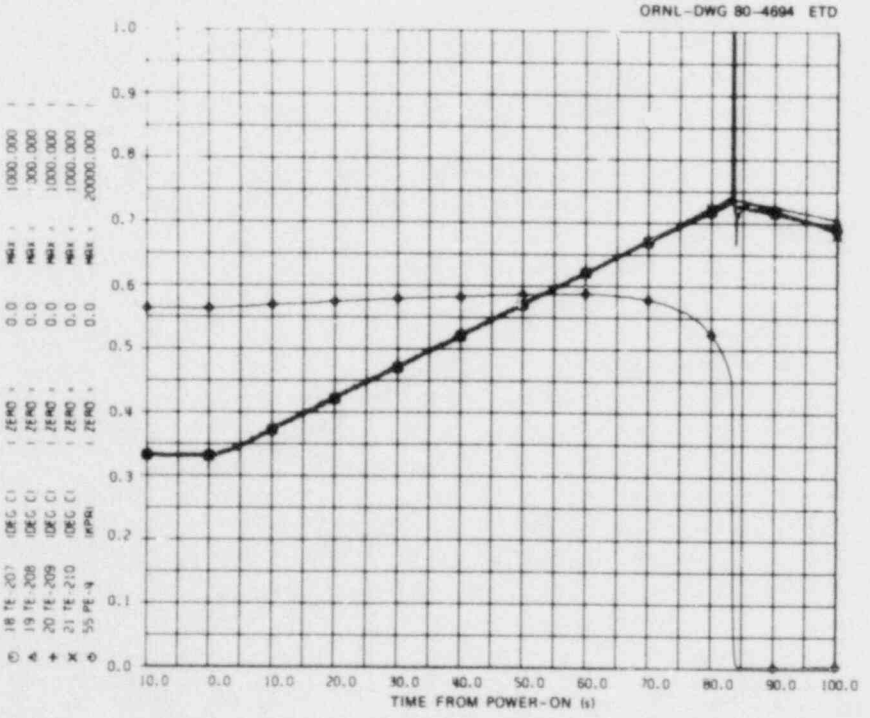

Fig. 2.52. Temperatures measured at 24-cm elevation in SR-65.

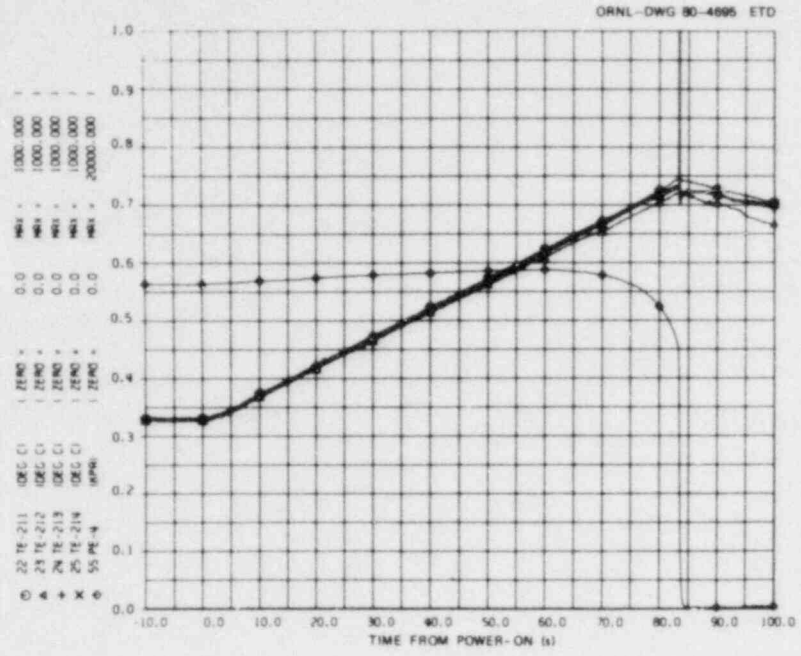

Fig. 2.53. Temperatures measured on upper portion of SR-65.

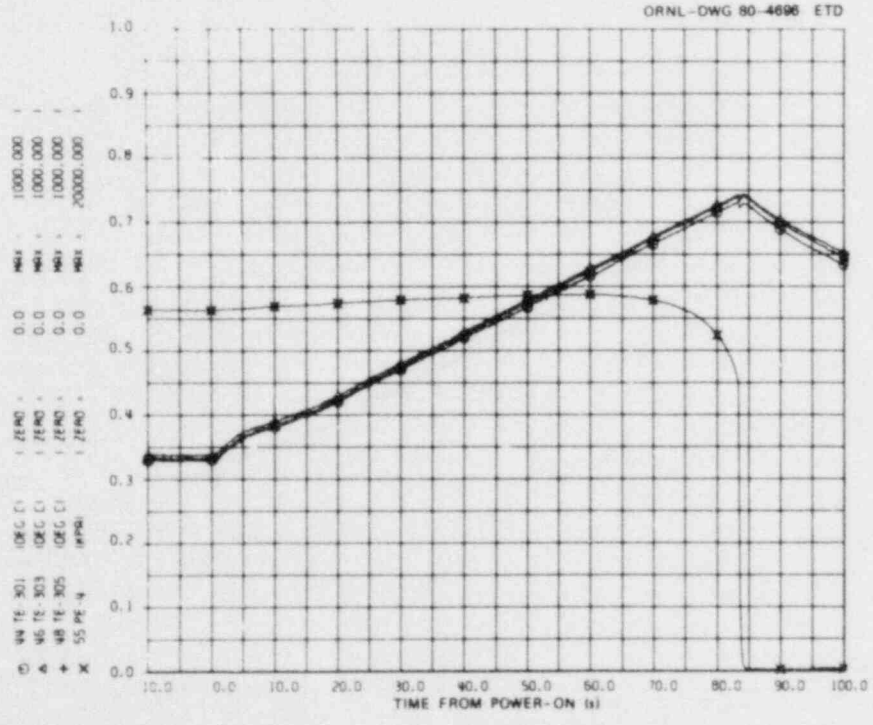

Fig. 2.54. Axial temperature distribution of heated shroud in SR-65.

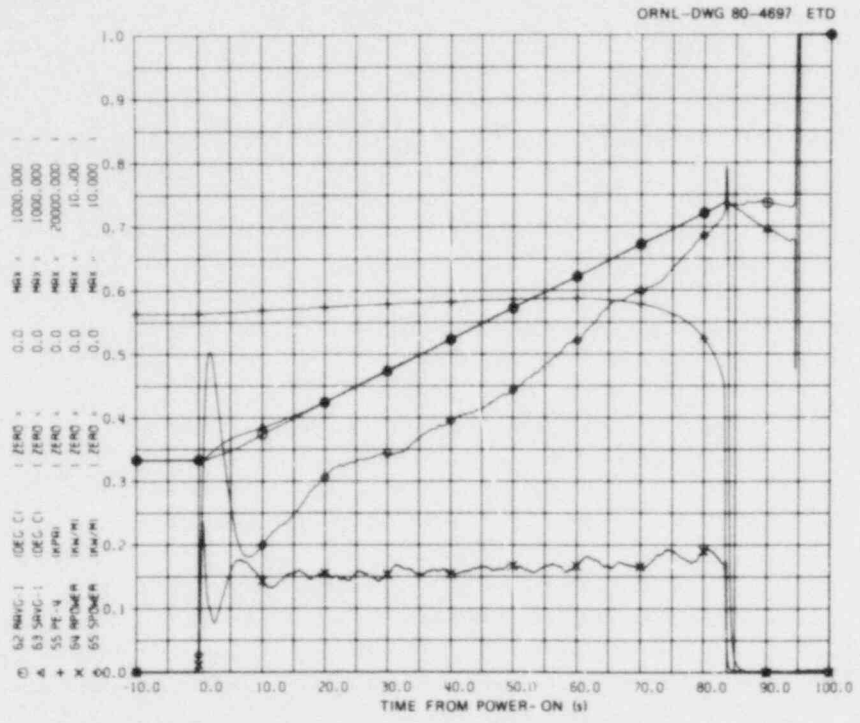

Fig. 2.55. Rod and shroud average temperatures, fuel simulator and shroud powers, and simulator pressure in SR-65.

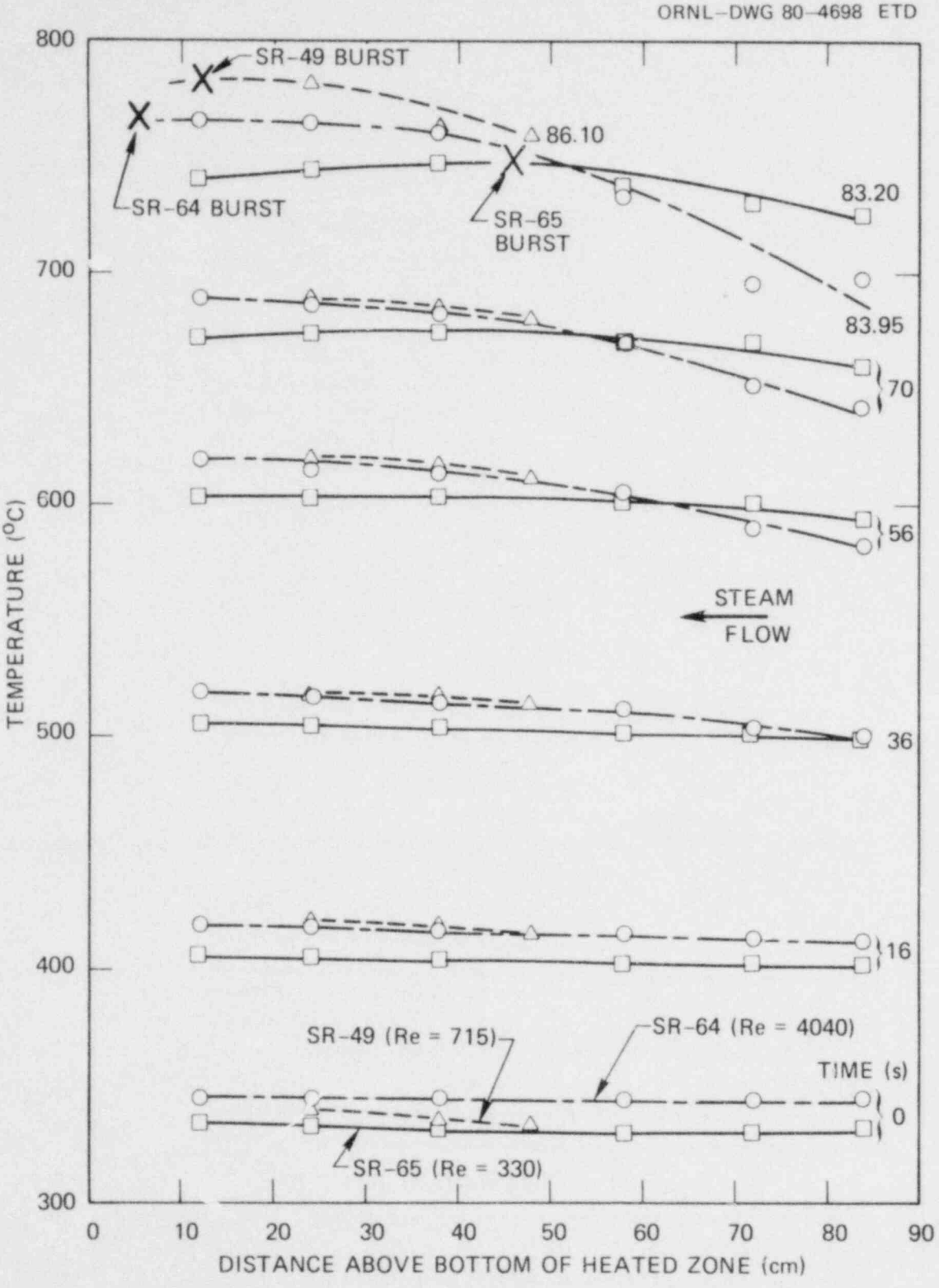

Fig. 2.56. Comparison of axial temperature distributions showing effect of different convective cooling conditions in SR-49, SR-64, and SR-65.

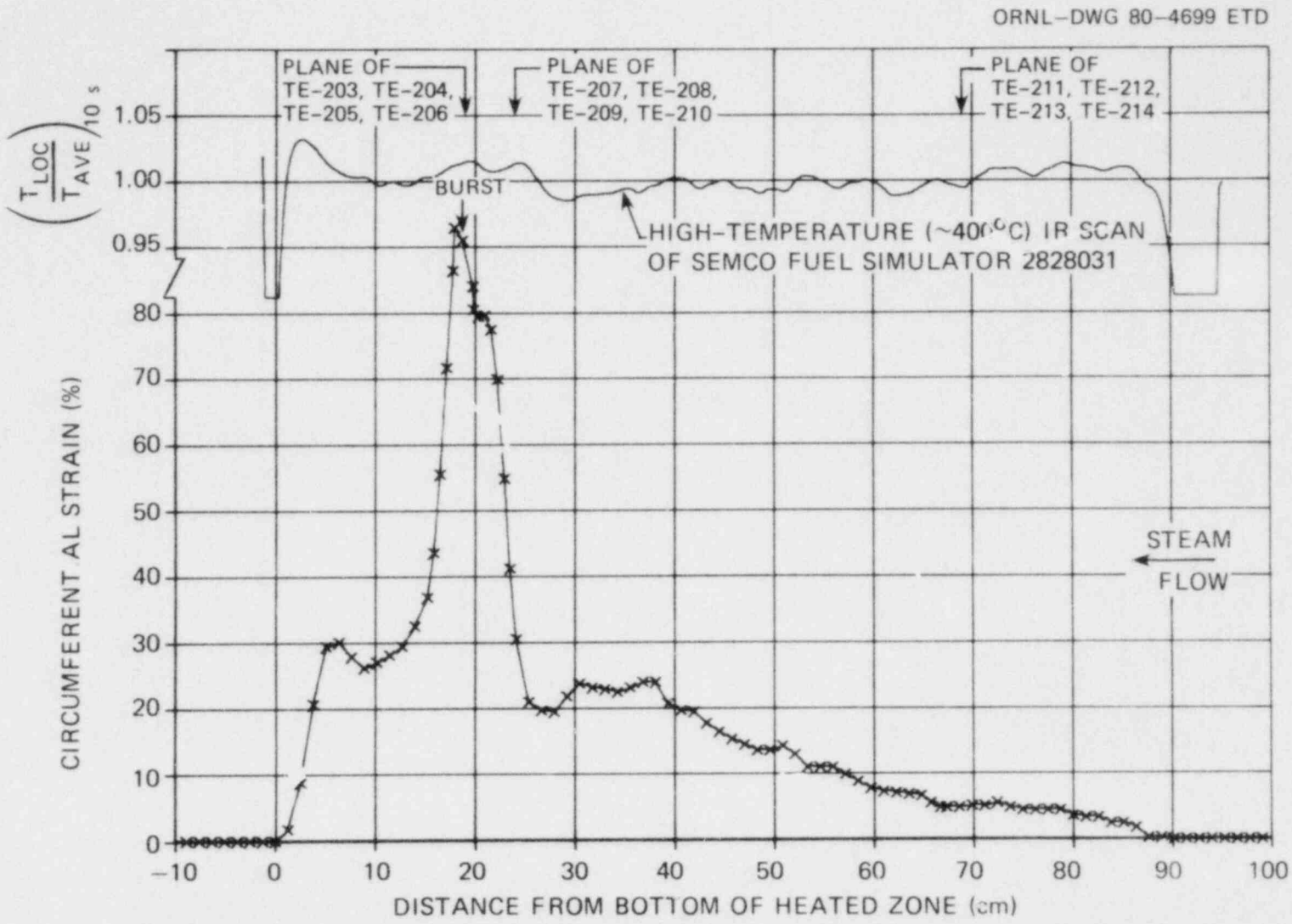

Fig. 2.57. Deformation profile of SR-51.

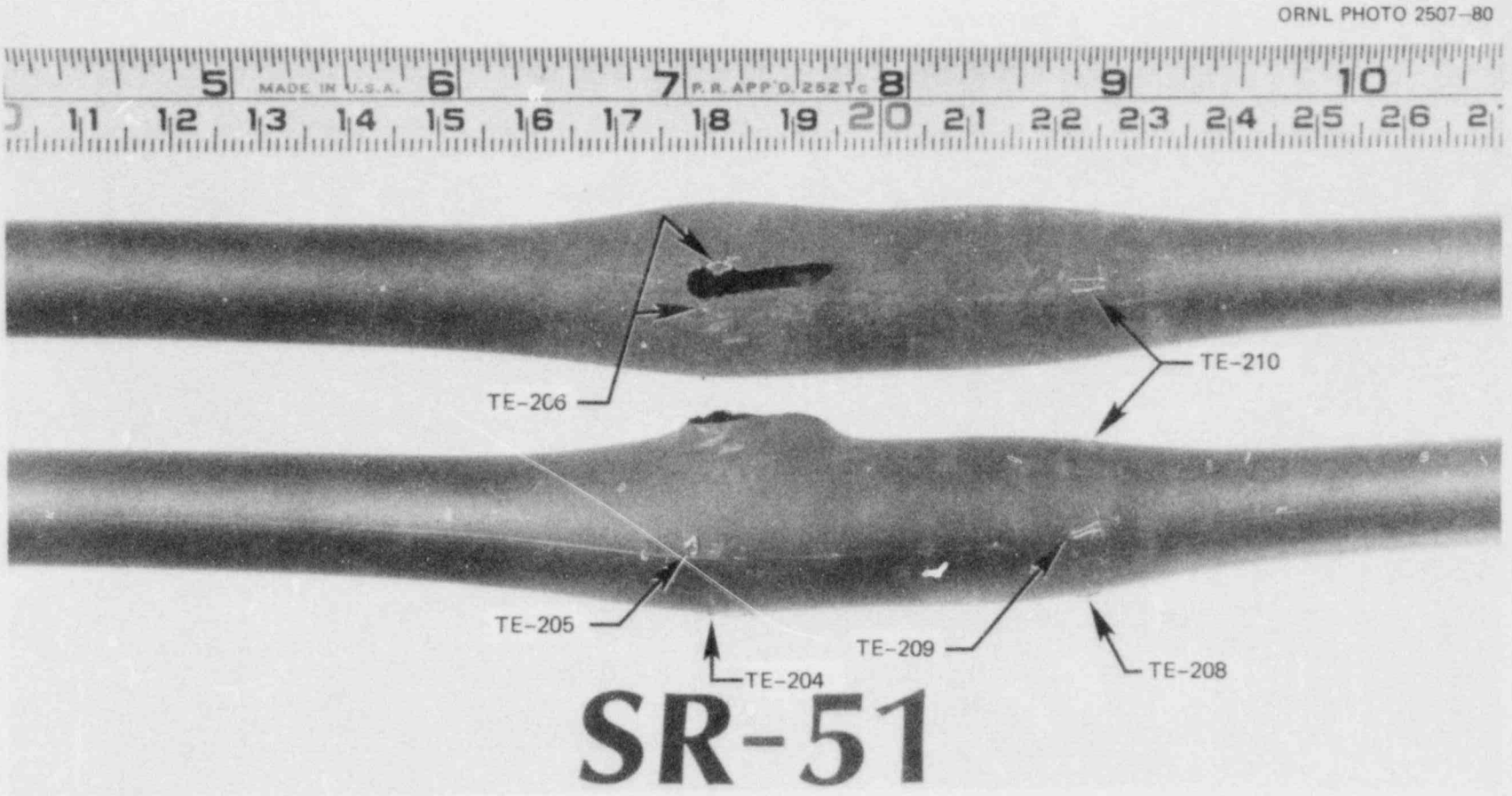

Fig. 2.58. Burst in SR-51.

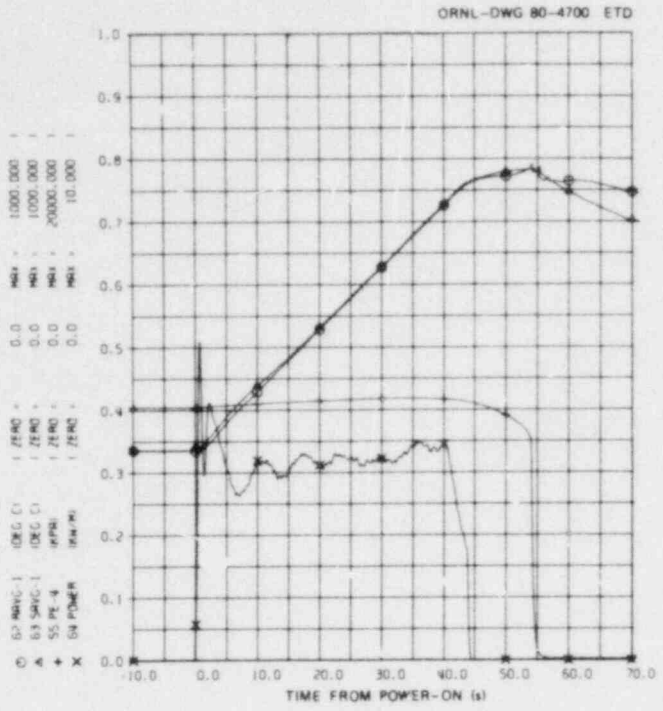

Fig. 2.59. Rod and shroud average temperatures and simulator power and pressure in SR-51.

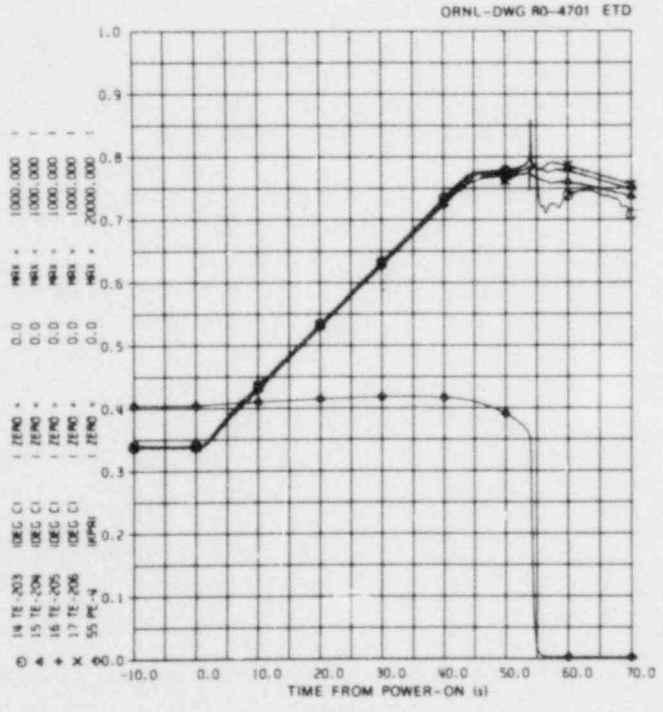

Fig. 2.60. Temperatures measured at 19-cm elevation in SR-51.

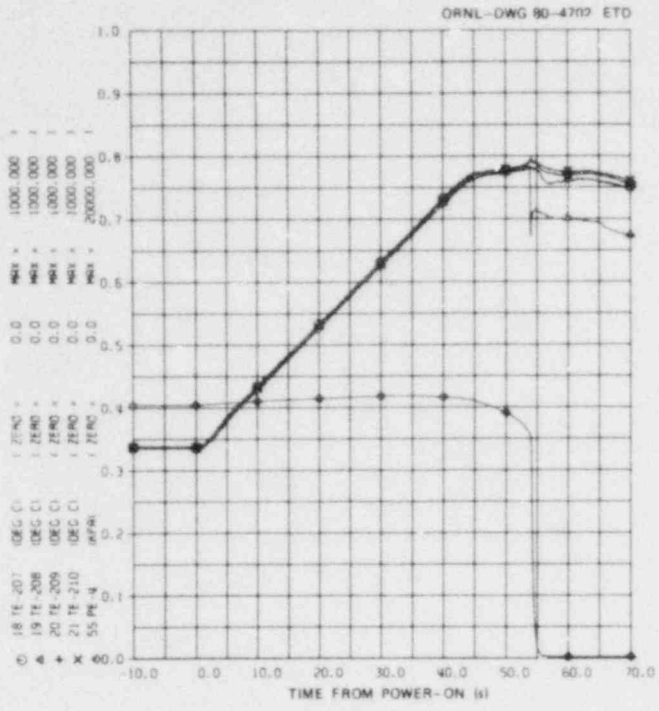

Fig. 2.61. Temperatures measured at 24-cm elevation in SR-51.

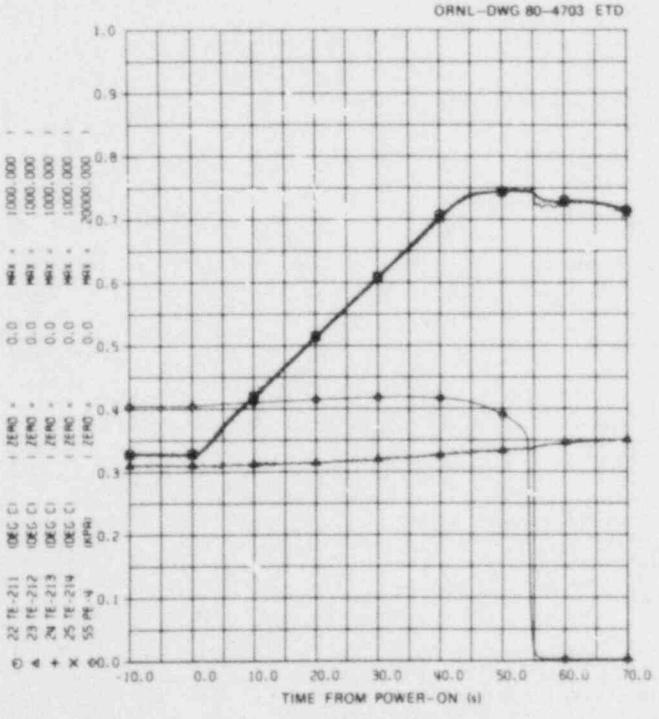

Fig. 2.62. Temperatures measured at 68.5-cm elevation in SR-51.

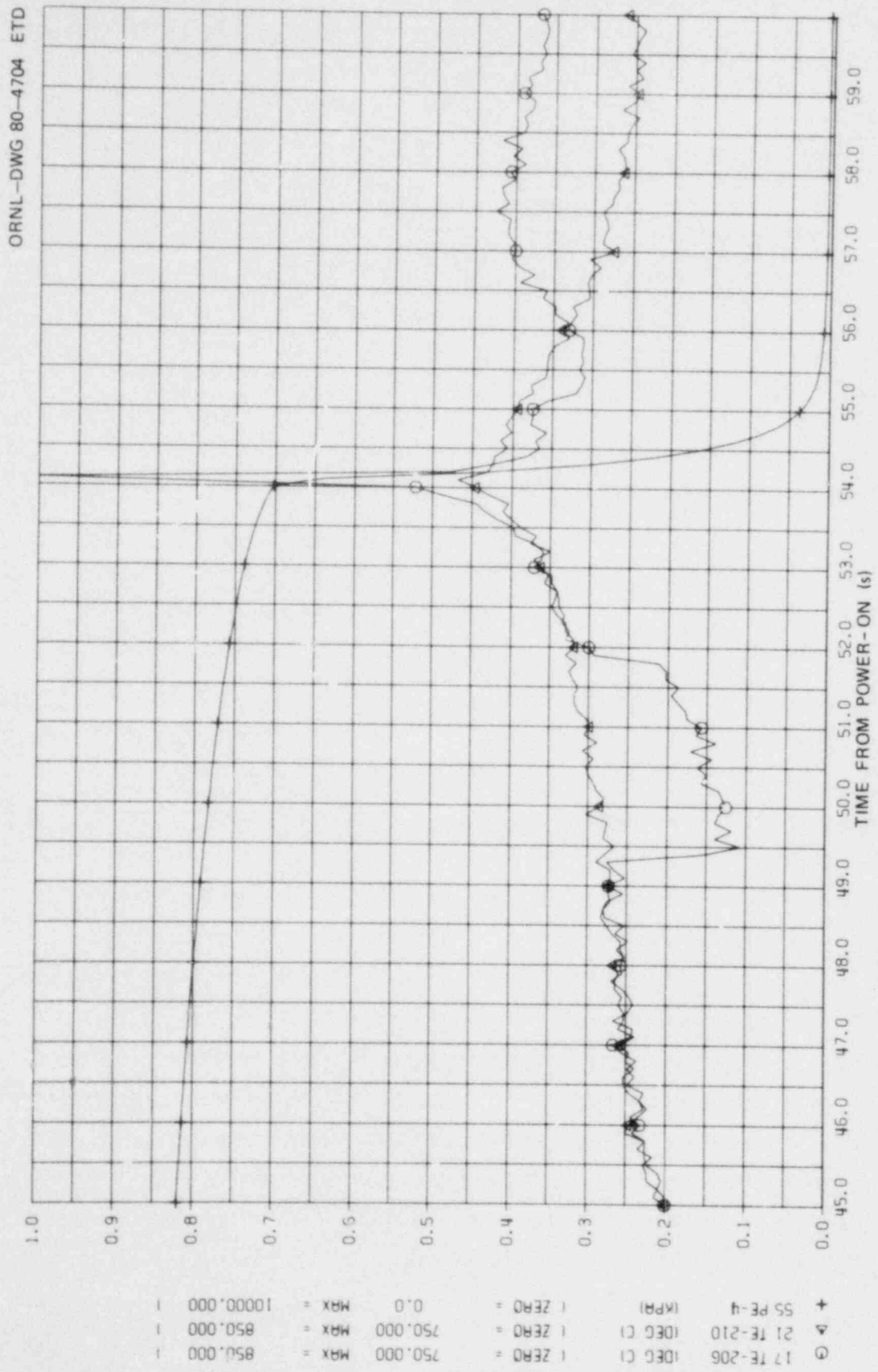

Fig. 2.63. Expanded-scale plot of TE-206 and TE-210 in SR-51.

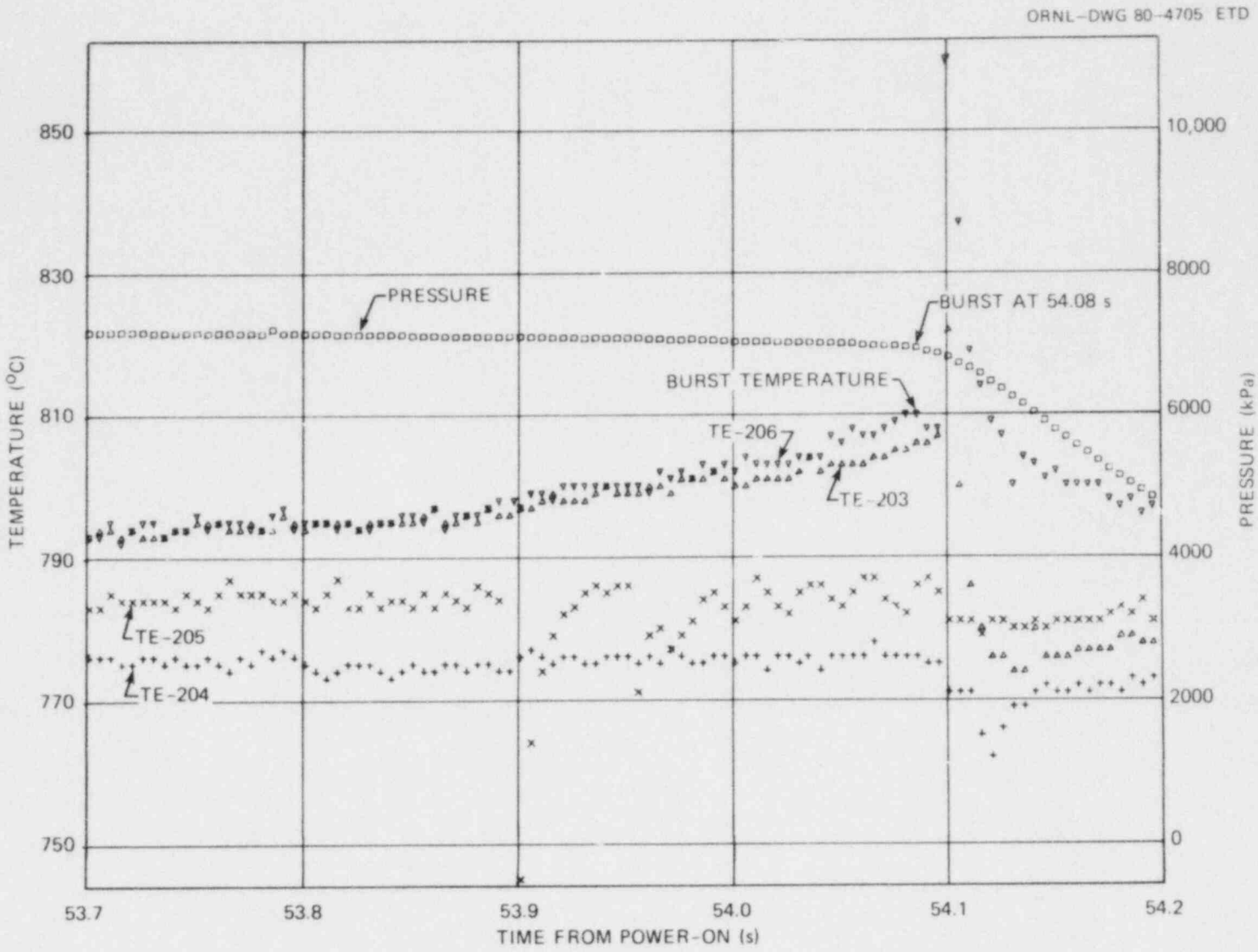

Fig. 2.64. Temperatures measured at 19-cm elevation at 5-ms intervals around burst time in SR-51.

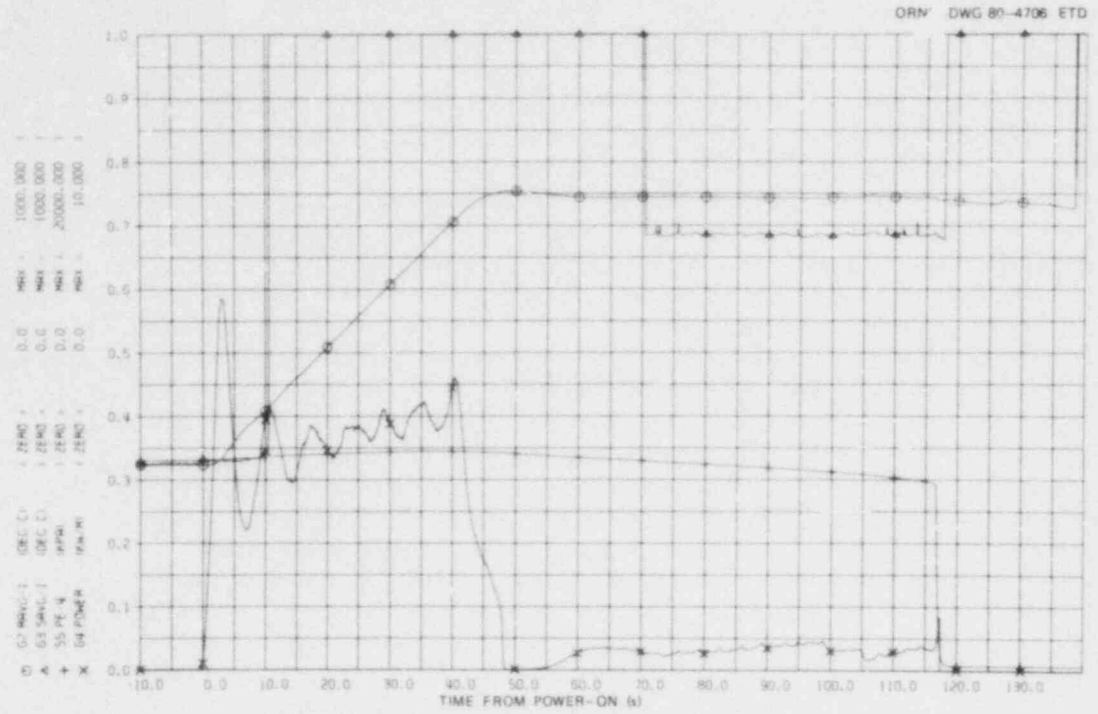

Fig. 2.65. Rod and shroud average temperatures and simulator pressure and power in SR-53. See text for explanation of shroud average temperature behavior.

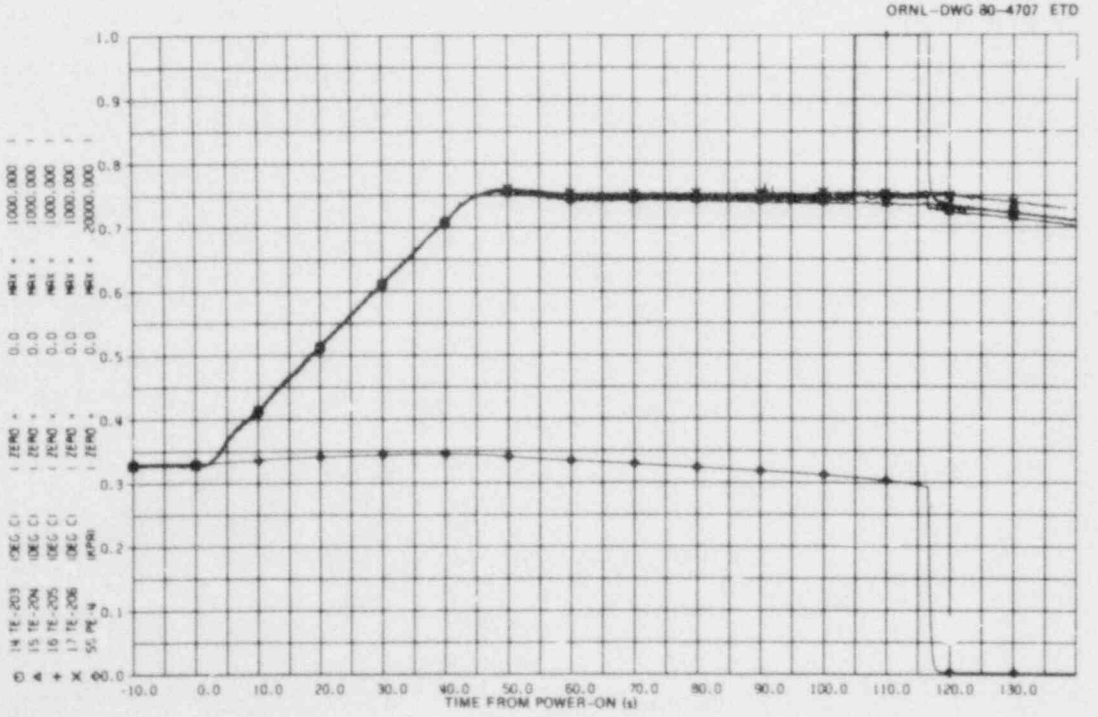

Fig. 2.66. Temperatures measured at 24-cm elevation in SR-53.

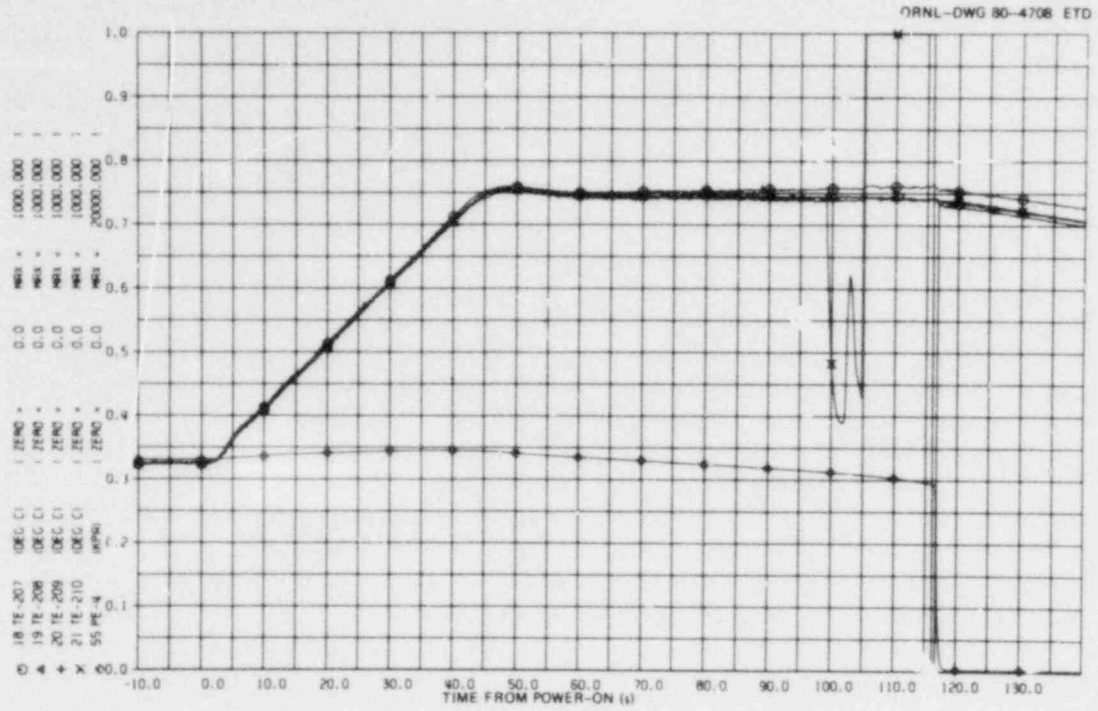

Fig. 2.67. Temperatures measured at 38-cm elevation in SR-53.

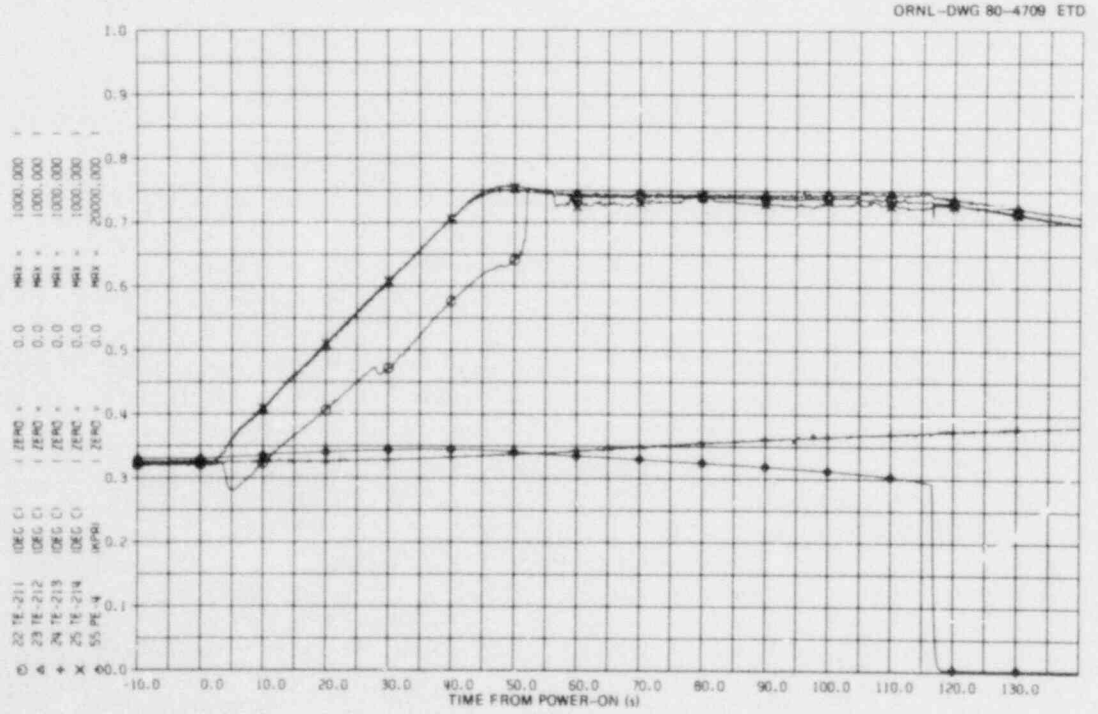

Fig. 2.68. Temperatures measured at 48-cm elevation in SR-53.

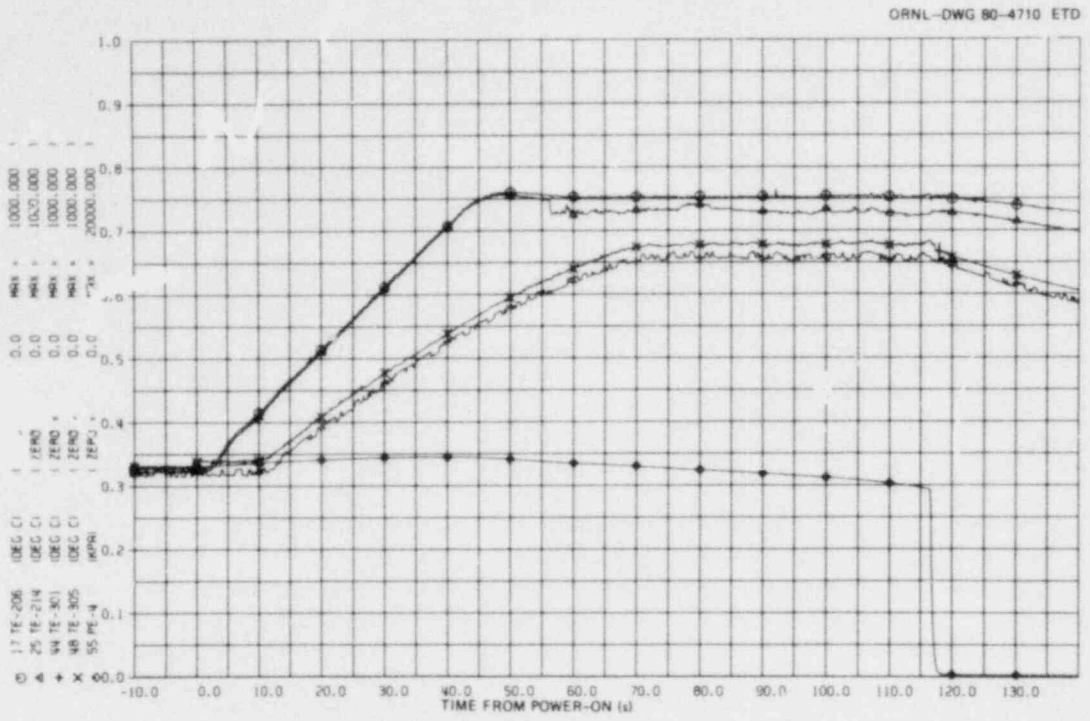

Fig. 2.69. Comparison of rod and shroud temperatures in SR-53.

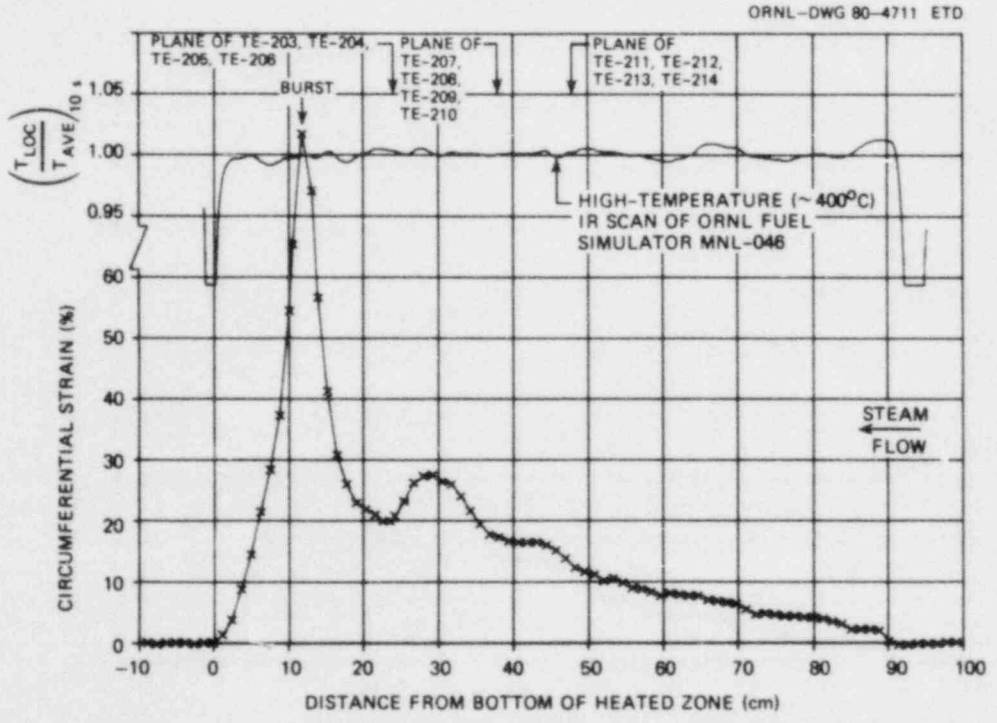

Fig. 2.70. Deformation profile of SR-53.

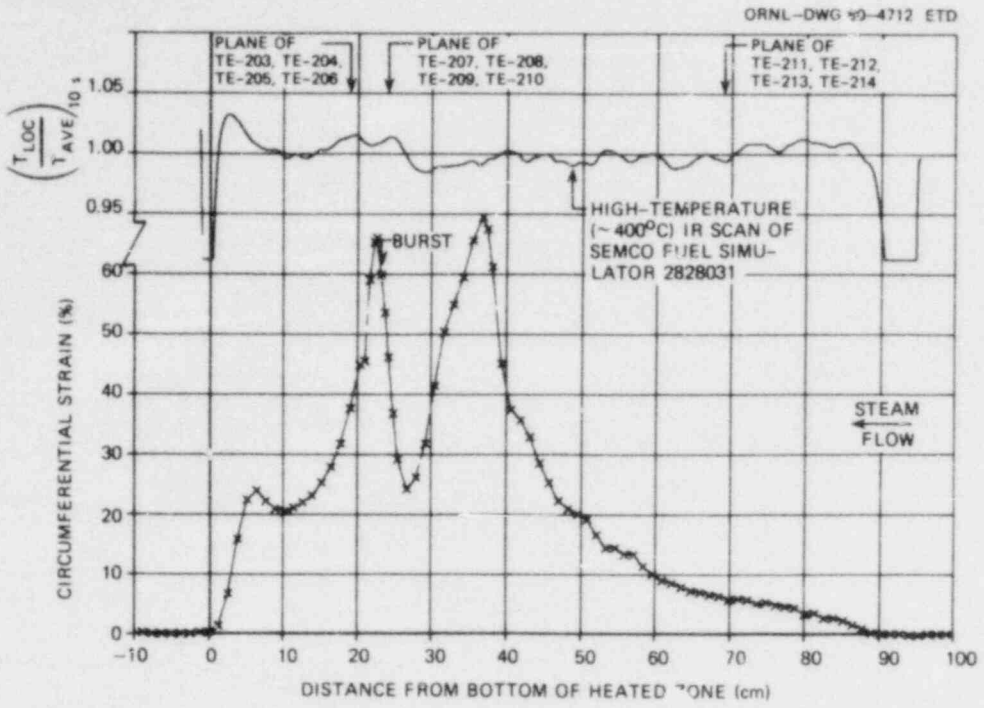

Fig. 2.71. Deformation profile of SR-56.

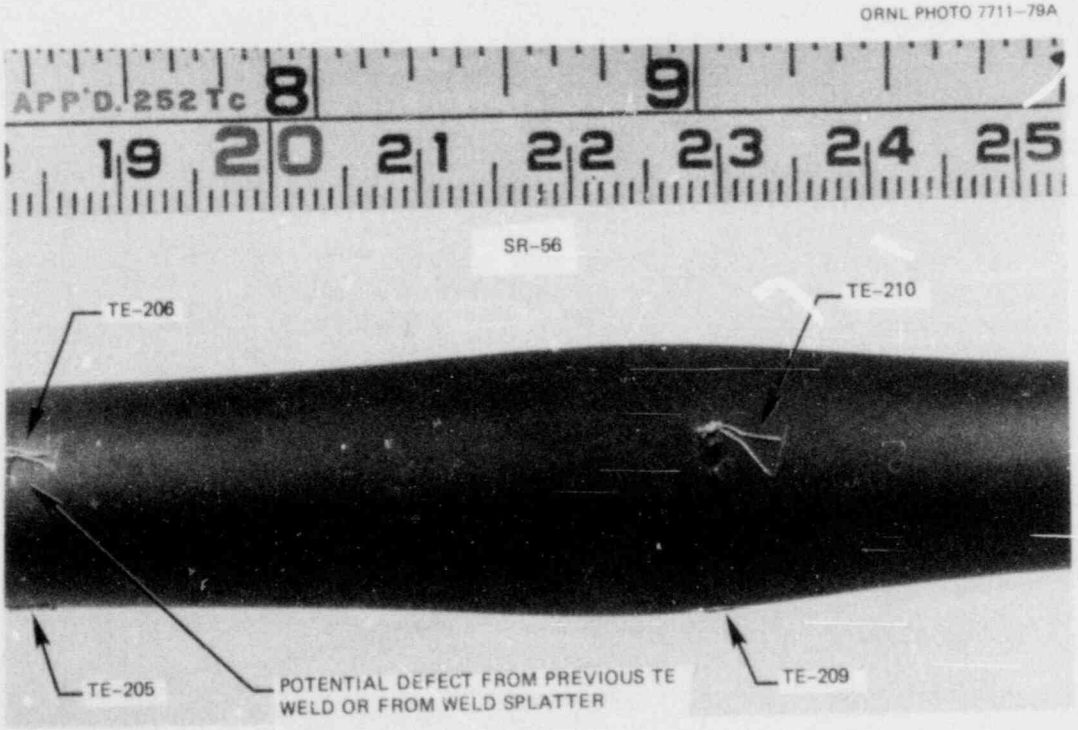

Fig. 2.72. Photograph of burst in SR-56 showing failure adjacent to TE-210.

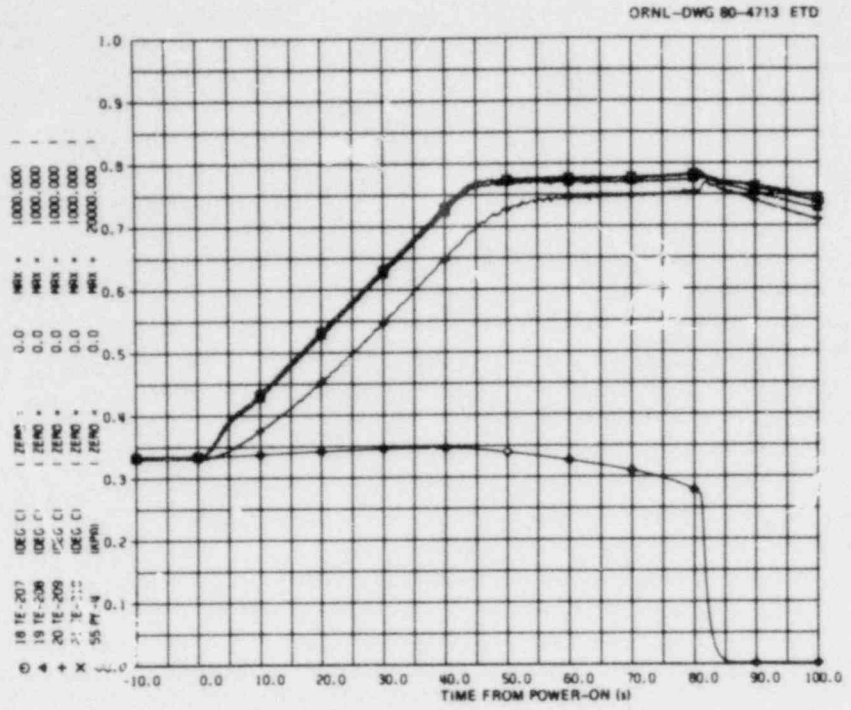

Fig. 2.73. Temperatures measured at burst elevation in SR-56.

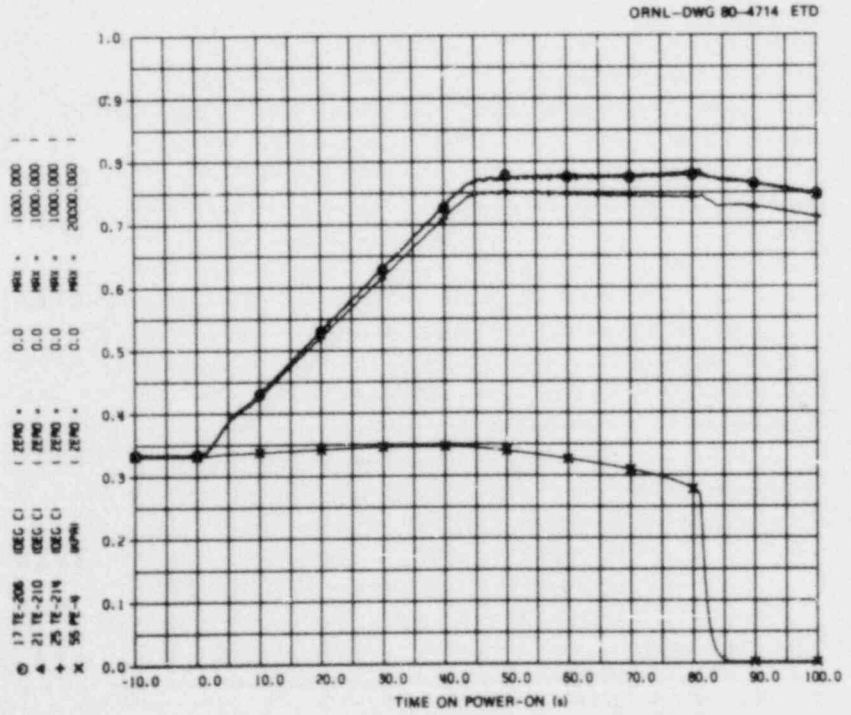

Fig. 2.74. Axial temperature distribution in SR-56.

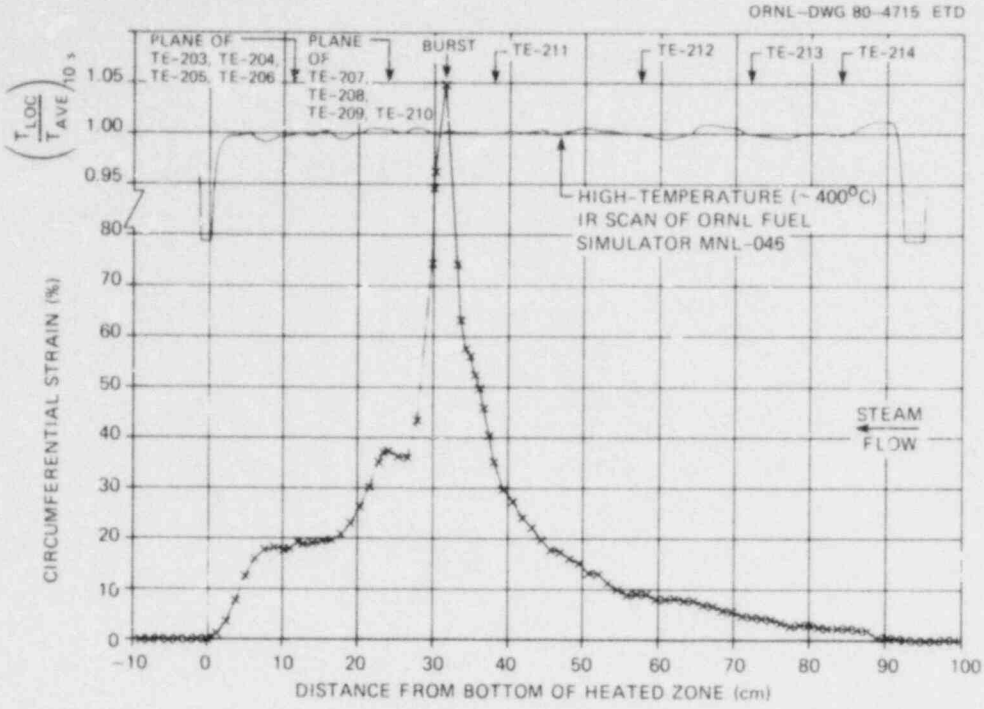

Fig. 2.75. Deformation profile of SR-57.

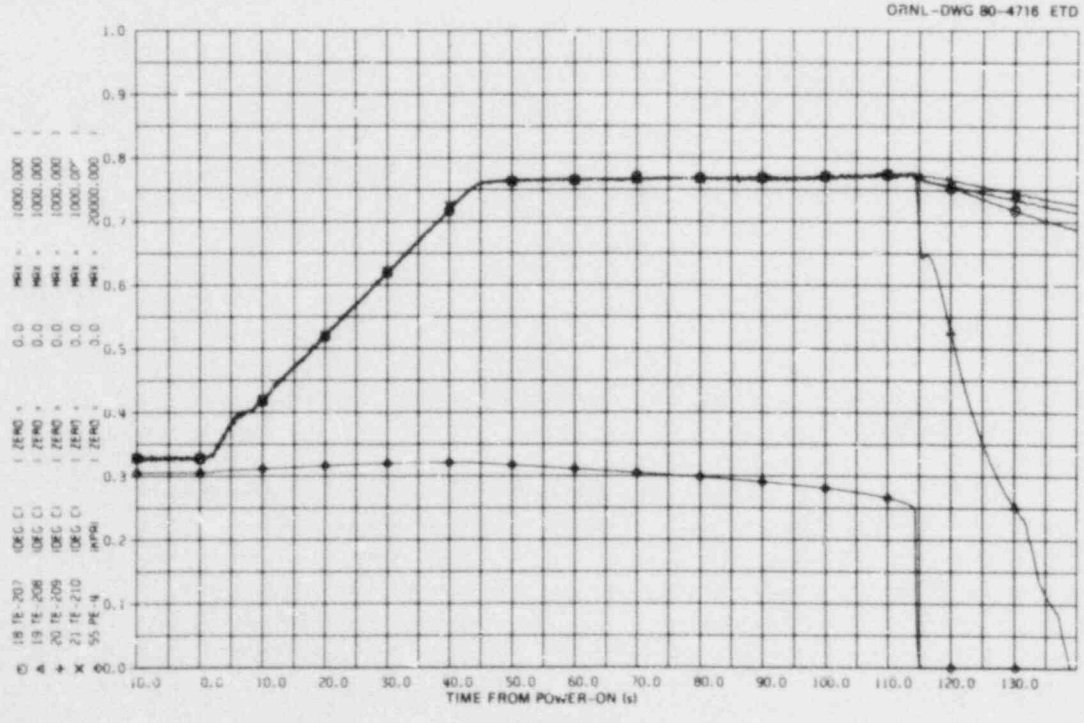

Fig. 2.76. Temperatures measured at 24-cm elevation in SR-57.

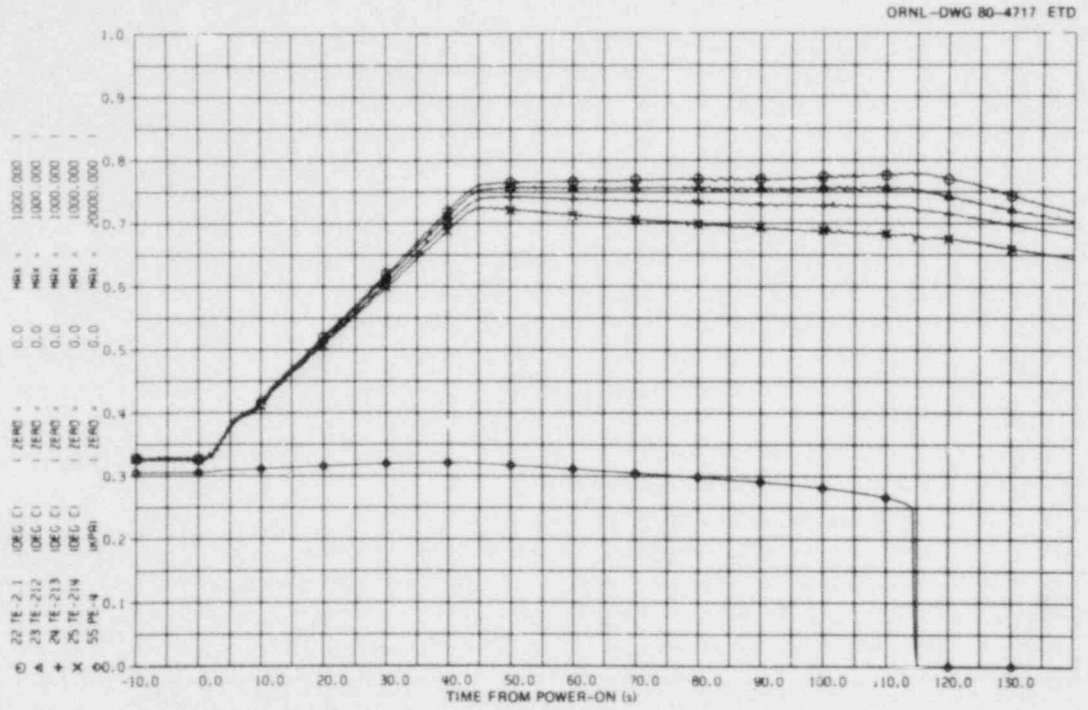

Fig. 2.77. Temperatures measured at the four upper instrumented locations in SR-57.

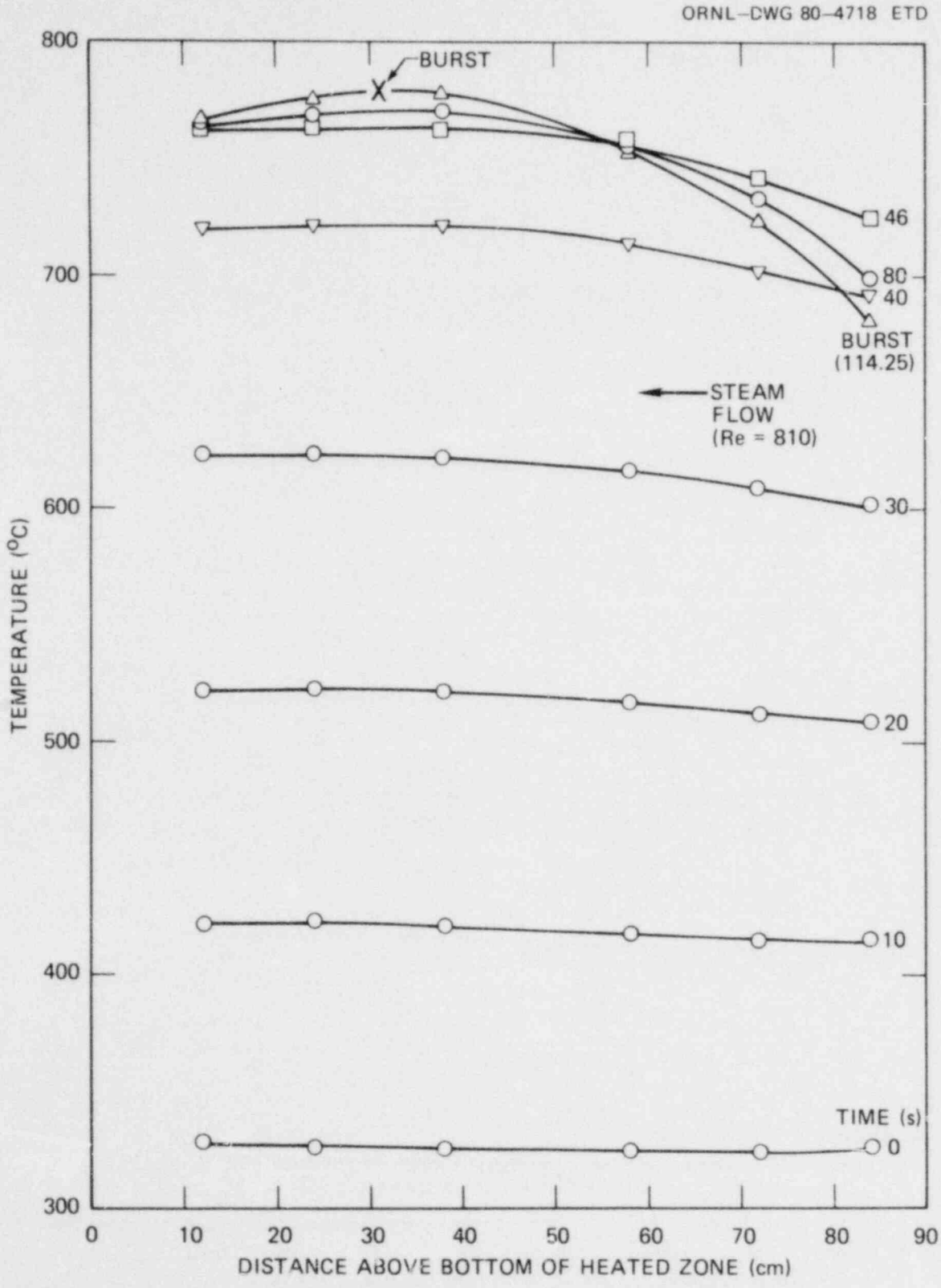

Fig. 2.78. Axial temperature distribution in SR-57.

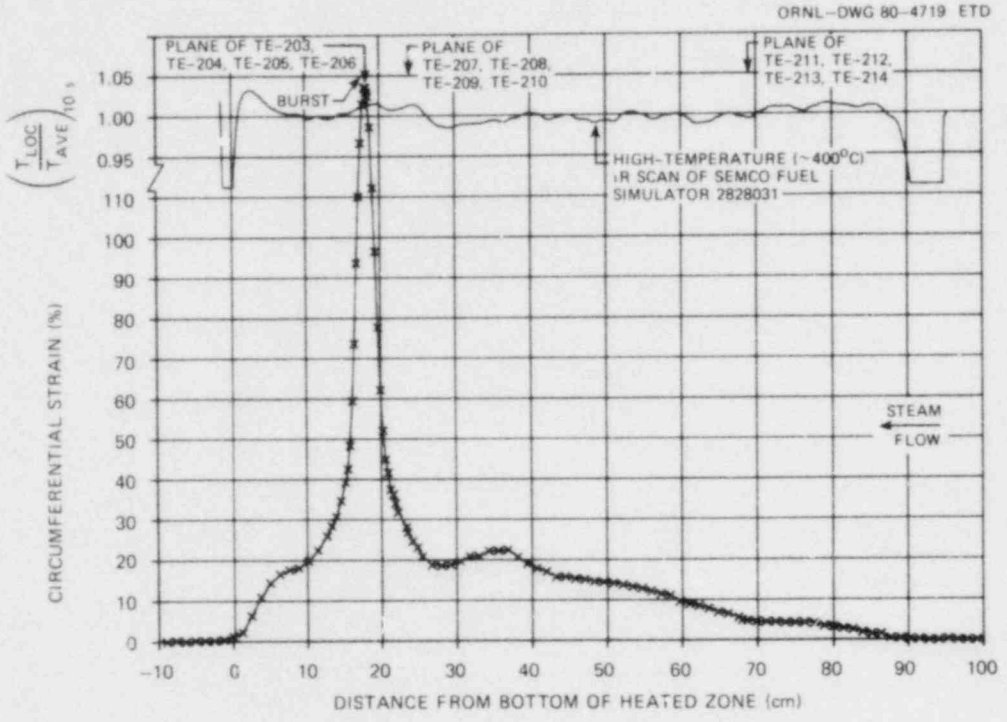

Fig. 2.79. Deformation profile of SR-58.

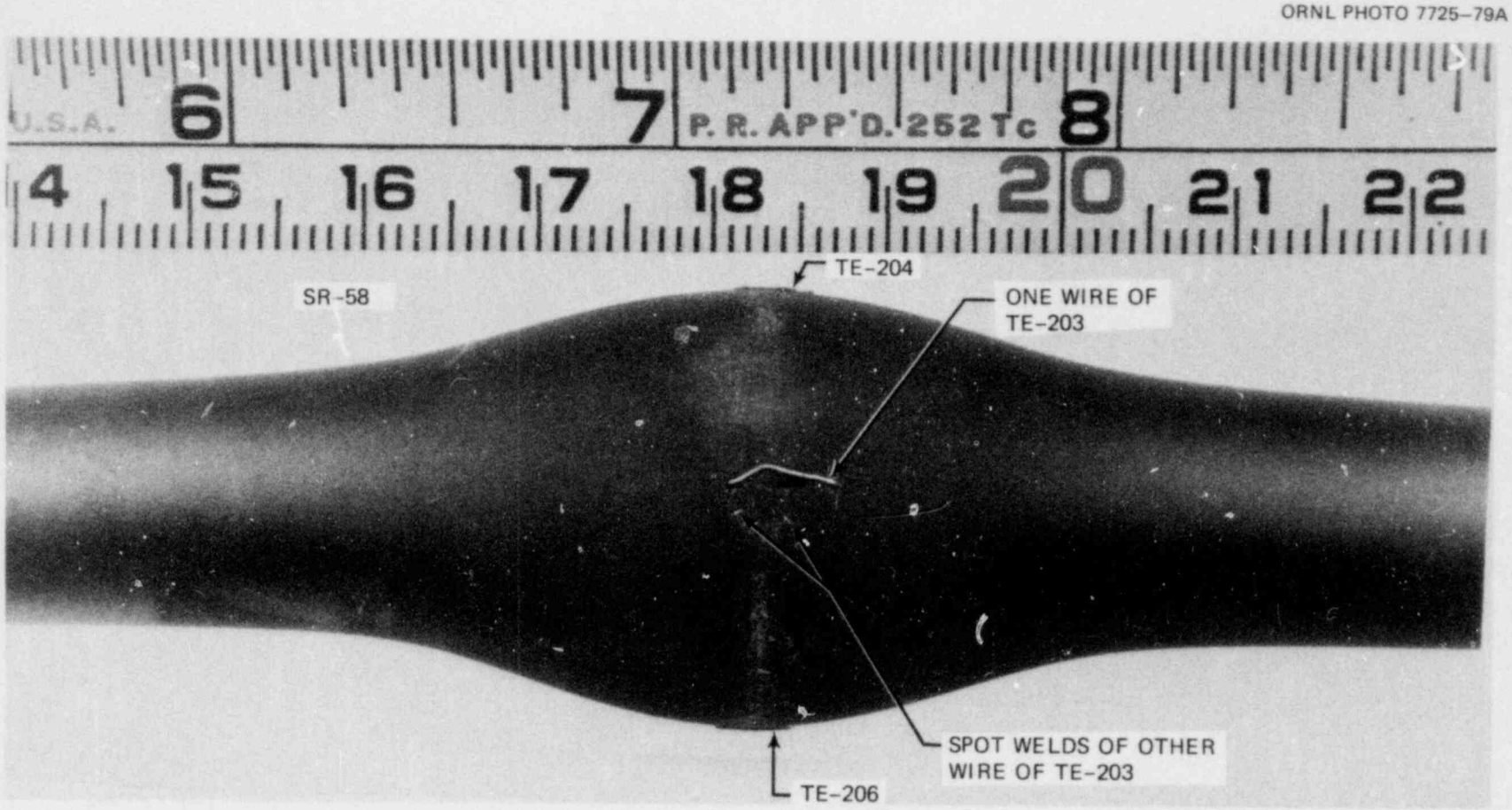

Fig. 2.80. Burst in SR-58 with thermocouple wires attached.

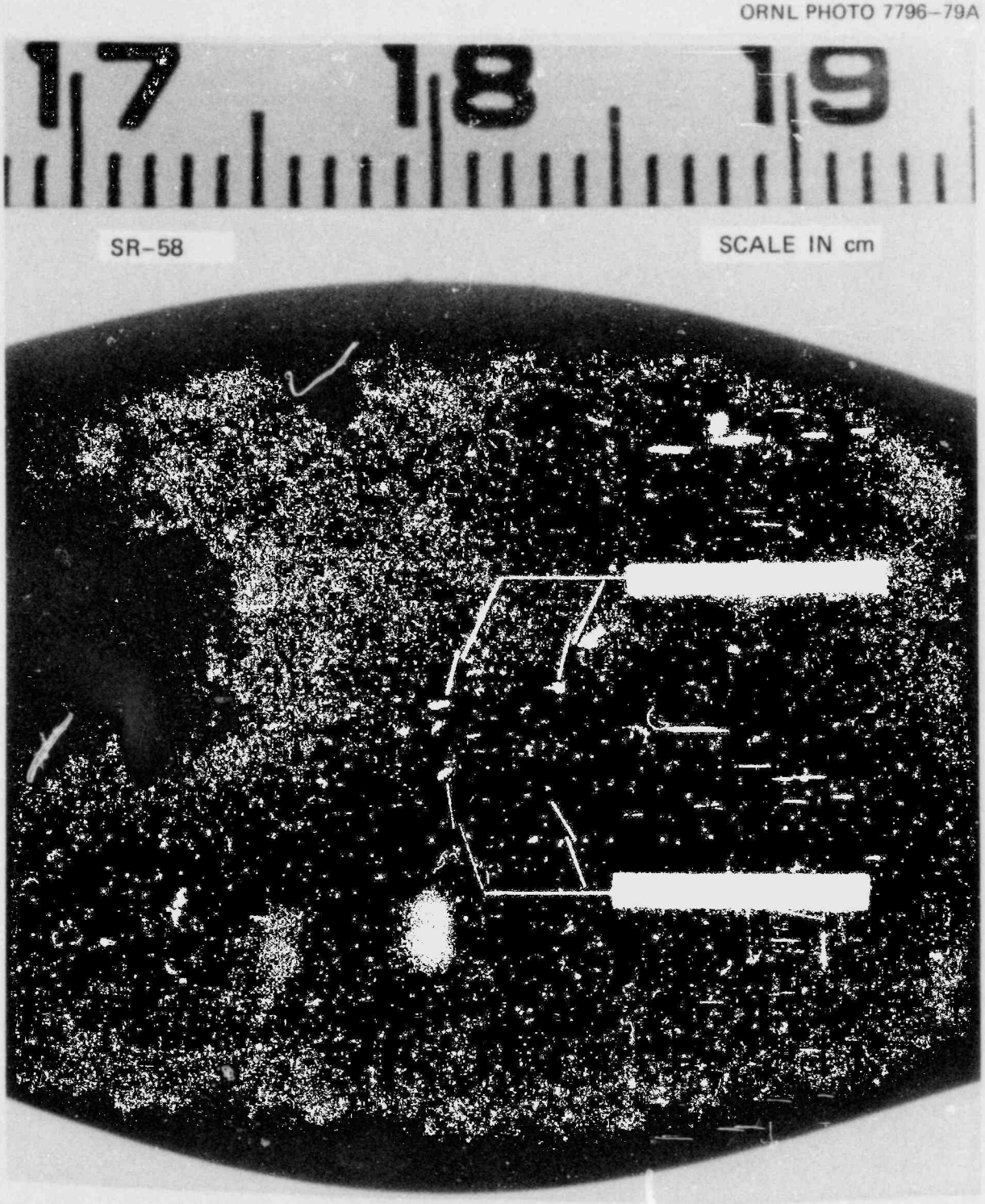

Fig. 2.81. Bursts in SR-58 with thermocouple wires removed.

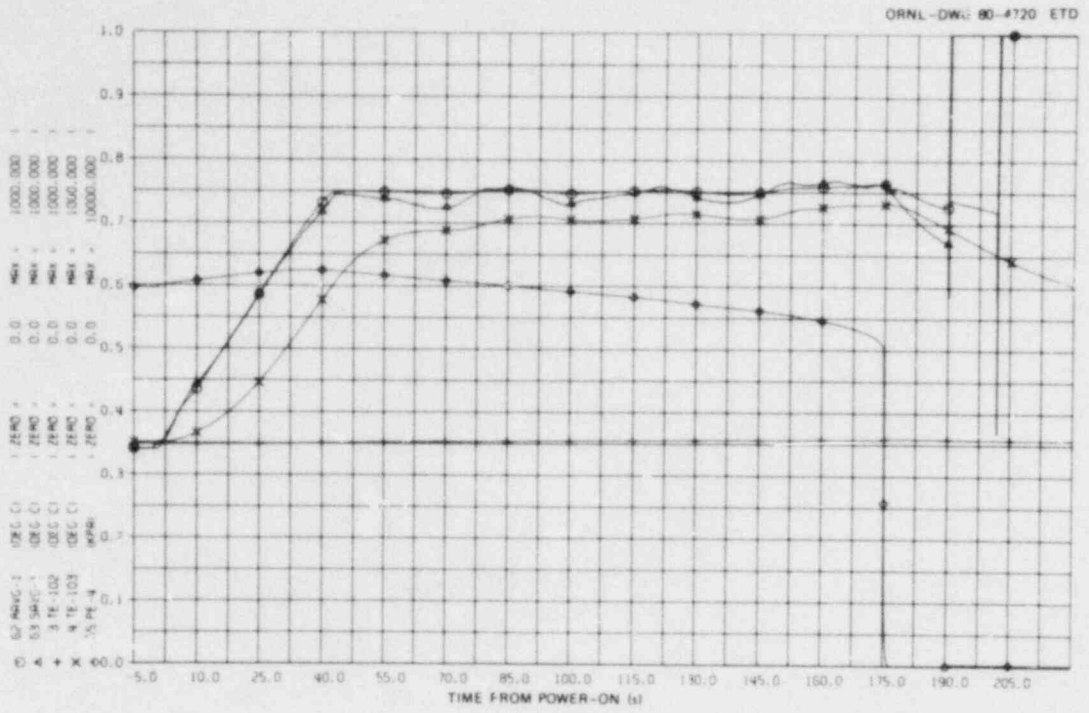

Fig. 2.82. Rod and shroud average temperatures, simulator pressure, and steam inlet and outlet temperatures in SR-58.

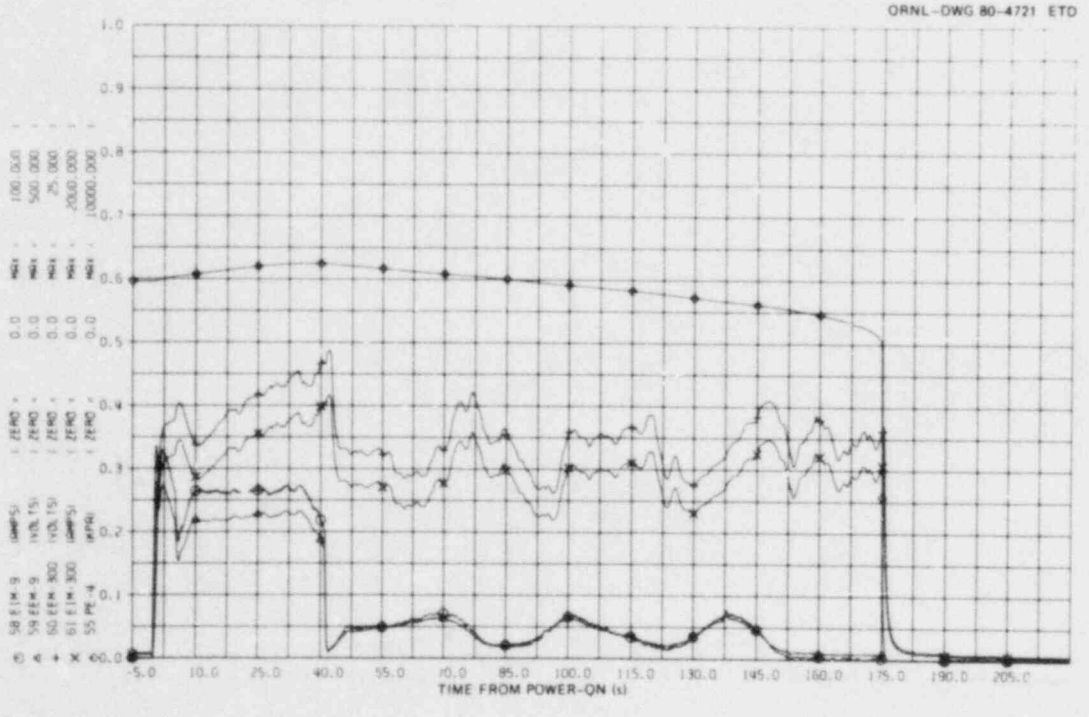

Fig. 2.83. Electrical power parameters in SR-58.

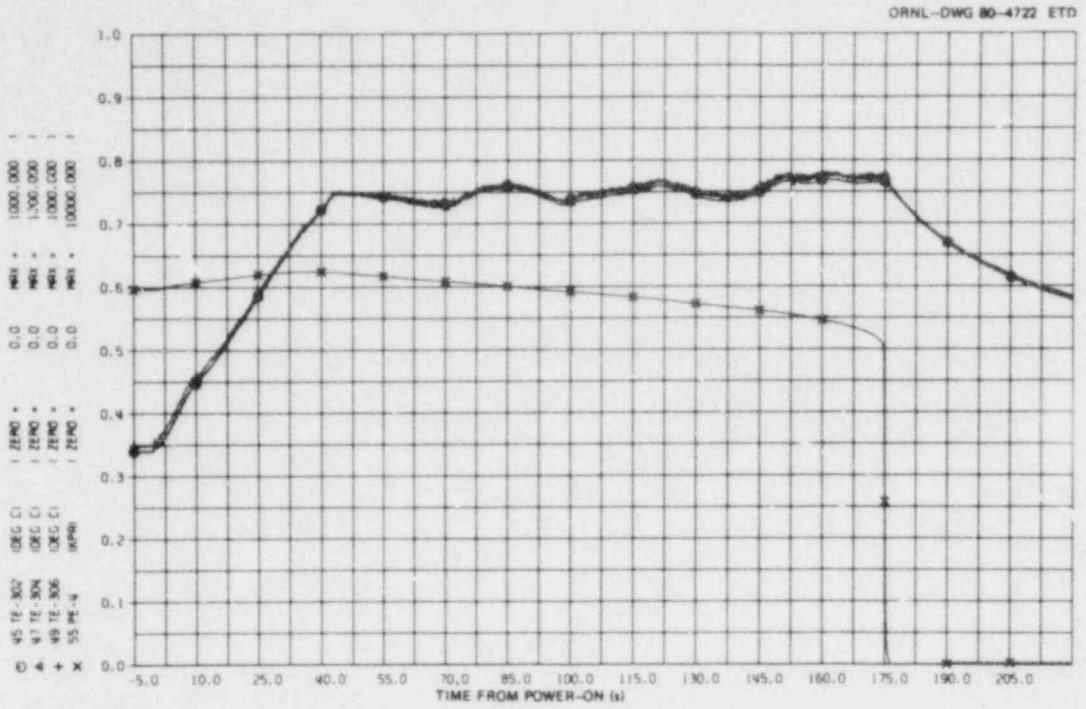

Fig. 2.84. Shroud axial temperature distribution in SR-58.

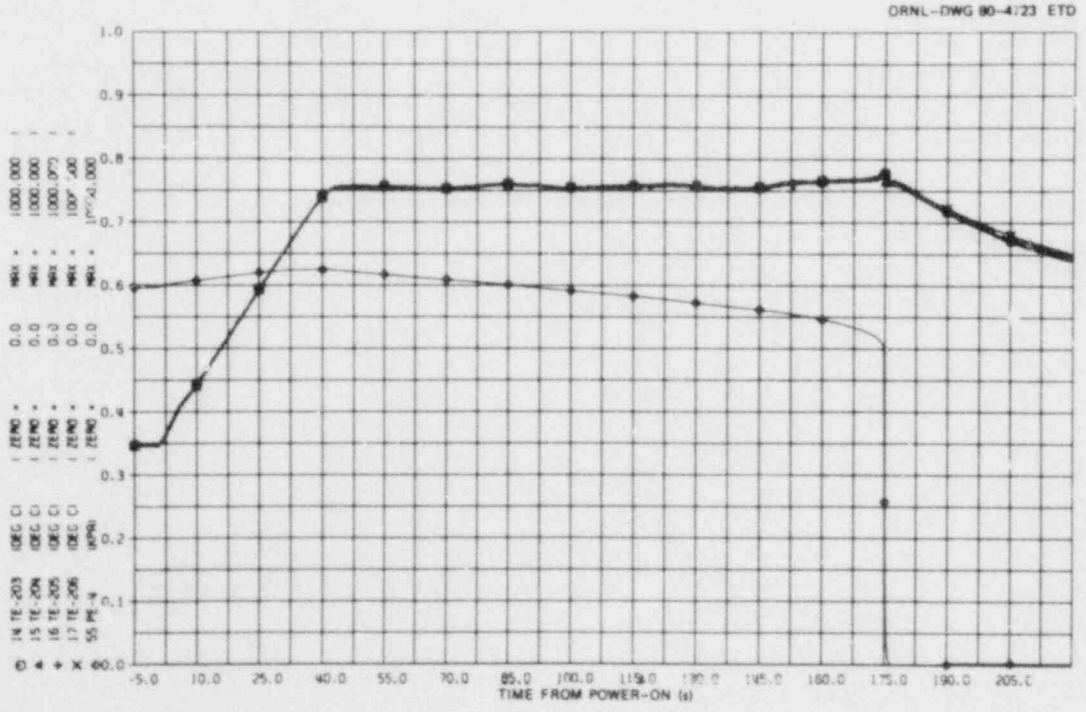

Fig. 2.85. Temperatures measured at burst elevation in SR-58.

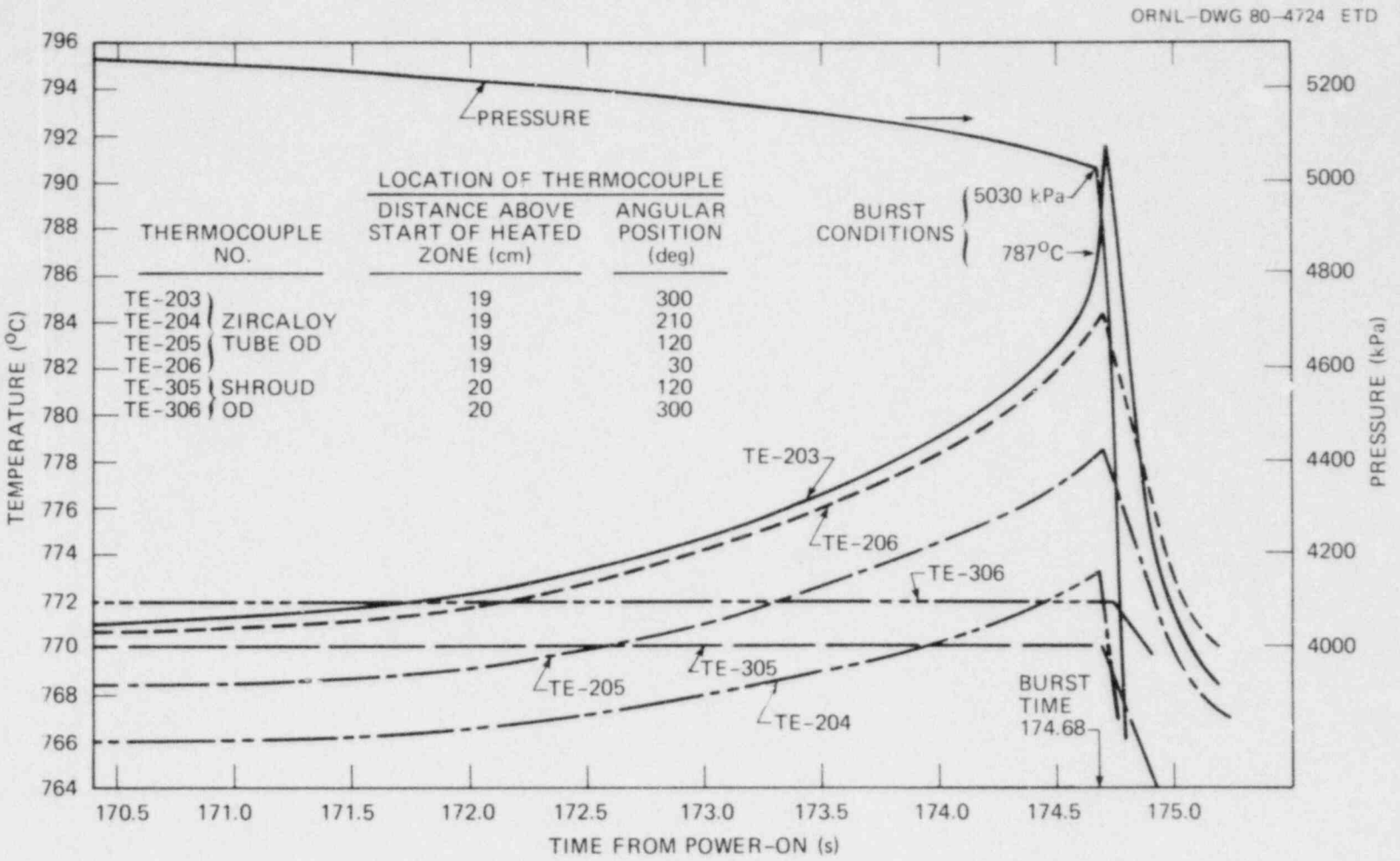

Fig. 2.86. Expanded-scale plot of temperature at burst elevation in SR-58.

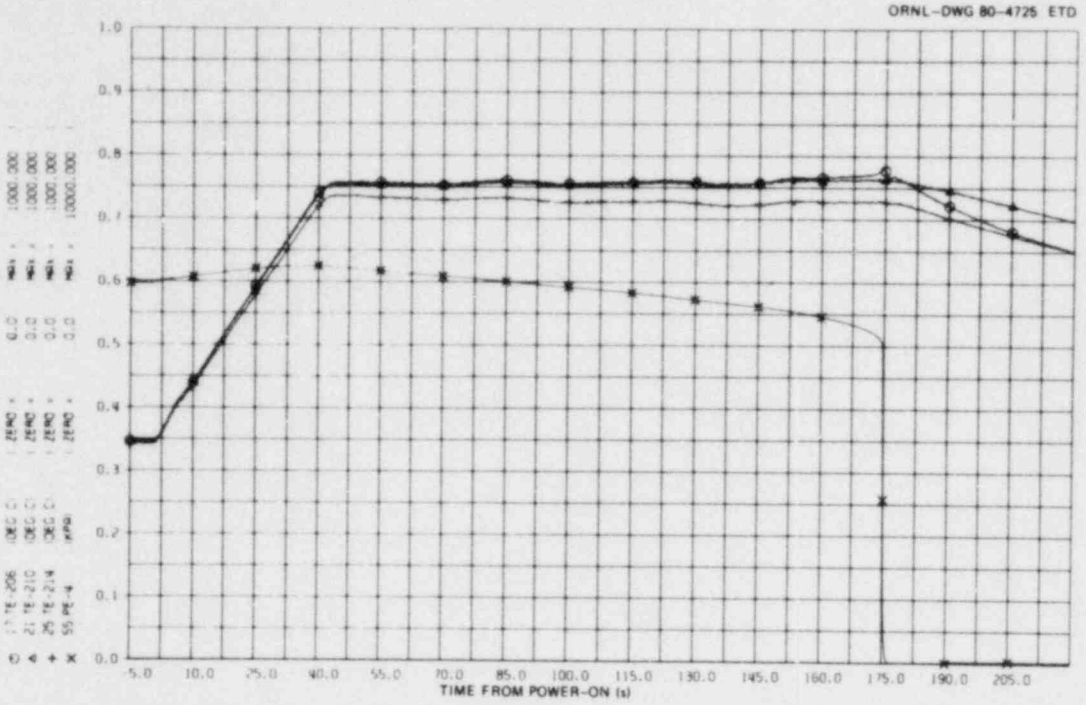

Fig. 2.87. Rod axial temperature distribution in SR-58.

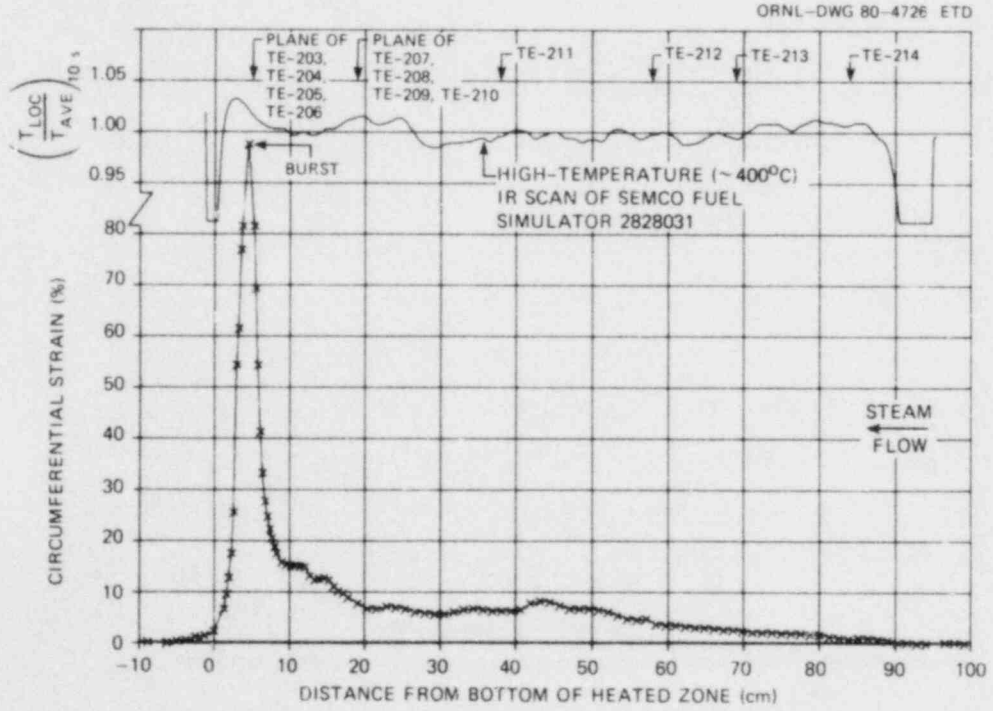

Fig. 2.88. Deformation profile of SR-63.

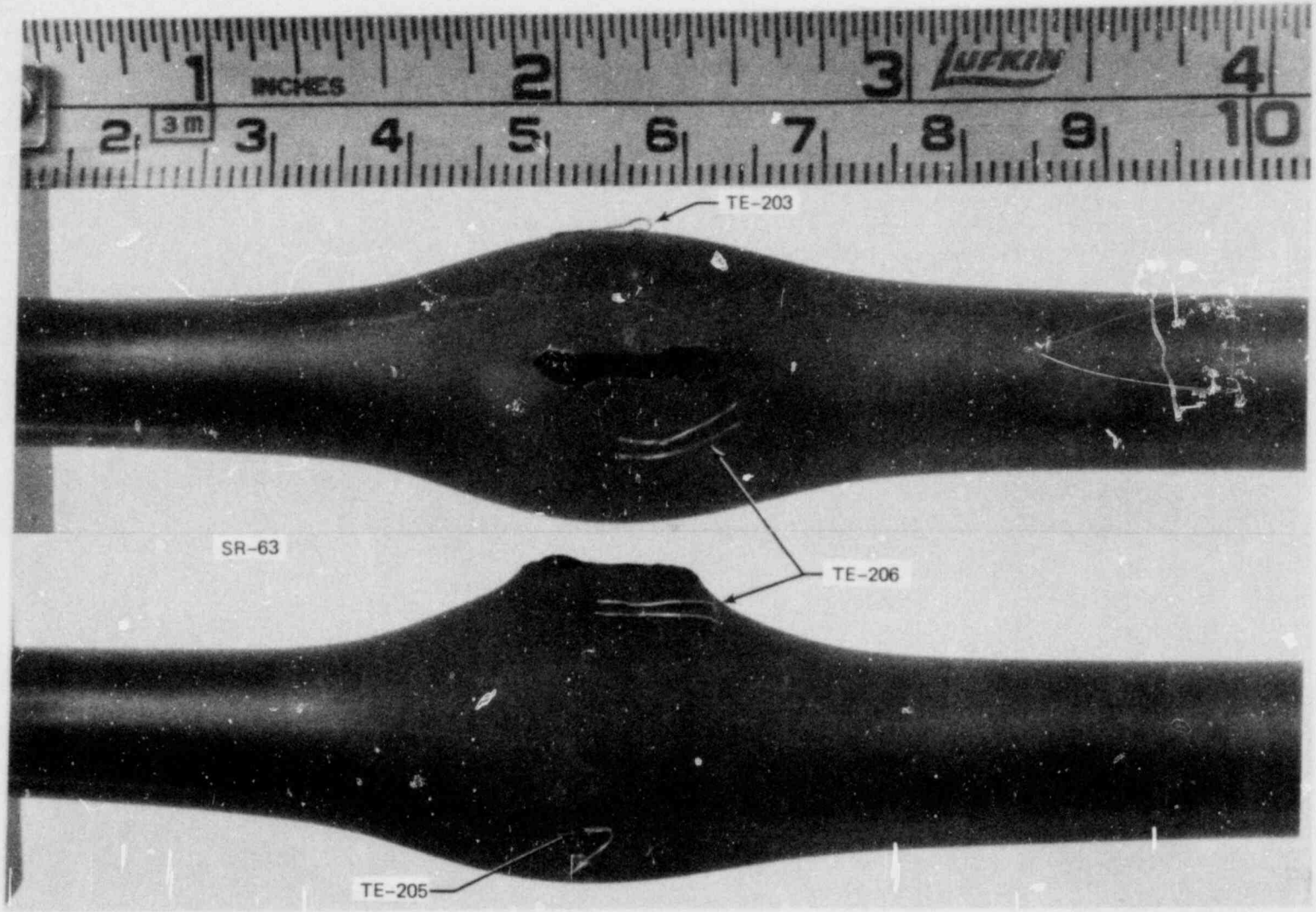

Fig. 2.89. Burst in SR-63.

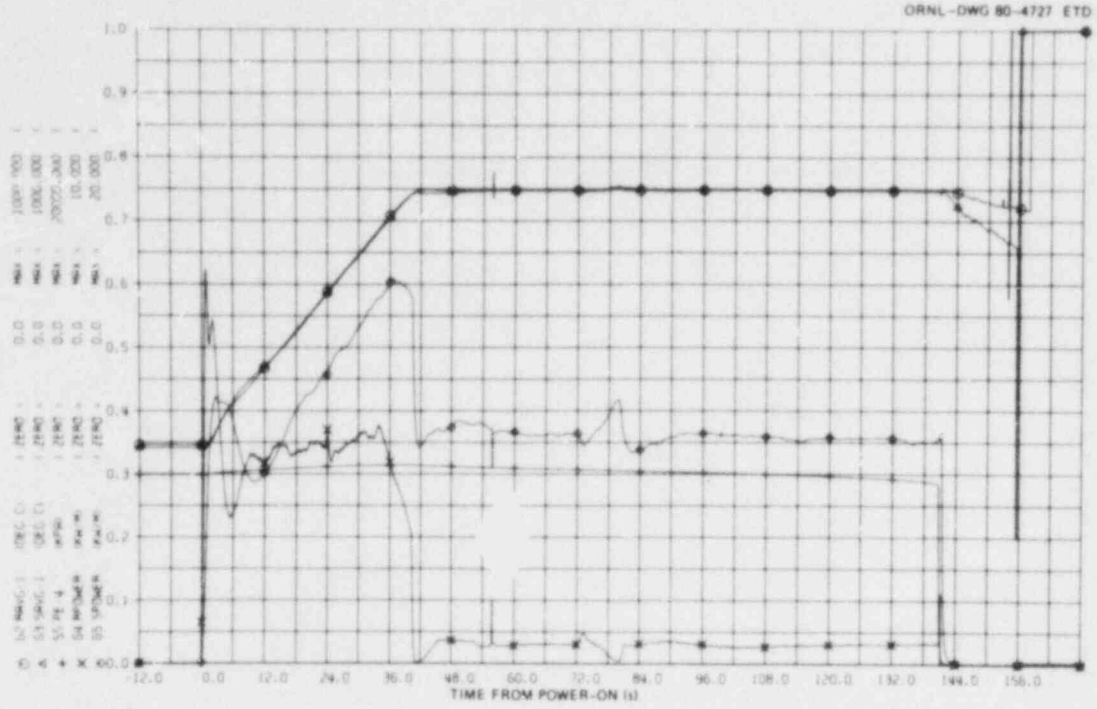

Fig. 2.90. Rod and shroud average temperatures and power levels in SR-63.

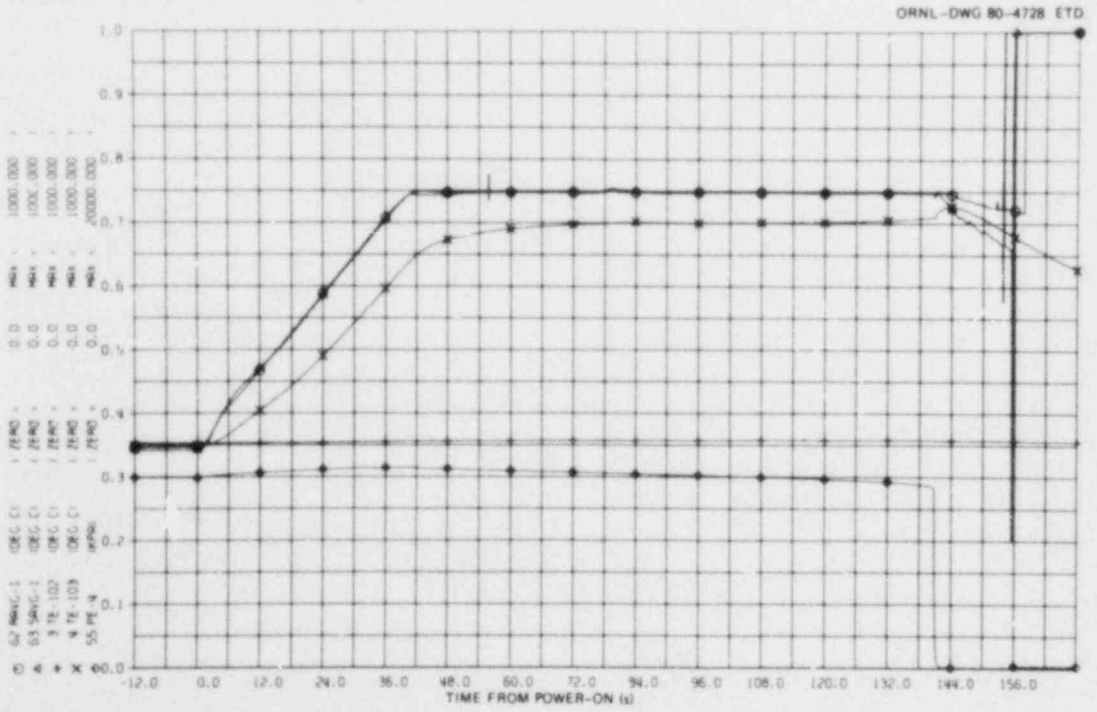

Fig. 2.91. Comparison of steam inlet and outlet temperatures with rod and shroud average temperatures in SR-63.

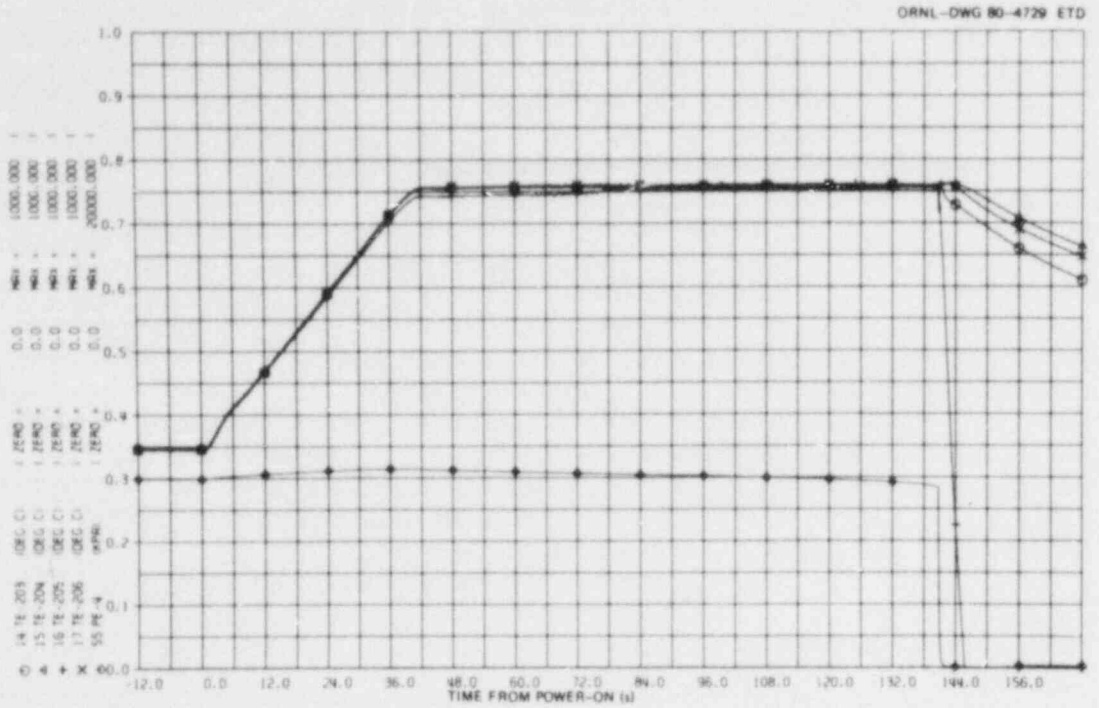

Fig. 2.92. Temperatures measured at burst elevation in SR-63.

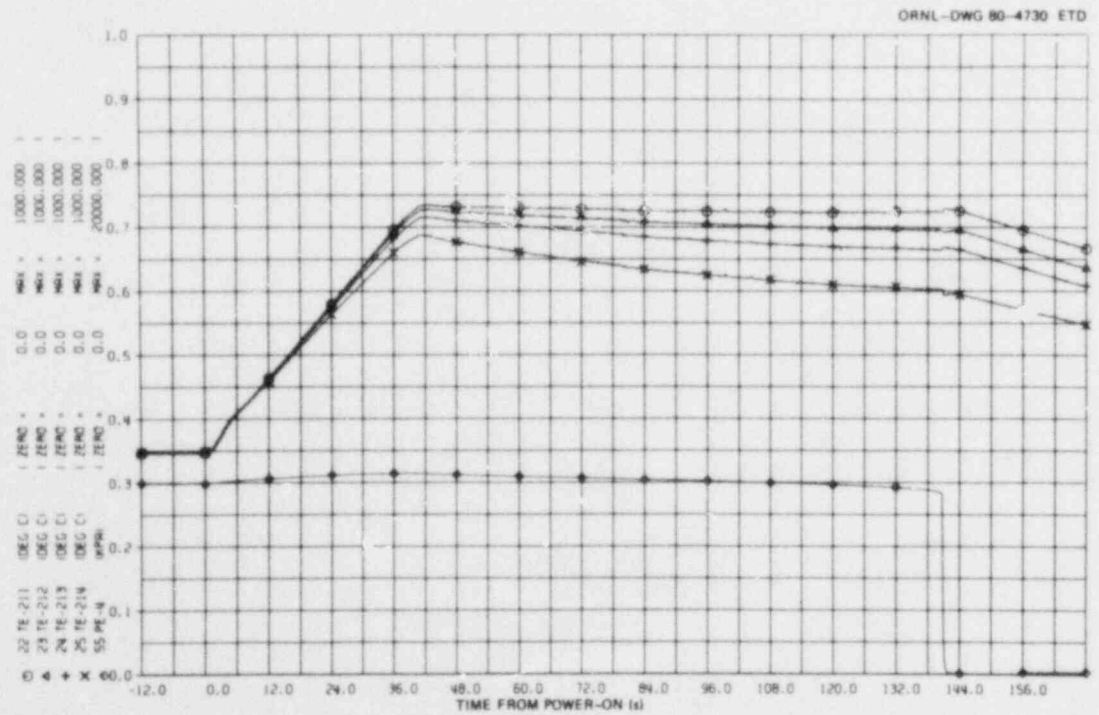

Fig. 2.93. Temperatures measured along upper portion of rod in SR-63.

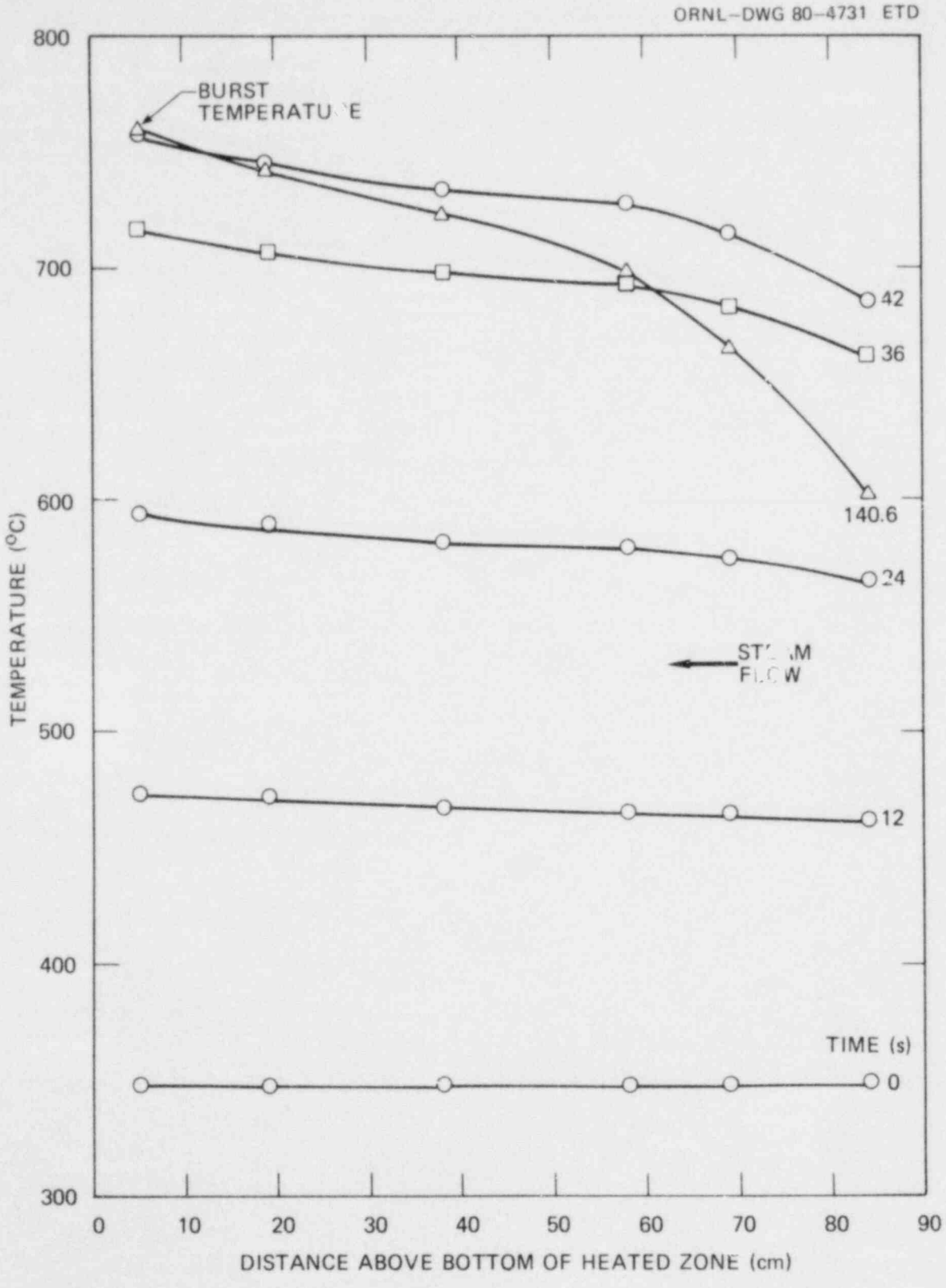

Fig. 2.94. Axial temperature distribution in SR-63.

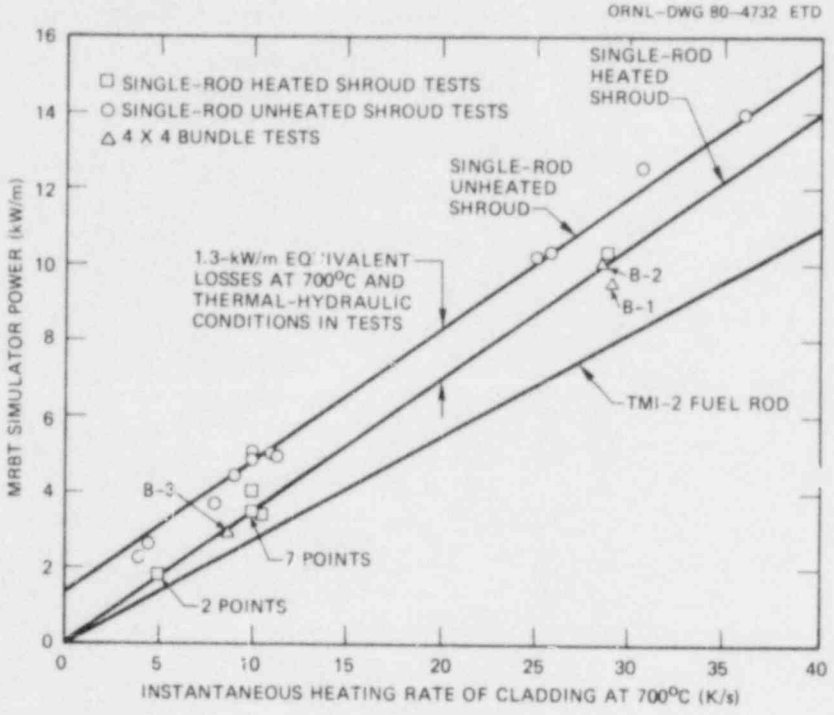

Fig. 2.95. Comparison of fuel simulator power requirements in heated and unheated shroud tests.

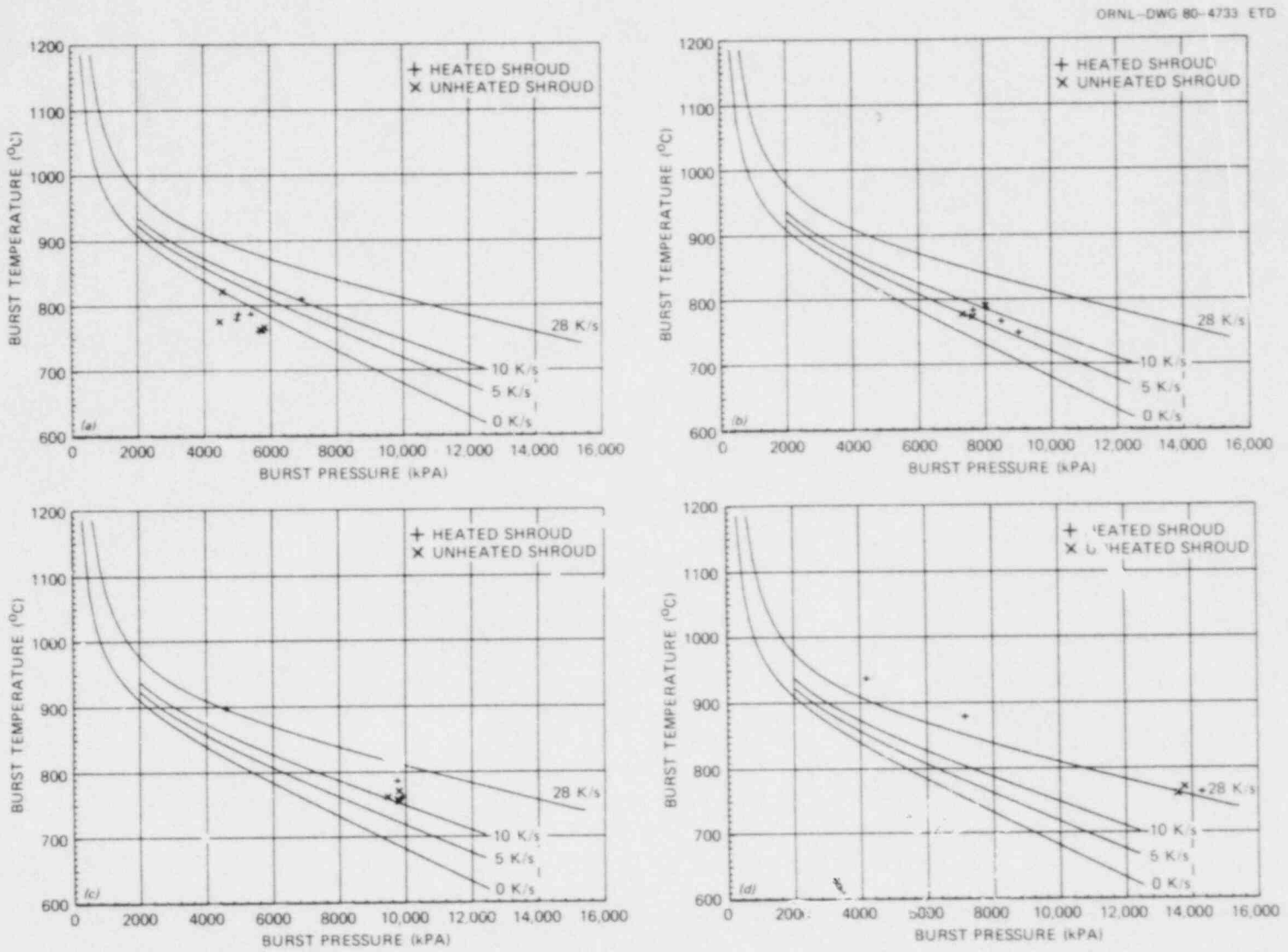

Fig. 2.96. Comparison of ORNL correlation with heated and unheated shroud test results for heating rates of (a) ~0 K/s, (b) 5 K/s, (c) 10 K/s, and (d) 28 K/s.

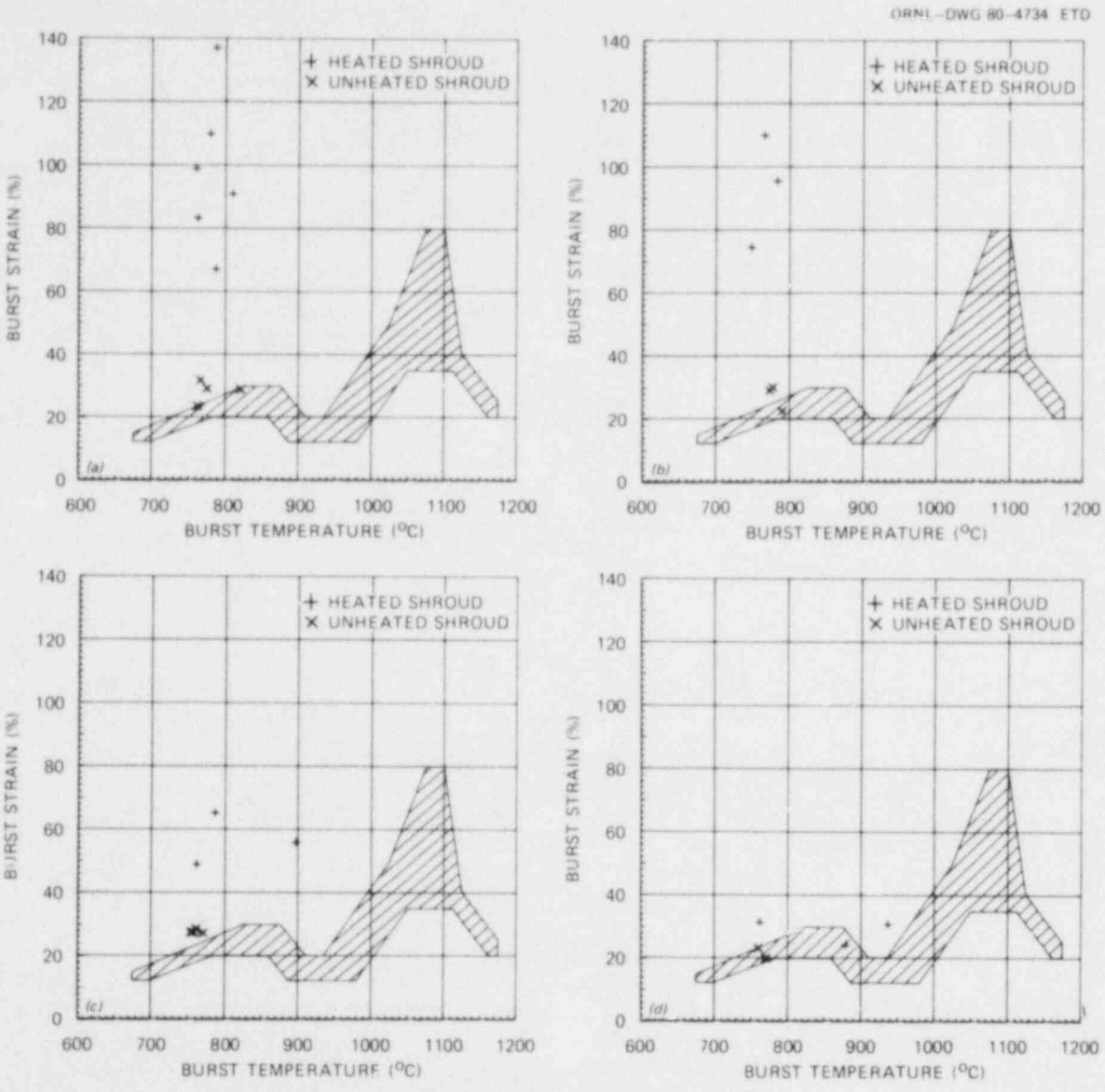

Fig. 2.97. Comparison of burst strain in heated and unheated shroud tests for heating rates of (a) ~0 K/s, (b) 5 K/s, (c) 10 K/s, and (d) 28 K/s.

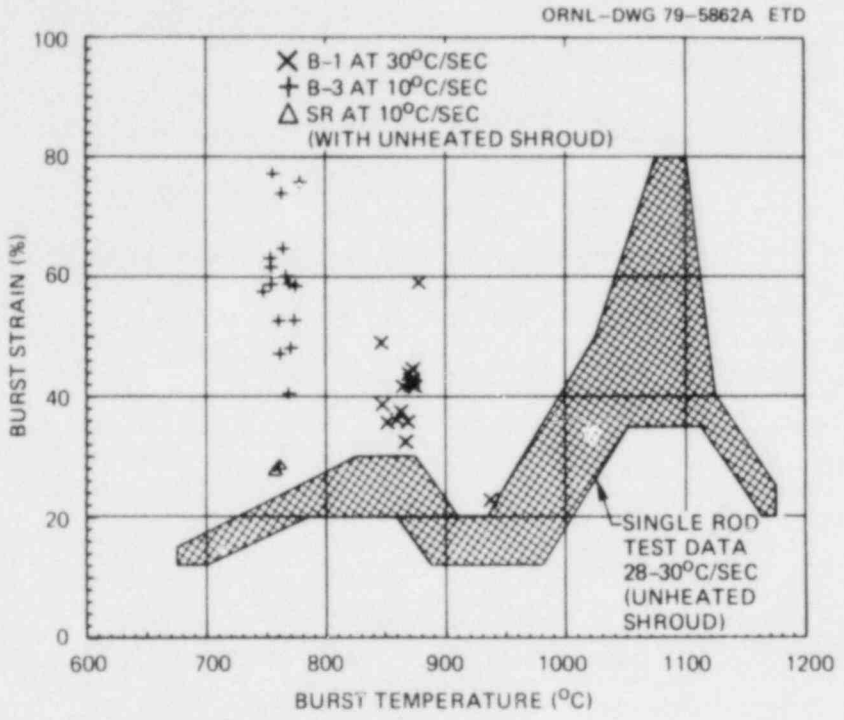

Fig. 2.98. Comparison of B-1 and B-3 burst strains with single-rod unheated shroud test data.

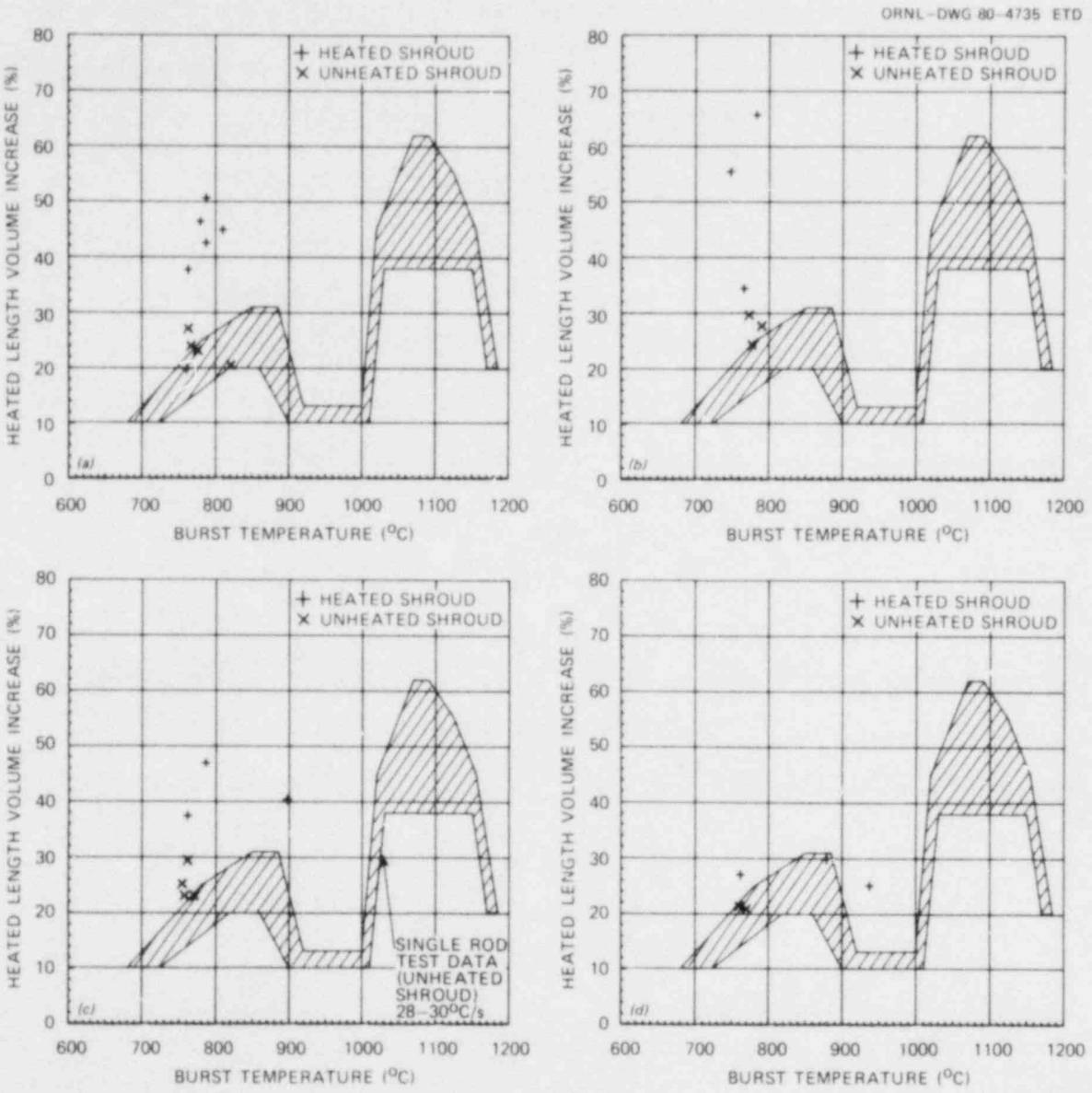

Fig. 2.99. Comparison of heated length volume increase in heated and unheated shroud tests for heating rates of (a) ~0 K/s, (b) 5 K/s, (c) 10 K/s, and (d) 28 K/s.

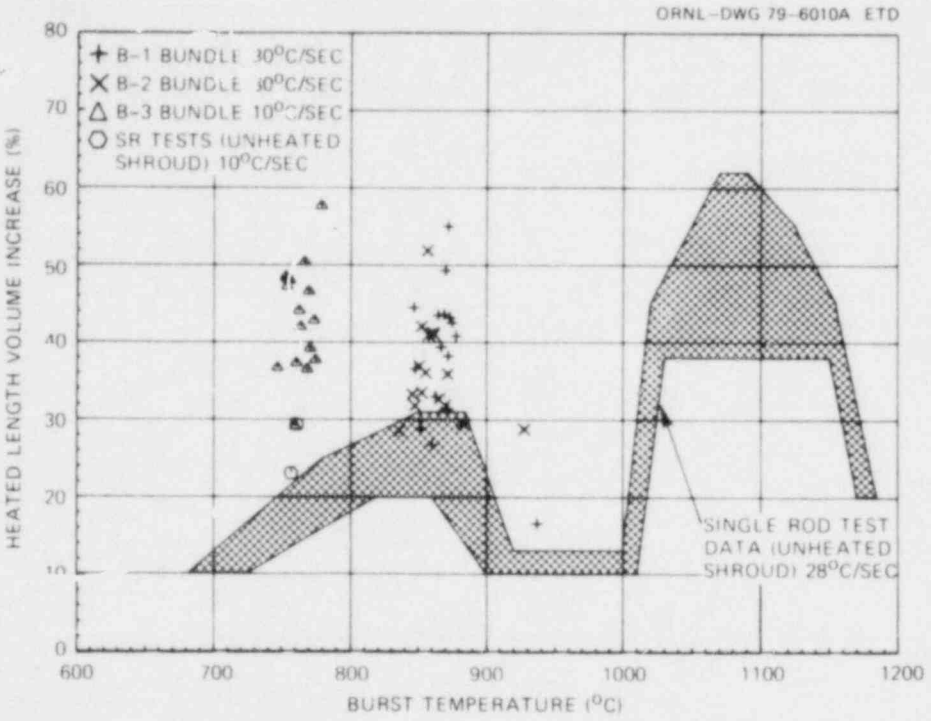

Fig. 2.100. Comparison of volume increase of B-1, B-2, and B-3 tubes with single-rod unheated shroud test data.

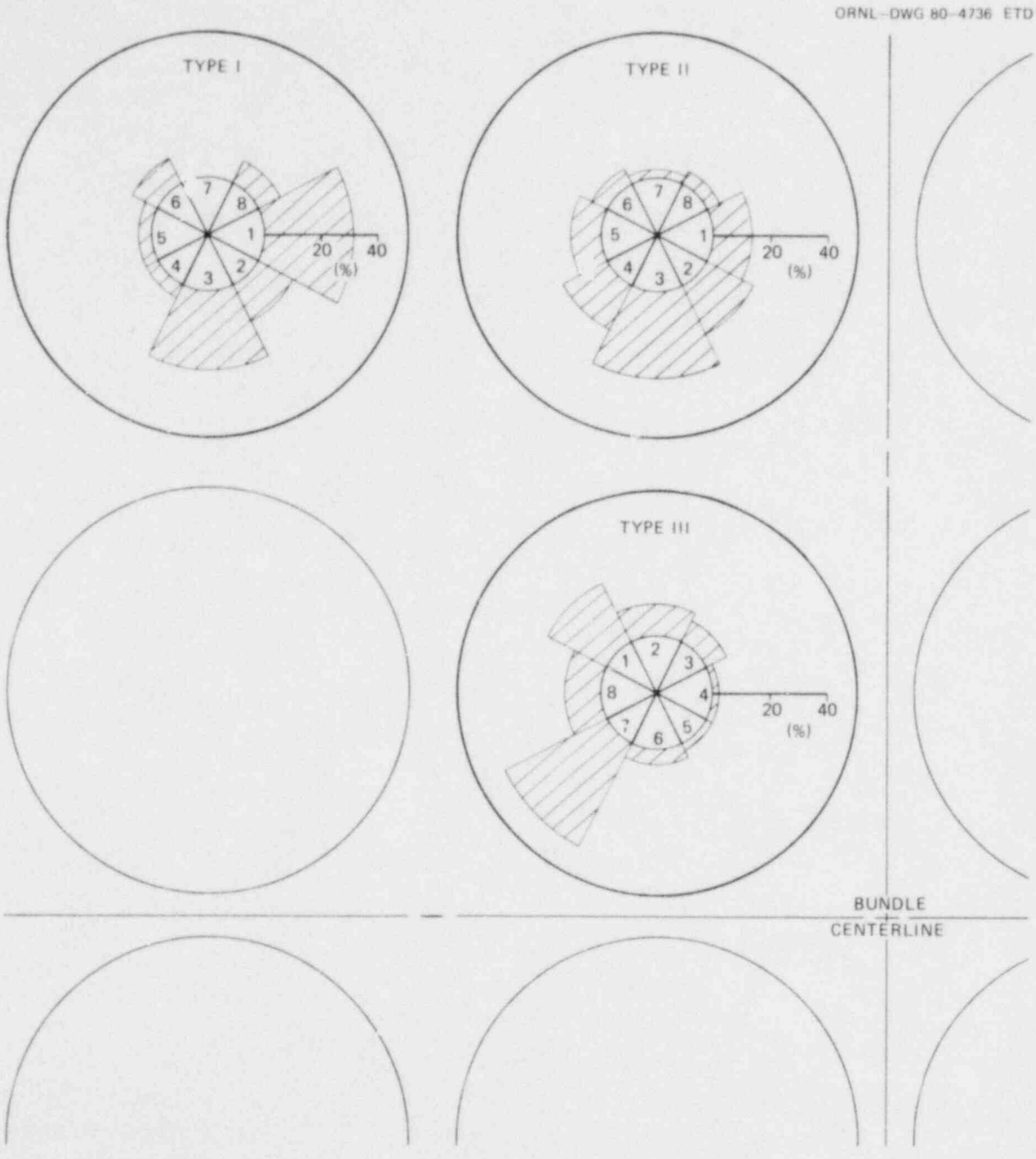

Fig. 2.101. Distribution of maximum wall thinning observations by view sector for the three rod types in B-3 test array.

3. DEVELOPMENT AND PROCUREMENT

3.1 Infrared Scanning Evaluation of Fuel Simulators and Fuel Pin Simulators

R. W. McCulloch S. D. Snyder
J. L. Crowley A. W. Longest

3.1.1 Summary

Significant temperature profile analyses of fuel simulators* and fuel pin simulators were completed during this reporting period. The last 34 ZrO_2-coated fuel simulators for bundle B-5 were given 10-s IR characterization scans for quality ranking, and the determination was made that the ZrO_2 coating process significantly influenced the transient surface temperature as indicated by the IR scans. All four quadrants of two ZrO_2-coated simulators were IR-scanned at various ramp rates to establish additional baseline information on their performance prior to their assembly into fuel pin simulators for bundle B-5. An uncoated fuel simulator (MNL-085) used in several recent single-rod tests, was given 10-s transient scans on all four quadrants as a surface uniformity check. The circumferential transient temperature uniformity was determined to be excellent for fuel simulators fabricated in the fuel pin simulators development laboratory. Two fuel pin simulators, one containing an uncoated fuel simulator and one containing a ZrO_2-coated fuel simulator, were given a series of tests to determine surface transient temperature profile uniformity. In addition, fuel pin simulators manufactured by the TOSHIBA Corporation (Tokyo, Japan) were received and

*To avoid misconceptions and confusion, we use the following terminology in our reports. By "fuel simulator," often abbreviated as FS (or FSs if more than one), we mean a long, slender, rod-type device that uses electrical energy to simulate the heating produced in a stack of nuclear fuel pellets. By "fuel pin simulator," often abbreviated as FPS or FPSs, we mean a composite assembly that consists of "Zircaloy fuel cladding" and a "fuel simulator." Thus, in the MRBT, "fuel pin simulators" are distinctively different (more inclusive) from "fuel simulators," whereas in other programs they are identical. Frequent use will be made of the term "simulator" without descriptive modifiers; in these situations the context will make clear which modifier is implied.

given nondestructive analysis. These simulators were ordered to the same specifications as those used by JAERI in cladding deformation studies, which are very similar to those of the MRBT Program at ORNL. One of the five was then destructively analyzed to obtain additional information, and a meeting was held with a TOSHIBA Corporation representative regarding the two simulator designs being tested in the two countries.

3.1.2 IR scan evaluation of ZrO_2 coated fuel simulators for bundle B-5

During this report period, the last 34 of the group of 75 fuel simulators prepared for possible use in B-5 were given the normal first-quadrant 10-s IR characterization scan after being ZrO_2 plasma sprayed. Most of the fuel simulator IR scans before and after coating were reasonably comparable in quality; but about one-third showed cyclic, step, or other significant changes in the axial profile after being coated. The profile abnormalities resulted from variables in the plasma-spraying process. Most of the simulators having these profile abnormalities were stripped of the nonuniform coating and recoated in an attempt to correct the defects; subsequent scans indicated that most defects were corrected. Figure 3.1 compares 10-s transient IR scans (all at ~480°C) of fuel simulator MNL-036 (1) in noncoated condition, (2) with a defective coating, and (3) after stripping and recoating.

Two of the ZrO_2-coated fuel simulators for B-5, MNL-026, and MNL-064 were IR-scanned at several different ramp rates and in four quadrants at the normal 40 K/s ramp rate (10-s IR scan). The four-quadrant scans of these two fuel simulators indicated that there were no significant differences in the axial temperature profiles for the four quadrants and that the coating was reasonably uniform circumferentially.

3.1.3 Evaluations of circumferential temperature uniformity

Uncoated simulator MNL-085 was given 10-s transient IR scans on each of the four quadrants. Figure 3.2 compares the four profiles and shows that the circumferential nonuniformity is insignificant. Even minor axial profile variations appear the same in all four quadrants. The

sheath circumferential temperature variations indicated by the four scans were within about 2°C. This difference is most likely due to variations in supply voltage, starting temperature, and contact resistance from scan to scan, not actual simulator variations.

3.1.4 Evaluation of fuel pin simulators containing coated and uncoated fuel simulators

Fuel pin simulator SR-55 (containing uncoated fuel simulator MNL-046) and fuel pin simulator SR-59 (containing ZrO_2-coated fuel simulator MNL-043) were given 10-s transient IR scans at 40 K/s ramp rates in four quadrants as well as 10 and 5 K/s scans in the first quadrant and two 35-s scans at 10 K/s with 30- and 105-s steady-state "hold" periods at the end of the transient. No significant differences in temperature profiles were noted between fuel pin simulators with coated fuel simulators and those with uncoated fuel simulators. However, the circumferential temperature uniformity of both fuel pin simulators was very poor compared with that of the fuel simulators. A maximum circumferential variation of ~26°C between the second and third quadrants can be determined from Fig. 3.3, which compares temperature profiles of fuel pin simulator SR-59 in the four quadrants. Axial variations from quadrant to quadrant are also pronounced. These data suggest that the fuel simulator is not centered within the Zircaloy clad of the fuel pin simulator. Although tolerances are small (on the order of 0.13 mm), the circumferential gap variations are thought to be the cause of the profile distortion. Although the fuel simulator might tend to stay centered better if the fuel pin simulator were tested in a vertical position, scanning equipment limitations permit scanning in only a horizontal position.

A comparison of the scans of SR-59 at the different ramp rates showed that a transient ramp rate of 40 K/s gave a total axial temperature profile variation of 23°C at 419°C average cladding temperature (5.5%). A 10 K/s ramp produced an 11°C (2.6%) temperature profile variation, and the 5 K/s ramp rate scan produced variations of only about 7°C (1.7%). Axial variations were reduced to 6°C (1.4%) when 30- to 105-s steady-state "hold periods" were included at the end of the transient.

A comparison of the scans of fuel pin simulator SR-55 at the different ramp rates is shown in Fig. 3.4. Similar IR scans of fuel simulator MNL-046, which was used in fuel pin simulator SR-55, are shown in Fig. 3.5. The expected smoothing out of the axial profile variations with decreasing power level is evident in both figures. A power of about 0.7 kW/m was required to maintain the "hold" temperature on both the fuel pin simulator and the fuel simulator. Figure 3.4 shows that the heating rate of 40 K/s (power ~15.5 kW/m) on this typical fuel pin simulator for single-rod testing gave a total first-quadrant axial temperature profile variation (over most of the heated zone length) of ~15°C, the heating rate of 10 K/s (power ~3.5 kW/m) produced ~8°C temperature profile variation, and the 5 K/s heating rate (power ~1.9 kW/m) produced ~6°C temperature profile variation. Axial variations were reduced to ~5°C when 30- and 105-s "hold periods" were included at the end of the 10 K/s transient. The power level of ~0.7 kW/m required for these "hold periods" with the fuel pin simulator in a horizontal position in air is considerably greater than the power required in some of our recent 760°C creep-rupture tests employing a heated shroud (see Sect. 2.2). Thus, temperature profile variations do not depend on heating rate alone but rather on the particular combination of power level and heat losses (to coolant and surroundings) producing the heating rate. Other factors affecting temperature profile variations include, of course, the uniformity of the initial temperature distribution, uniformity of heat losses, and effects of the cladding deformation process on heat transfer.

3.1.5 Evaluation of JAERI fuel pin simulators

Five fuel pin simulators were received from a Japanese manufacturer for evaluation. These simulators were ordered from the same supplier (TOSHIBA Corporation) and to the same specifications as those used by JAERI in their cladding deformation studies. Evaluation included IR scanning, radiographic analysis, electrical tests, and dissection of one of the five fuel pin simulators.

All five simulators were scanned under a variety of conditions similar to those used for scanning SR-55 and SR-59. In addition, one

was scanned at 10 and 5 K/s in three quadrants (outer thermocouple attachments to the clad prohibited scanning for the fourth quadrant).

Figures 3.6 through 3.11 summarize the scanning results, typical of all five simulators. Figure 3.6(a) was intended to be a 1-s transient to a temperature level of ~80°C, using the same power level as that employed on ORNL fuel pin simulator transient IR scans. However, the design of the Japanese simulator was such that a 2- to 4-s lag occurred from the time of application of power to the start of the temperature transient. This characteristic precluded achieving results comparable to those of the normal 1-s transient scan. The procedure was modified to include a steady-state scan at ~65°C [Fig. 3.6(b)] as the starting point to produce a level of ~80°C in the 1-s transient shown in Fig. 3.6(c). This resulted in a transient that could be qualitatively compared with the ORNL 1-s transient scans.

Figure 3.6(d) shows the 1-s transient obtained by heating the Zircaloy tube instead of the internal fuel simulator. It indicates a significant degree of contact variation between the Zircaloy cladding and the inside pellets. Dissection of a fuel pin simulator revealed that Al_2O_3 pellets were used to contain six equally spaced 0.6-mm-diam W-3% Re wires which ran parallel to the axis with a radial gap of ~0.06 mm between the pellets and the clad ID. The large difference in surface area between the heat-generating W-Re wires and the Zircaloy cladding, combined with the gas gaps between the wires and pellets and between the pellets and cladding, resulted in the observed time lag in the transient tests. The relatively large axial temperature variations, especially pronounced at the heating rate of 40 K/s, are thought to be caused by nonuniform gas gaps between the pellets and the cladding. As in the case of the ORNL fuel pin simulators the scanning was done with the simulators in a horizontal position.

Figures 3.7 through 3.9 show 40, 10, and 5 K/s transient IR scans, respectively. The axial temperature variations were ~60°C (15%) for the 40 K/s scan but reduced to 30 and 12°C (6 and 3%) for the 10 and 5 K/s ramps, respectively. The axial variations remained at about this level for the transient plus steady-state tests shown in Figs. 3.10 and 3.11.

A comparison of the ORNL and Japanese fuel pin simulator transient performance indicates that at the higher ramp rates (40 and 10 K/s) the ORNL fuel pin simulator profile is much more uniform. However, at the lower ramp rates (5 and 10 K/s followed by steady state), the difference is much less. Since many JAERI bundle tests are conducted at these lower ramp rates, the two designs appear to be qualitatively equivalent, with the ORNL units being somewhat more uniform.

One significant difference in the two fuel pin simulator designs is that the W-3% Re heating wire of the TOSHIBA simulator has a much higher (and positive) temperature coefficient of resistance than the Kanthal A-1 used in the ORNL simulator. Because of this, a hot spot would tend to cause an increase in local heat generation (a 50°C increase in element temperature results in a 2% increase in local heat generation at ~1000°C heating element temperature). This effect might be important under certain test conditions, such as perhaps in a test where initial temperatures are not axially uniform.

Mr. C. Hiruta, a representative of TOSHIBA Corporation, discussed both the Japanese and ORNL designs with ORNL on September 17, 1979. He was very helpful in answering questions regarding the Japanese fuel pin simulator, and he noted that the simulators we evaluated were the third generation design. The design was the responsibility of Dr. Kawasaki of JAERI. Fabrication was developed jointly by Dr. Kawasaki and TOSHIBA engineers. The division of TOSHIBA Corporation responsible for production of the simulators is primarily a metals fabrication facility that manufactures W-Re wire but does not normally fabricate fuel pin simulators. Their effort on the fuel pin simulator was closely coordinated with Dr. Kawasaki, with most of the development under the guidance of his staff.

3.1.6 Destructive examination of a TOSHIBA fuel pin simulator

Typical assembled and partially disassembled TOSHIBA fuel pin simulators are shown in Fig. 3.12. Figure 3.13 shows enlarged views of a cladding thermocouple holder, with and without a thermocouple installed. A relatively large separation distance between the thermocouple junction and

the cladding is present in this design. An enlarged view of the lower end of the fuel pin simulator is shown in Fig. 3.14, in which two ceramic seals, a power lead, and a pressurization tube and valve can be seen. Radiographs revealed the presence of an ~10-cm-long metal-braid section on the lower power lead inside the large-diameter section at the left in Fig. 3.14, apparently to accommodate differential length changes between the cladding and internal parts during a test.

One of the simulators, fuel pin simulator No. 334, is being destructively examined. This simulator was sectioned below the ceramic seal at the top end, and the Zircaloy cladding tube was removed (after its lower end was cut) as shown in Fig. 3.12(b). The 85-cm-long heated section corresponds to the discoloration zone that is visible on the cladding (produced during the IR-scanning in air to temperatures of ~500°C) in both views of Fig. 3.12 and also, as shown in Fig. 3.12(b), to the length of longer Al_2O_3 pellets in between the shorter Al_2O_3 sleeves on the unheated ends.

An enlarged view of the upper end of the heated section of a simulator is shown in Fig. 3.15, where three of the shorter Al_2O_3 sleeves have been removed. This view shows the six W-3% Re heating element wires where they emerge from the holes in the top Al_2O_3 pellet and attach to the upper iron lead section. A similar design is used at the lower end of the heated zone.

3.2 Thermocouple Procurement

W. A. Bird* J. H. Holladay*

Delivery was completed on the order for 300 Inconel-sheathed (0.71-mm-OD) type K thermocouples for the B-5 fuel pin simulators. As reported in the previous report, in-house fabrication from bulk material prevented late delivery of the order from delaying the assembly of fuel pin simulators. Receiving inspection revealed that 32 of the 300 thermocouples failed to meet the room temperature insulation resistance requirements. These were returned to the factory for repair.

---

*Instrumentation and Controls Division.

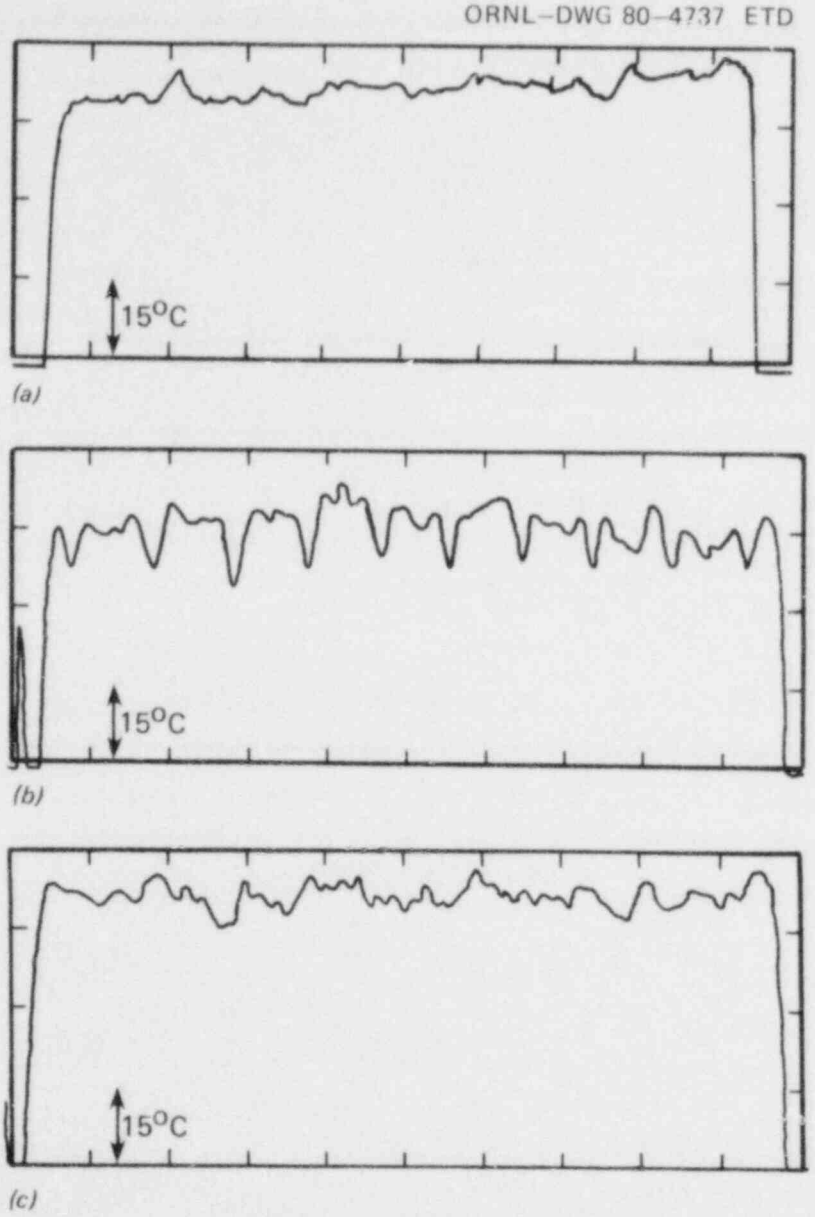

Fig. 3.1. Comparison of 10-s transient IR scan of fuel simulator (a) without ZrO_2 coating, (b) with defective ZrO_2 coating, and (c) with acceptable ZrO_2 coating.

ORNL-DWG 80-4738 ETD

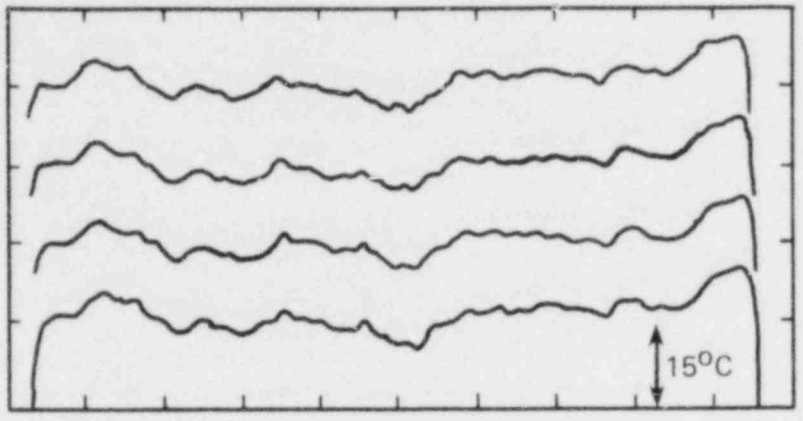

QUADRANT	T_{MAX} (°C)
1	444
2	446
3	446
4	445

Fig. 3.2. Comparison of 10-s transient temperature profiles of the four quadrants of uncoated simulator MNL-085.

ORNL-DWG 80-4739 ETD

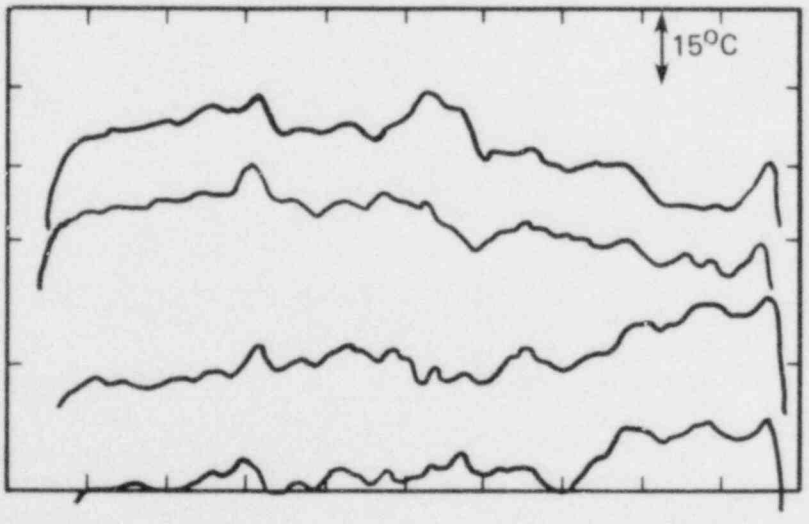

QUADRANT	T_{MAX} (°C)
1	429
2	443
3	426
4	428

Fig. 3.3. Comparison of 10-s transient temperature profiles of the four quadrants of fuel pin simulator SR-59.

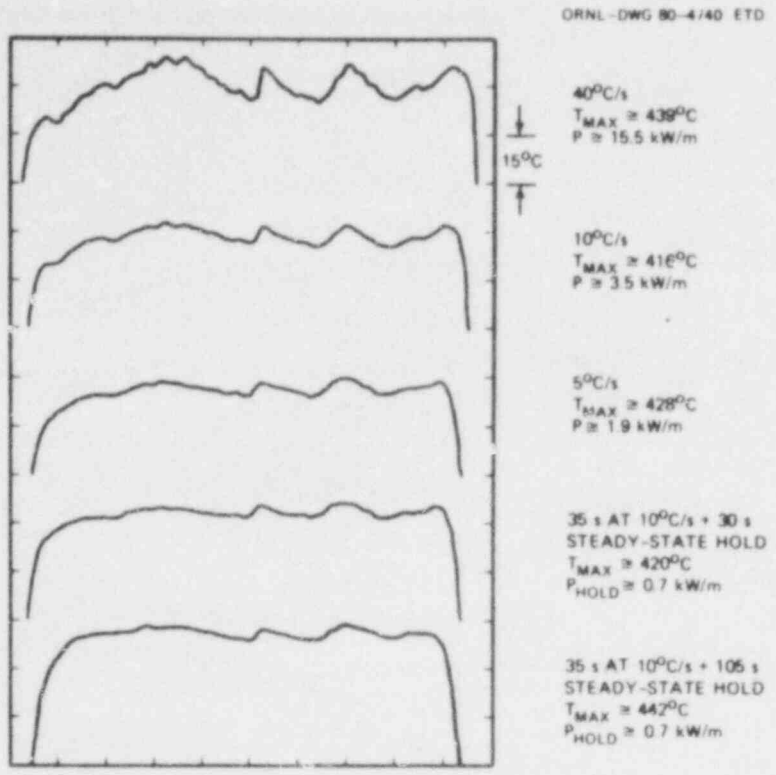

Fig. 3.4. First-quadrant IR scans of fuel pin simulator SR-55 at various cladding heating rates.

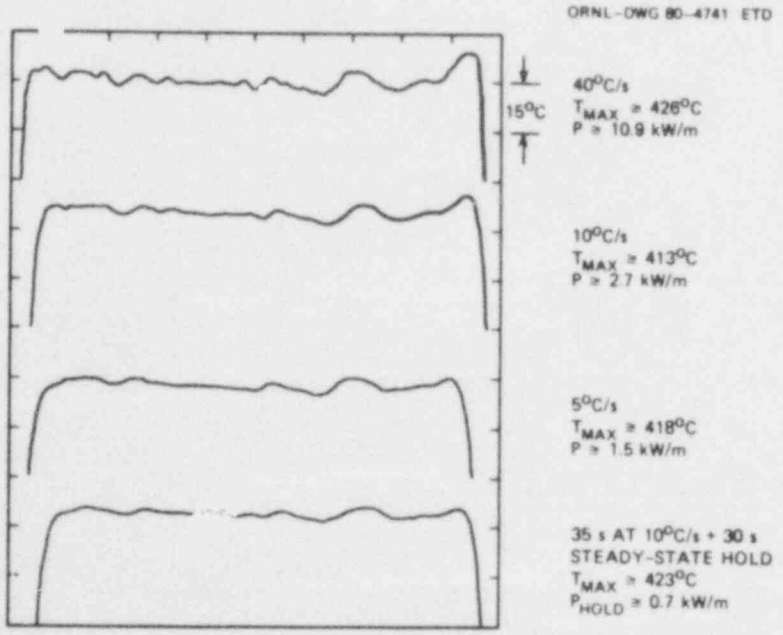

Fig. 3.5. First-quadrant IR scans of fuel simulator MNL-046 at various heating rates.

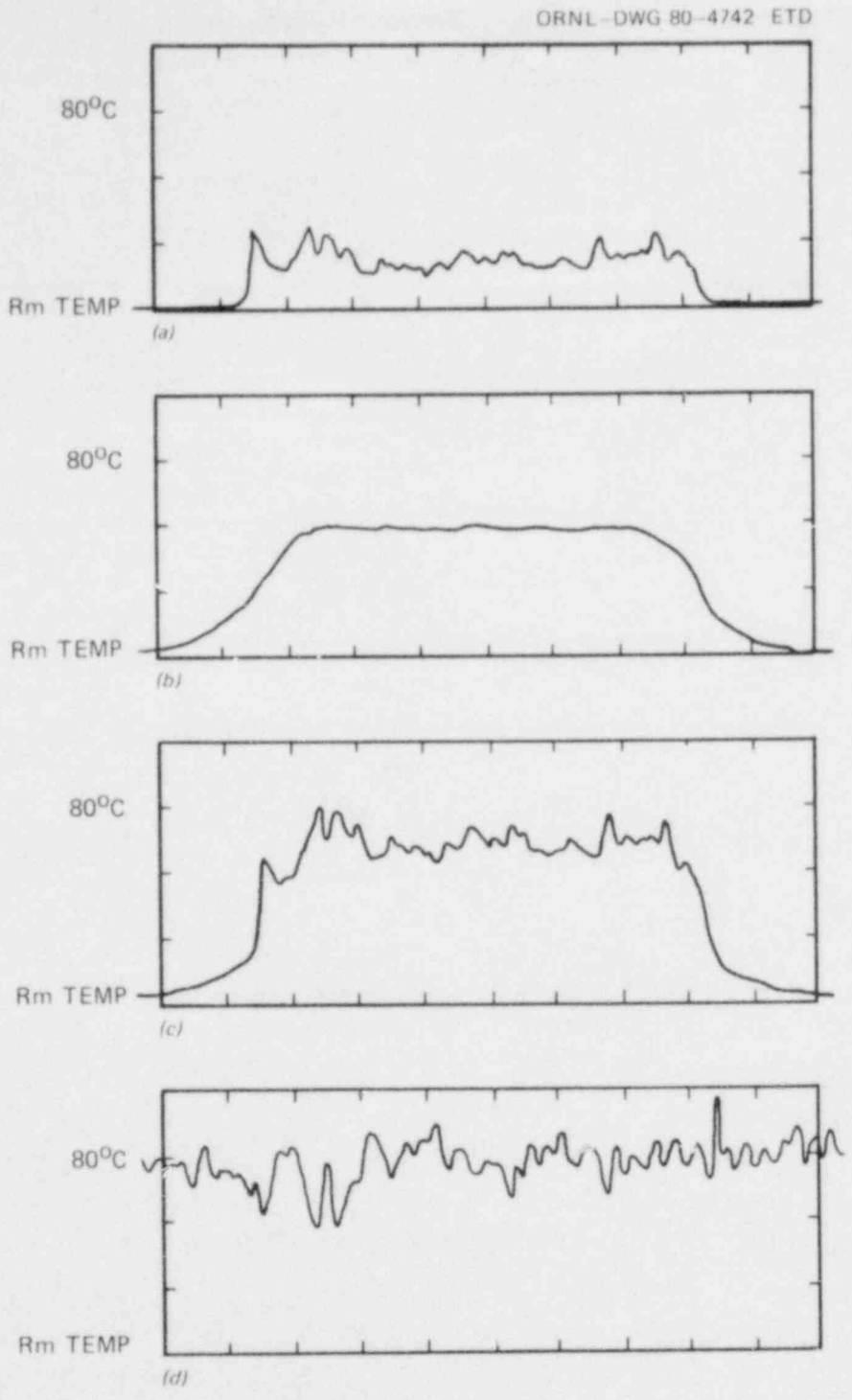

Fig. 3.6. Typical low-temperature IR scans of TOSHIBA fuel pin simulators: (a) normal 1-s transient, (b) steady-state heating of fuel pin simulator, (c) 1-s transient starting from steady-state temperature distribution in (b) above, (d) 1-s transient heating of fuel pin simulator cladding.

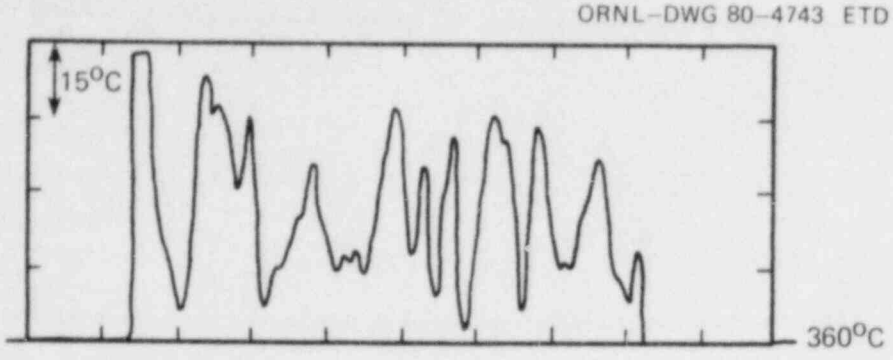

Fig. 3.7. Typical 10-s transient temperature profile of TOSHIBA fuel pin simulator with heating rate of 40 K/s.

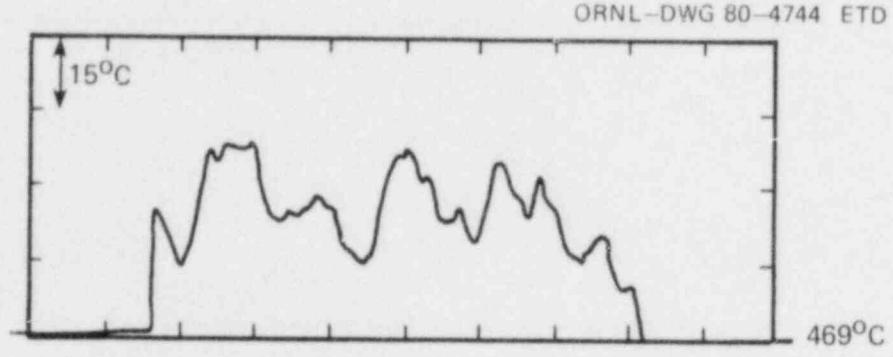

Fig. 3.8. Typical 40-s transient temperature profile of TOSHIBA fuel pin simulator with heating rate of 10 K/s.

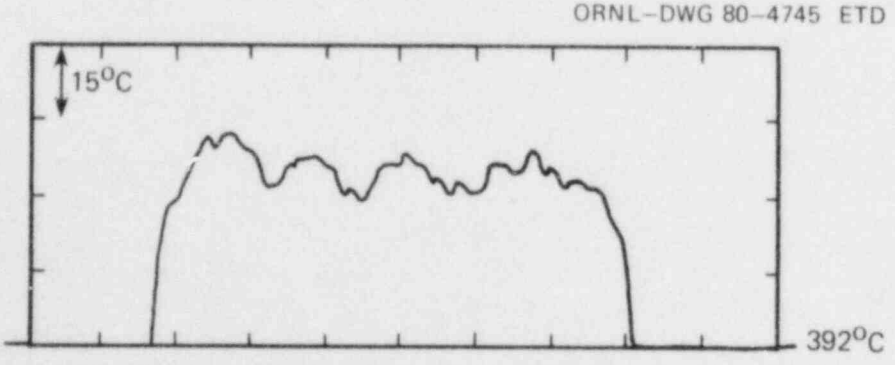

Fig. 3.9. Typical 80-s transient temperature profile of TOSHIBA fuel pin simulator with heating rate of 5 K/s.

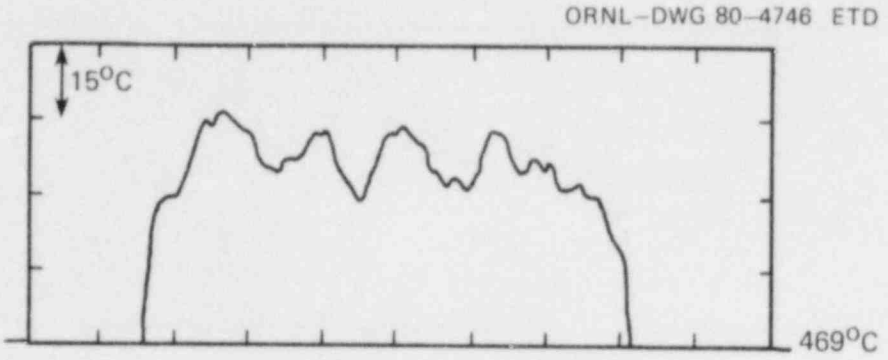

Fig. 3.10. Typical 30-s high-temperature steady-state temperature scan of TOSHIBA fuel pin simulator achieved by heating to hold temperature at a rate of 10 K/s and then reducing power to maintain hold temperature for 30 s.

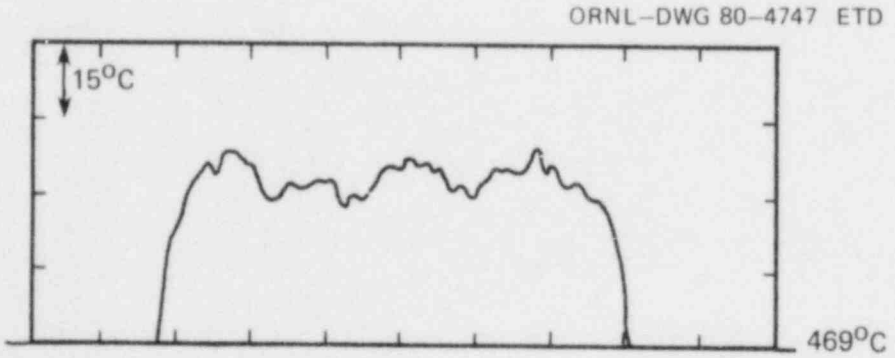

Fig. 3.11. Typical 105-s high-temperature steady-state temperature profile of TOSHIBA fuel pin simulator. Scan taken 75 s after that in Fig. 3.10.

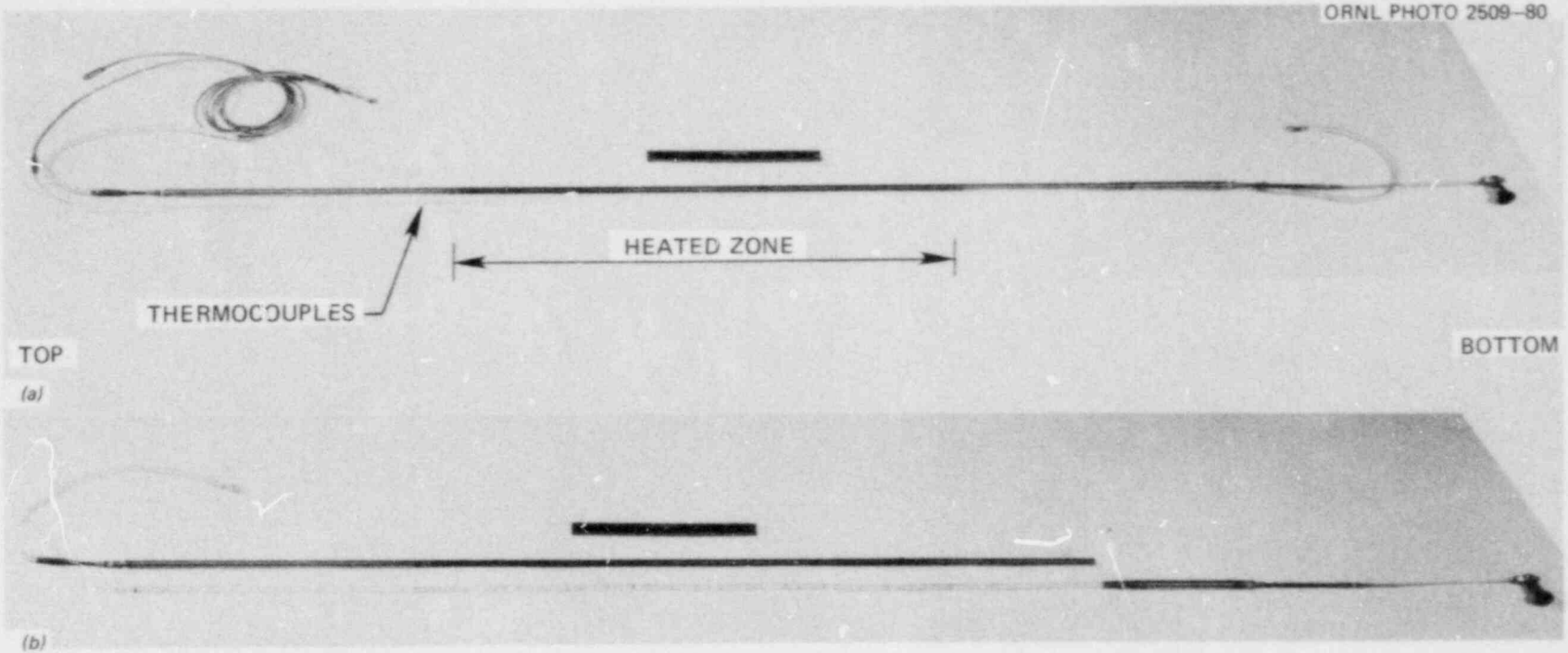

Fig. 3.12. Typical TOSHIBA fuel pin simulators. (a) FPS 800 fully assembled and (b) FPS 334 with Zircaloy tube removed.

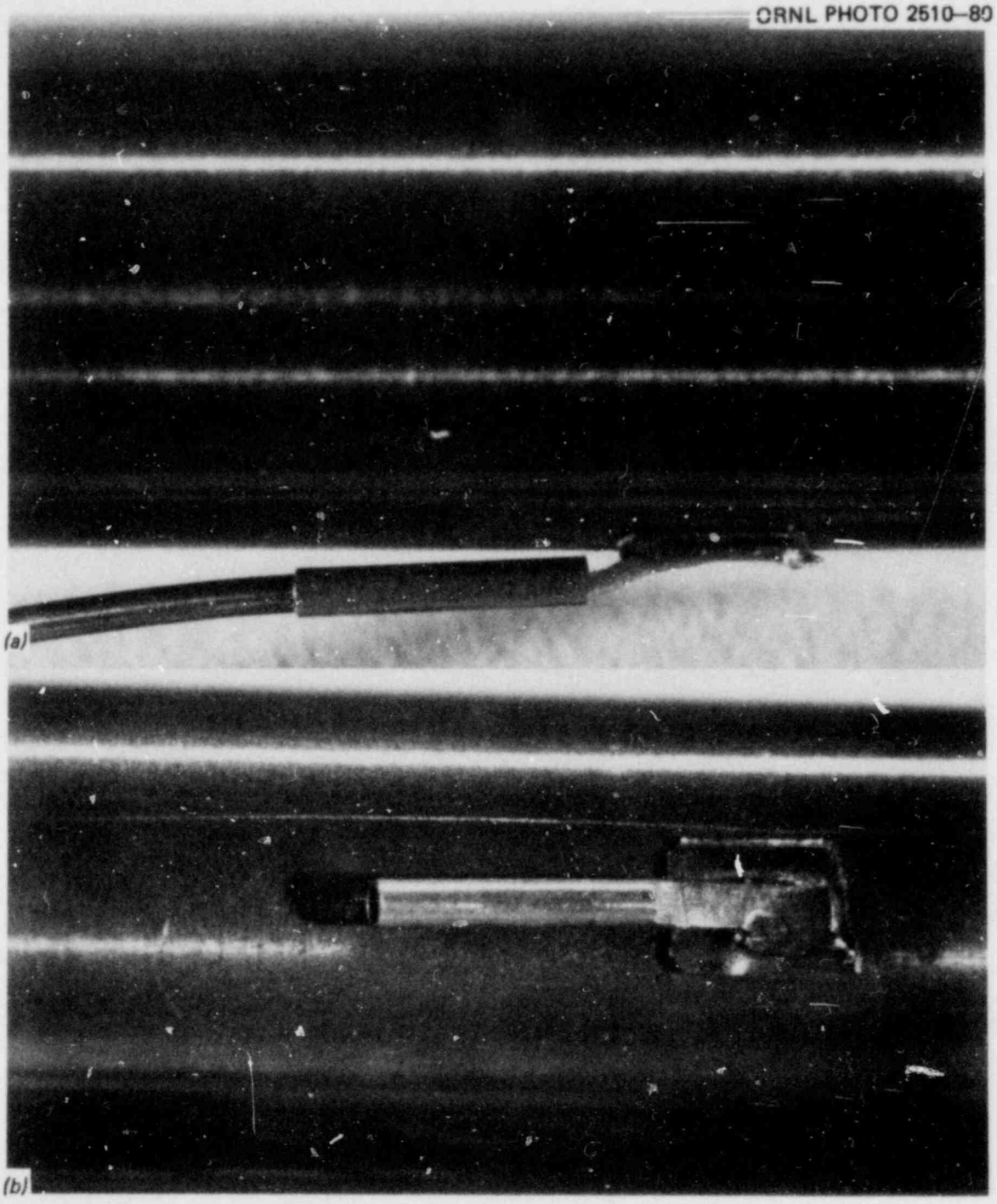

Fig. 3.13. Cladding thermocouple attachment on TOSHIBA fuel pin simulator (a) with thermocouple inserted and (b) without thermocouple.

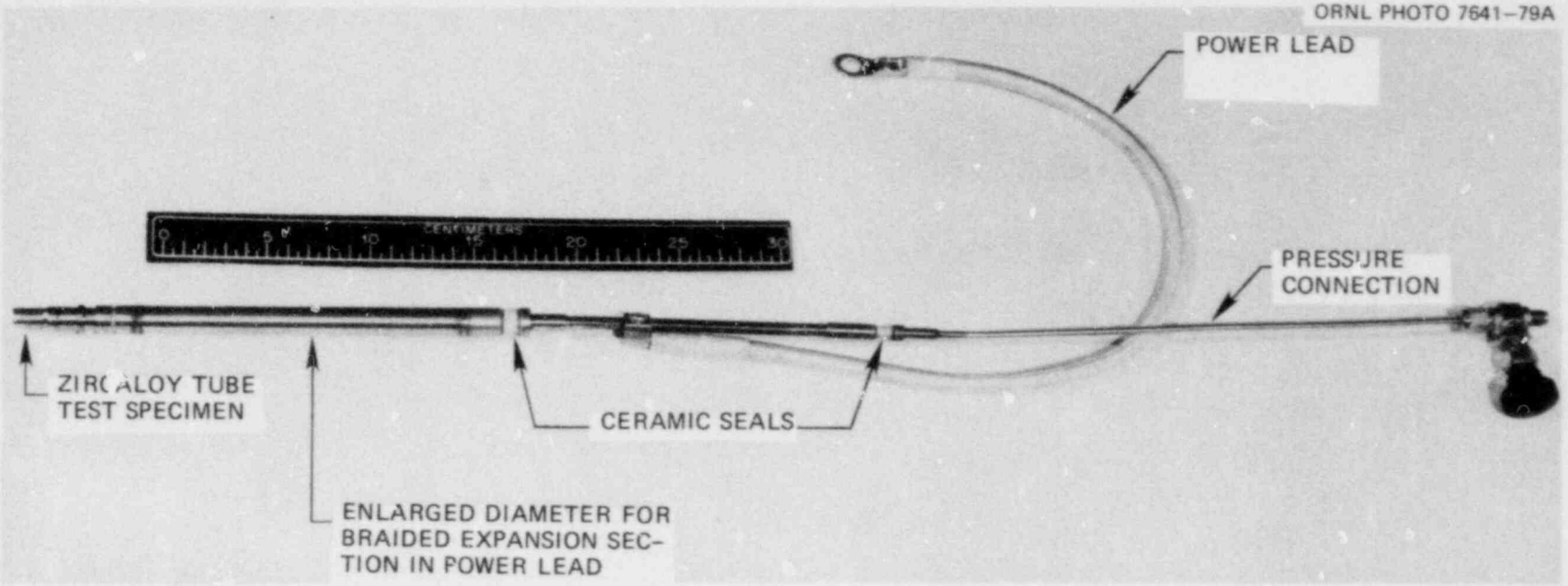

Fig. 3.14. Details of lower end construction of TOSHIBA fuel pin simulator.

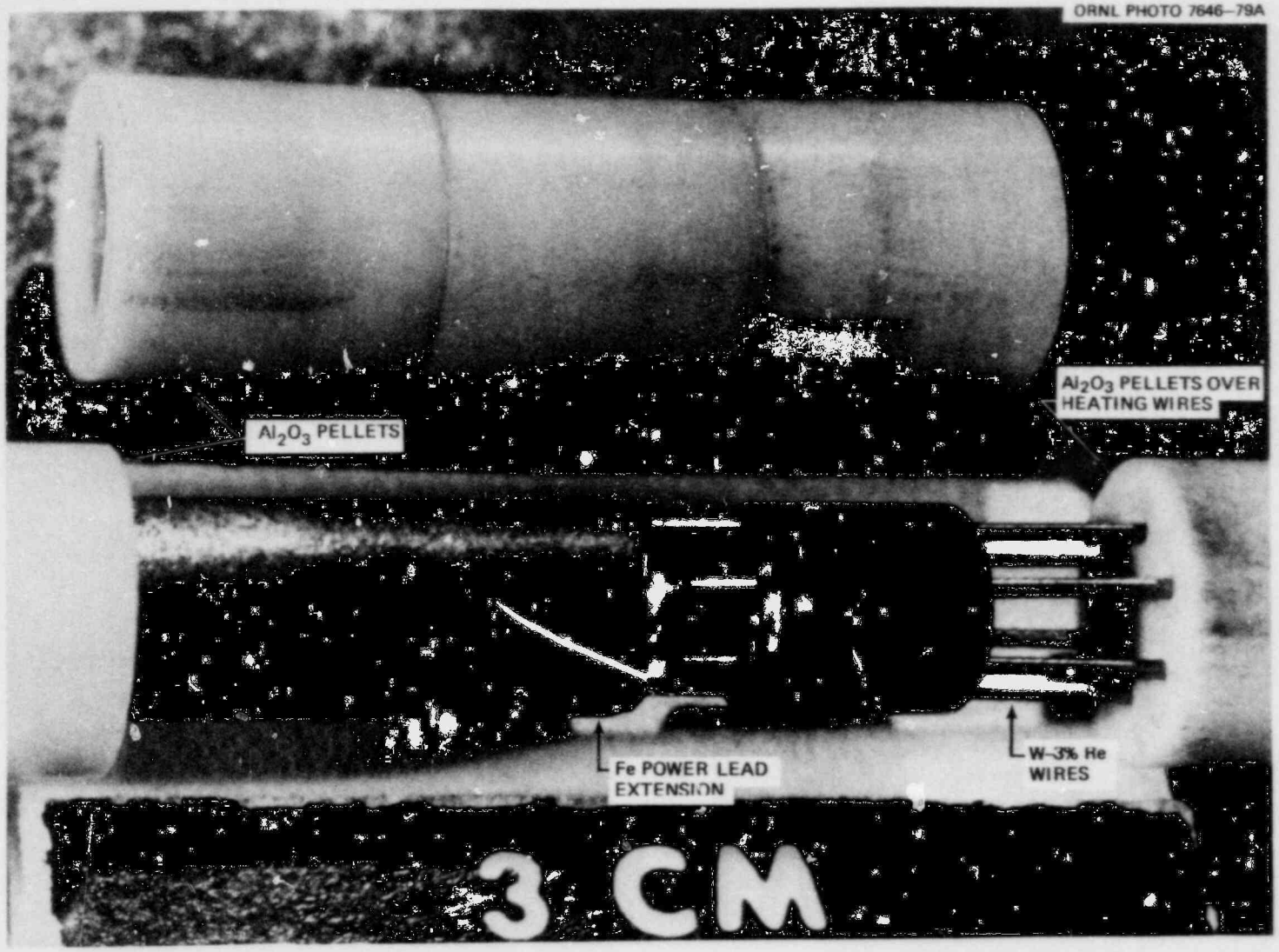

Fig. 3.15. Details of upper end construction of TOSHIBA fuel simulator.

4. DESIGN, FABRICATION, AND EQUIPMENT MODIFICATIONS

4.1 B-5 Fuel Pin Simulator Assembly

J. L. Crowley A. W. Longest

Assembly of the 64 fuel pin simulators needed for the 8 × 8 bundle B-5, which began in May 1979, is continuing satisfactorily toward the scheduled completion date of February 1, 1980. Approximately 90% of the 64 simulators were assembled as of December 31, 1979. As described in the preceding progress report,[8] the fuel pin simulator design, including the fuel simulator (internal heater), is basically the same as for the previous 4 × 4 bundles; and essentially the same assembly techniques and procedures are being used. Detailed as-built data for each individual fuel pin simulator are being recorded and will be summarized and reported in a subsequent progress report when all of the fuel pin simulators have been assembled.

Preparation of the fuel simulators for B-5, which was started in January 1979, was completed during this report period. Fuel simulator preparation includes grooving to provide pathways for the fuel pin simulator internal thermocouples, plasma spray coating of the heated zone with a protective coating of ZrO_2, and 10-s IR scanning to characterize transient axial heat generation distribution. As mentioned in the preceding progress report, a group of 75 fuel simulators, all fabricated by the ORNL Fuel Rod Simulator Technology Laboratory, were selected for preparation and possible use in B-5 fuel pin simulators. The uniformity of the axial heat generation distributions of these simulators (as indicated by transient IR scanning before preparation) was generally as good as or better than the best ones used in the previous 4 × 4 bundle tests.

Review of the grooving inspection data showed that all but one of the 75 fuel simulators have grooves within dimensional tolerances or sufficiently close to the specified tolerances to be acceptable for use in B-5. Coating inspection data indicated all 75 coated fuel simulators to be acceptable. However, a comparison of 10-s IR scans obtained before and after fuel simulator preparation showed that the ZrO_2 coatings introduced

additional variations in the scans (see Sect. 3.1). About one-third of the B-5 group of coated fuel simulators showed changes in the IR scans that were greater than we judged to be acceptable based on results obtained immediately after checkout of the coating equipment. Those in this category were stripped of ZrO_2 and recoated (after checkout and adjustment of the equipment) with reasonably good results. The final postpreparation 10-s IR scan variations are generally less than ±2.5% of the mean value, compared to pre-preparation variations of less than ±2% of the mean value. (A majority of the fuel simulators have pre-preparation 10-s IR scan variations of less than ±1-1/2% of the mean value.) Additional information obtained from the IR scan evaluation of the B-5 fuel simulators is given in Sect. 3.1.

As preparation of the fuel simulators was completed, the ones judged to be of the highest quality were assigned to the 64 positions in the bundle in much the same manner as was done for the previous bundle tests. In general, those with the most uniform axial heat generation distributions, as indicated by the 10-s IR characterization scans, were assigned to the innermost positions and the least uniform ones to the outermost positions.

4.2 Multirod Test Facility Expansion for B-5 Test

W. A. Bird* J. L. Crowley

The expansion effort was continued during this report period with the actual installation work beginning in November. The expansion, to allow testing of a 64-rod bundle, includes additional instrumentation to provide a total capability of 300 thermocouple channels and 65 pressure channels. Also included in the expansion is the capability of temperature controls for both bundle and shroud (which has been described in previous reports[7,8]). Drafting was completed on 2[illegible] drawings and 33 revised drawings.

New equipment received and being installed includes thermocouple reference boxes and pressure transducers. Power supplies for the pressure

*Instrumentation and Controls Division.

transducers have been ordered but not yet received. The manifold for pressurizing and monitoring individual fuel pin simulator pressures during the test transient has been fabricated but not yet installed. The facility expansion is expected to be complete by mid-March.

4.3 Data Acquisition System and Software for B-5 Test

A. F. Johnson F. R. Gibson

Activity during this period consisted mainly of modifying data acquisition system (DAS) software. This software upgrade was necessary so that the Thermal-Hydraulic Test Facility (THTF), Instrument Development Loop (IDL), and MRBT could all use, where applicable, the same DAS software and hardware with minimal conflict.

New MRBT data reduction programs are being written for the Computer Sciences Division's IBM computers. These programs will be written to handle new upgraded DAS data formats and larger MRBT bundle sizes.

4.4 Single-Rod Test Facility Modifications

D. B. Lloyd J. L. Crowley
R. F. Haynes

Operation of the single-rod test facility, described previously, pointed to several areas where further improvements were possible. It was found that the ceramic-like material (Mykroy) used to fabricate the thermocouple feed-through strip distorted when subjected to typical burst temperatures. Macor, a machinable ceramic material, has been substituted and found to be acceptable. It is, by nature, more brittle than the Mykroy, but it is dimensionally stable at our operating temperatures and has not presented any problems in either the assembly or disassembly of the test equipment.

A heater was installed on the flange of the test vessel to provide a more uniform temperature for the beginning of the burst transient. The upper flange is in direct contact with the support frame and thus represents a substantial heat sink.

A support ring was attached to the top flange of the test assembly to provide support for the thermocouple heads. Because the type S thermocouple wires, which are reused in the single-rod tests, are very fragile, the support ring is expected to prolong the life of the thermocouples. The support with identified thermocouple head locations also facilitates the pretest checkout procedures.

5. OPERATIONS

A. W. Longest W. A. Bird*
D. B. Lloyd R. F. Haynes

An important new series of single-rod tests incorporating a heated shroud was begun during this report period. Earlier demonstration tests of the heated shroud assembly, shroud portable power supply, and fuel pin simulator and shroud temperature controllers were described in the preceding progress report.[8] Those tests indicated good performance of the new systems and implied that the heated shroud assembly would permit single-rod testing under thermal conditions closely matching those in a bundle; with a very similar thermal environment, tube deformation behavior should approximate that in a bundle, with the exception of the possible influences of rod-to-rod interactions and radial restraint.

Eighteen fuel pin simulators were assembled and tested in the new single-rod heated shroud assembly. For tests numbered SR-47 through SR-62, a nominal steam flow rate of 5.8×10^{-4} kg/s was maintained; this flow rate and the resulting Reynolds number (~700) were approximately the same as in the previous sequence of single-rod unheated shroud tests. (This nominal flow rate is that referred to hereafter as "normal.") In contrast, SR-63 was run with a steam flow rate nearly 7 times higher than that for the preceding 15 tests, and consequently the Reynolds number was on the order of 5000. For SR-64, the flow rate was set at an intermediate value of about 5-1/2 times the normal value, resulting in a Reynolds number of about 4000. In addition to these two high-flow-rate tests, one test with lower-than-normal steam flow rate (SR-65) was conducted to closely match the bundle B-3 mass flux of 0.28 $kg \cdot m^{-2} \cdot s^{-1}$. This flow of about 2.7×10^{-4} kg/s resulted in a Reynolds number of about 330 (Table 5.1). The tests were conducted at various cladding heating rates up to 28 K/s. The heated shroud was utilized (powered) in all tests except SR-48, SR-54, and SR-55. One of the fuel simulators (SEMCO 2828031) used in seven of the present test series was also used for many previous tests in the older unheated shroud assembly. The remaining 11 tests were performed

*Instrumentation and Controls Division.

Table 5.1. Burst tests conducted in the MRBT single-rod heated shroud assembly

Test	Fuel simulator	Test type	Cladding heating rate (K/s)	Nominal burst temperature (°C)	Shroud powered	Flow rate (10^{-4} kg/s)	Mass flux ($kg \cdot m^{-2} \cdot s^{-1}$)
SR-47	SEMCO-031	Transient	10	760	Yes	5.96	0.625
SR-48	MNL-085	Transient	10	760	No	5.95	0.624
SR-49	MNL-046	Transient	5	760	Yes	5.80	0.608
SR-50	MNL-009	Transient	10	860	Yes	6.16	0.646
SR-51	SEMCO-031	Creep-rupture	0	760	Yes	6.10	0.640
SR-52	MNL-085	Transient	10	760	Yes	6.04	0.634
SR-53	MNL-046	Creep-rupture	0	760	Yes	5.80	0.608
SR-54	SEMCO-031	Transient	10	760	No	6.28	0.659
SR-55	MNL-046	Transient	5	760	No	6.06	0.636
SR-56	SEMCO-031	Creep-rupture	0	760	Yes	5.80	0.608
SR-57	MNL-046	Creep-rupture	0	760	Yes	6.58	0.691
SR-58	SEMCO-031	Creep-rupture	0	760	Yes	5.88	0.616
SR-60	MNL-009	Transient	28	860	Yes	6.07	0.636
SR-61	SEMCO-031	Transient	28	760	Yes	5.81	0.609
SR-62	MNL-009	Transient	28	920	Yes	6.01	0.631
SR-63	SEMCO-031	Creep-rupture	0	760	Yes	40.7	4.27
SR-64	MNL-046	Transient	5	760	Yes	32.7	3.43
SR-65	MNL-046	Transient	5	760	Yes	2.67	0.280

with 3 new fuel simulators (MNL-009, MNL-046, or MNL-085) recently fabricated by the ORNL Fuel Rod Simulator Technology Laboratory.

A few of the tests in the new series were of a preliminary nature and designed to reveal general differences between single-rod tests performed in the unheated shroud facility and those conducted in the present facility. Other tests allowed investigation of the effects of varying heating rate on deformation. Tests SR-63, SR-64, and SR-65 were undertaken to determine the significance of steam flow rate coupled with other variables such as heating rate.

The results of these 18 tests in the heated shroud assembly (SR-47 through SR-58 and SR-60 through SR-65) are presented and discussed in Sect. 2.2.

REFERENCES

1. R. H. Chapman, *Multirod Burst Test Program Quart. Prog. Rep. for January–March 1976*, ORNL/NUREG/TM-36.

2. R. H. Chapman, *Multirod Burst Test Program Quart. Prog. Rep. for April–June 1977*, ORNL/NUREG/TM-135.

3. R. H. Chapman, *Multirod Burst Test Program Prog. Rep. for July–December 1977*, NUREG/CR-0103 (ORNL/NUREG/TM-200).

4. R. H. Chapman, *Multirod Burst Test Program Prog. Rep. for January–March 1978*, NUREG/CR-0225 (ORNL/NUREG/TM-217).

5. R. H. Chapman et al., *Effect of Creep Time and Heating Rate on Deformation of Zircaloy-4 Tubes Tested in Steam with Internal Heaters*, NUREG/CR-0343 (ORNL/NUREG/TM-245) (October 1978).

6. R. H. Chapman, *Multirod Burst Test Program Prog. Rep. for July–December 1978*, NUREG/CR-0655 (ORNL/NUREG/TM-297).

7. A. W. Longest, *Multirod Burst Test Program Prog. Rep. for January–March 1979*, NUREG/CR-0817 (ORNL/NUREG/TM-323).

8. R. H. Chapman, *Multirod Burst Test Program Prog. Rep. for April–June 1979*, NUREG/CR-1023 (ORNL/NUREG/TM-351).

9. J. F. Mincey, *Steady-State Axial Pressure Losses Along the Exterior of Deformed Fuel Cladding: Multirod Burst Test (MRBT) Bundles B-1 and B-2*, NUREG/CR-1011 (ORNL/NUREG/TM-350) (January 1980).

10. R. H. Chapman et al., *Bundle B-1 Test Data*, ORNL/NUREG/TM-322 (June 1979).

11. R. H. Chapman et al., *Bundle B-2 Test Data*, ORNL/NUREG/TM-337 (August 1979).

12. R. H. Chapman et al., *Bundle B-3 Test Data*, ORNL/NUREG/TM-360 (January 1980).

13. E. D. Hindle and C. A. Mann, *Deformation of PWR Cladding Following a Loss-of-Coolant Accident*, UKAEA Report ND-R-362(S) (July 1979).

14. E. D. Hindle and C. A. Mann, *Zircaloy PWR Fuel Cladding Deformation Tests Under Mainly Convective Cooling Conditions*, UKAEA Report ND-R-364(S) (May 1979).

NUREG/CR-1450
ORNL/NUREG/TM-392
Dist. Category R3

Internal Distribution

1. M. Bender
2. K. R. Carr
3-7. R. H. Chapman
8. W. G. Craddick
9. J. L. Crowley
10. R. F. Haynes
11. D. O. Hobson
12. A. F. Johnson
13. D. B. Lloyd
14. A. W. Longest
15. A. P. Malinauskas
16. R. W. McCulloch
17. C. A. Mills
18. F. R. Mynatt
19. F. H. Neill
20. H. R. Payne
21-22. J. L. Rich
23. R. D. Stulting
24. H. E. Trammell
25. J. D. White
26. Patent Office
27. Nuclear Safety Information Center
28. Central Research Library
29. Document Reference Section
30-31. Laboratory Records Department
32. Laboratory Records (RC)

External Distribution

33. Office of Assistant Manager for Energy Research and Development, DOE, ORO, Oak Ridge, TN 37830
34. Director, Reactor Division, DOE, ORO, Oak Ridge, TN 37830
35. M. L. Picklesimer, Division of Reactor Safety Research, Office of Nuclear Regulatory Research, NRC, Washington, DC 20555
36. T. Howe, EG&G Idaho, Inc., INEL, Idaho Falls, ID 83401
37. D. L. Hagrman, EG&G Idaho, Inc., INEL, Idaho Falls, ID 83401
38. R. R. Hobbins, EG&G Idaho, Inc., INEL, Idaho Falls, ID 83401
39. J. R. Larson, EG&G Idaho, Inc., INEL, Idaho Falls, ID 83401
40. C. R. Hann, Battelle Northwest Laboratory, P.O. Box 999, Richland, WA 99352
41. M. Fischer, PNS-Leitung, Gesellschaft für Kernforschung, Postfach 3640, 75 Karlsruhe, FRG
42-43. Technical Information Center, DOE, Oak Ridge, TN 37830
44-443. Distribution as shown for NRC category R3 (NTIS-10)

☆U.S. GOVERNMENT PRINTING OFFICE: 1980-640-245/206